

B10
3431

Synthesis of Nanocomposite Material with Quest of Antimicrobial Properties

A thesis submitted in the partial fulfilment of the
Requirement for the degree of

**DOCTOR OF PHILOSOPHY
IN
MICROBIOLOGY**



By
Ishrat Bano

Department of Microbiology
Quaid-i-Azam University
Islamabad, Pakistan
2013



The Quest for Antimicrobial Properties of Nanocomposite Material (Ag-TiO₂)



BY
ISHRAT BANO

Supervisor:

Prof. Abdul Hameed
Department of Microbiology

Quaid-i-Azam University
Islamabad, Pakistan

Co-Supervisor:

Dr. R. Vasnat Kumar
Department of Materials Science &
Metallurgy

University of Cambridge
UK

(2013)


Dedication

**To my beloved parents who raised their daughters to be confident
and successful in their lives.**

CERTIFICATE


This thesis by **Ishat Bano** is accepted in its present form by the Department of Microbiology, Quaid-i-Azam University, Islamabad, as fulfilling the thesis requirement for the degree of Doctor of Philosophy in Microbiology.

Supervisor



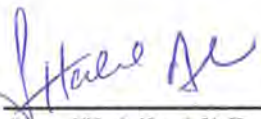
(Prof. Dr. A. Hameed)

External examiner



(Prof. Dr. Azra Khanum)

External examiner



(Dr. Habib Ali Bokhari)

Chairperson



(Prof. Dr. Safia Ahmed)

Dated: 21-01-2014

Table of Content

Topic	Page No.
List of Tables	I
List of Figures	II
List of Abbreviations	V
Acknowledgements	VII
Abstract	IX
Chapter 1 Introduction	1
Chapter 2 Literature Review	112
Chapter 3 Materials & Methods	52
Chapter 4 Results and Discussion	80
Chapter 5	114
Conclusion	133
Future Recommendation	135
List of Publications	136
References	137

LIST OF TABLES

Table No.	Title	Page No.
1.1	Classification of Nanomaterials	3
2.1	Properties of TiO ₂ polymorphs	17
3.1	Chemicals used in the experiment	53
3.2	Chemicals used in synthesis of Ag-TiO ₂ Nanocomposite	59
3.3	Composition of Luria Bertani (LB) Broth	61
3.4	Variables used in the Experiments	64
4.1	BET Surface Area, Crystallite size (XRD) of Ag-TiO ₂ Nanocomposite	106
5.1	The reactions relating conduction band electron and valence band hole	130

LIST OF FIGURES

Fig No.	Title	Page No.
2.1	The Size of Nanomaterials In Comparison To Other structures On The Length Scale	13
2.2	Crystallographic Structure of TiO ₂	16
2.3	Applications of Sol-gel Process	29
2.4	Photocatalytic mechanism	35
2.5	Light Energy greater than band gap	38
2.6	Integration of silver nanoparticles traps photo generated electrons and assists longer charge separation	40
2.7	Electron accumulation in core-shell Ag/ TiO ₂ in UV irradiation	41
2.8	TiO ₂ photocatalytic splitting of water	47
2.9	Self cleaning windows from Pilkington Activ10	48
2.10	DSSC (Dye sensitised solar cell)	49
3.1	Chemical structure of Titanium iso propoxide	52
3.2	Flow chart showing synthesis of TiO ₂ nanopowder via Sol-Gel process	56
3.3	LB Broth	61
3.4	Viable Colony Counting Method by Serial Dilution	63
3.5	PANalytical vertical X-ray Diffractometer	65
3.6	Bragg's Law	66
3.7	Transmission Electron Microscope (TEM) Mechanism	71
3.8	Components Of a Typical UV Vis Spectroscopy	73
3.9	Zetasizer Malvern 3000 HAS	76
4.1	(a,b) XRD of TiO ₂ synthesized via standard sol-gel method (volume ratio TIP: ethanol: water = 1:1:1)	82
4.2	(a,b) SEM images of TiO ₂ NPs synthesised by standard sol-gel method (volume ratio TIP: ethanol: water = 1:1:1) at pH=7 (a) 10,000X (b) 90,000X.	84

4.3	Standard Sol-Gel Synthesis of TiO ₂ NPs	85
4.4	TiO ₂ gel particles dried at room temperature	86
4.5	FEGSEM analysis of TiO ₂ synthesized by pure TIP.	88
4.6	XRD of TiO ₂ prepared by sol gel	90
4.7	(a) Size variations of primary particles (estimated from FEGSEM) and crystallites (estimated from XRD) (b) Secondary particles (estimated from FEGSEM)	92
4.8	Nucleation and growth of TiO ₂ in primary particles	93
4.9	FEGSEM images of TiO ₂ NPs synthesised by ethanol-stabilised TIP (volume ratio TIP/ethanol = 5/0, 5/1, and 5/5). The samples are annealed at 150 °C/1h, 400 °C/1 hour with heating rate of 10 °C/min.	95
4.10	Temporal analysis of FEGSEM of TiO ₂ synthesised by ethanol-stabilised TIP	97
4.11	Temporal analysis of FEGSEM of TiO ₂ synthesised by ethanol-stabilised TIP.	98
4.12	Temporal analysis of XRD for TiO ₂ NPs prepared by ethanol-stabilised TIP. (volume ratio TIP/methanol = 1/0.1, aged 8 hours).	99
4.13	XRD Patterns of a) TiO ₂ b) Ag-TiO ₂ nanocomposite	105
4.14	BET Surface area and pore size of Ag-TiO ₂ nanocomposite	106
4.15	UV-Vis Spectra of Ag-TiO ₂ photosynthesised at pH=3	107
4.16	TEM Image of Ag-TiO ₂ showing the deposits of Ag on TiO ₂ Nanoparticles at pH 3	109
4.17	The Corresponding EDX Spectrum of Ag-TiO ₂ nanocomposite at pH3	109
4.18	(a, b) The SEM images of Ag-TiO ₂ nanocomposite at pH 3 and pH 9	111
5.1	Bactericidal effect of various Ag-TiO ₂ concentration on <i>E. coli</i>	120

	(2×10^5 CFU ml ⁻¹)	
5.2	Ag-TiO ₂ Bactericidal Efficiency (2×10^5 CFU ml ⁻¹)	121
5.3	Bactericidal Effect of TiO ₂ and Ag-TiO ₂ in UV and Dark (2×10^5 CFU ml ⁻¹) (pH 7.1, Ag-TiO ₂ 1.0 g/l)	122
5.4	(a) Untreated Bacterial cells	124
	(b) Treated bacterial cells showing damage of the cell membrane	
5.5	Transmission electron micrographs of <i>E. coli</i> sections prepared from specimens, which had not been exposed to Ag-TiO ₂ nanoparticles.	126
5.6	TEM of <i>E. coli</i> sections post treatment with Ag-TiO ₂ nanoparticles (Transverse Section)	127
5.7	TEM of <i>E. coli</i> sections post treatment With Ag-TiO ₂ nanoparticles (Longitudinal sections of the bacteria are shown)	127
5.8	Proposed mechanism of Ag-TiO ₂ bactericidal activity (a,b,c)	130

List Of Abbreviations

Å	Angstrom
AES	Auger Electron spectroscopy
Ag	Silver
AN	Nucleophilic addition reaction
Au	Gold
BEI	Back scattered electrons
BET	Brunauer–Emmett–Teller (BET)
BSE	Back-scattered electrons
°C	Centigrade
CB	Conduction band
CFU	Colony forming unit
CVD	Chemical vapour deposition
CTAB	Cetyl trimethyl ammonium bromide
DNA	Deoxy ribonucleic acid
DSSC	Dye sensitised solar cells
e-	excited electron
E-beam	Electron beam
<i>E.coli</i>	<i>Escheria coli</i>
ESR	Electron Spin resonance
FESEM	Field emission scanning electron microscopy
FEGSEM	Field Emission Gun-Scanning Electron Microscopes
FT-IR	Fourier transform infrared spectroscopy
FWHM	Full width at half maximum
g	gram
GIXRD	Glancing incidence x-ray photoelectron spectroscopy
h ⁺	positive hole
H ₂ O	Water
HRTEM	High resolution transmission electron microscopy
LB	Lauria Bertani
m	meter
mL	mili litre

MRSA	Methicillin-resistant <i>Staphylococcus aureus</i>
Nm	nanometre
NP	Nanoparticles
OD	Optical density
OR	alkoxide
Pd	Pladium
Pt	Platinum
PVC	Physical vapour deposition
PVD	Physical vapour deposition
R	Rutile
SE	Secondary electrons
SEM	Scanning electron microscopy
Sn	Tin
SN	Nucleophilic substitution reaction
STEM	Specimen current and transmitted electrons
TEOS	Tetra ethyl orthosilicate
Ti	Titanium
TGA	Thermogravimetric analysis
TIP	Titanium isopropoxide
TTIP	Titanium tetraisopropoxide
UV	Ultraviolet light
Um	micro meter
UL	micro litre
VB	Valence band
VOC	Volatile organic compound
wt %	weight %
XANES	X-ray absorption near edge spectroscopy
XPS	X-ray photoelectron spectroscopy
XRD	X-ray diffraction

ACKNOWLEDGEMENTS

If one were to consider the significant milestones in their own lives, it would become necessary to also consider those who have made these milestones possible. Here, I will do my best to acknowledge the people who have made this thesis a reality.

First and foremost, I would like to thank Allah almighty for blessing me with everything I ever wish for and I send countless salam to Prophet Hazrat Muhammad (peace be upon Him).

I would like to pay gratitude to my thesis supervisor, Prof. Abdul Hameed and Dr Vasant Kumar: Prof Abdul Hameed, who has been supporting and guiding me through the research work since the very beginning of my research career in Pakistan. His guidance and support extended my vision as a conscript researcher. His help has been beyond my expectations, and I truly appreciate it from the core.

Dr Vasant Kumar, I could not have had a better mentor to teach scientific thinking and writing. His guidance during the course of this work allowed me to grow as a scientist. I also would like to thank him for the opportunities to travel to conferences such a great amount. I tremendously enjoyed all the trips taken in the past few years. The people I have met during these trips have made my life richer and my research better.

I wish to express my gratitude to Prof Safia Ahmed, Professor and Chairperson, Department of Microbiology, Quaid-i-Azam University, Islamabad. I extend my acknowledgement to Dr Fariha Hassan and all the Microbiology department faculty members.

My entire family has been incredibly supportive during the whole PhD. Ammi and Abbu, thanks for everything. Your love and unwavering support has always been the bedrock upon which every worthwhile achievement in my life has been built. I never would have made it through this thesis writing process without their constant assistance. Samreen, thanks for “understanding” all my science from a business perspective. My sisters, nephews and nieces thanks for your unconditional love.

Thanks to all the present and former group members of the Materials Science Lab throughout the years. It has been fantastic sharing a lab with you. A special thanks to Julia and Collin, for all the academics and personal help during my stay at Cambridge and being a fantastic host for various special events.

Finally, I would like to acknowledge the financial support received from the UNESCO-L'Oreal, in the form of Research fellowship.

ABSTRACT

Nanomaterials are drawing great attention because of their very small size ranging between 1 to 100 nm. Owing to their small size, nanomaterials possess exceptional biological, chemical, thermal, optical and mechanical characteristics and have prospective applications in various fields.

Noble metal (Au, Pt, Pd and Ag, etc.) nanoparticles are of major concern owing to their exclusive properties predominantly in sterilization and antimicrobial purposes. Since Silver is much cheaper than the other noble metals, thus development of high performance silver based nanomaterials is of immense importance. Small particle size and good dispersion of silver are the two key parameters determining its performances. To achieve these two features, deposition of silver onto less expensive supporting materials such as metal oxides has been generally practiced. Titanium dioxide (TiO_2) is considered the most promising metal oxide due to its high efficiency, chemical stability, non-toxicity, and low cost for degradation.

In the first phase of the research TiO_2 nanoparticles were prepared by sol gel method and were coated with Ag by photo deposition from an aqueous solution of AgNO_3 at various pH levels ranging from 1 to 10 in a titania sol, under UV light. The as-prepared nanocomposite particles were characterized by UV-Vis absorption spectroscopy, transmission electron microscopy (TEM), X-ray diffraction (XRD) and N_2 adsorption/desorption method at liquid nitrogen temperature (-196°C) from Brunauer–Emmett–Teller (BET) measurements.

It is shown that at a Ag loading of 1.25 wt% on TiO_2 a high surface area nanocomposite morphology corresponding to an average of one Ag nanoparticle per titania nanoparticle was achieved. The diameter of the titania crystallites / particles

were in the range of 10 - 20 nm while the size of Ag particles attached to the larger titania particles were 3 ± 1 nm as deduced from crystallite size by XRD and particle size by TEM. Ag recovery by photo harvesting from the solution was nearly 100 %. TEM micrographs revealed that Ag-coated TiO_2 nanoparticles showed a sharp increase in the degree of agglomeration for nanocomposites prepared at basic pH values, with a corresponding sharp decrease in BET surface area especially at $\text{pH} > 9$. The BET surface area of the Ag- TiO_2 nanoparticles was nearly constant at around a value of $140 \text{ m}^2 \text{ g}^{-1}$ at all pH from 1 - 8 with an anomalous maximum of $164 \text{ m}^2 \text{ g}^{-1}$ when prepared from a sol at pH of 4, and a sharp decrease to $78 \text{ m}^2 \text{ g}^{-1}$ at pH of 10.

In the second phase, an *In vitro* photocatalytic bactericidal effect of Ag- TiO_2 nanocomposite was evaluated using *E.coli* as a model organism. Transmission electron micrographs have been used to illustrate the treated and untreated cells, giving insight into the possible mechanism underlying the interaction of Ag- TiO_2 nanocomposite with the bacterial cell.

Highly dispersed, Ag- TiO_2 nanocomposite is used with an average particle size of less than 20nm. Bactericidal analysis was carried out in Luria Bertani medium on solid agar plates with various illumination time and different concentrations of Ag- TiO_2 nanocomposite. Transmission electron microscope (TEM) analysis of bacterial section was used to detect the effect of irradiation of Ag- TiO_2 nanocomposite on the ultra structure of the bacterial cell in order to reveal possible cellular damage. The mechanism underlying the action of photo excited Ag- TiO_2 nanocomposite on *E.coli* cell membrane is also evaluated. The results confirmed that *E. coli* cells after contact with Ag- TiO_2 nanocomposite was damaged showing membrane disorganization. This causes the enhanced level of membrane permeability leading to buildup of Ag- TiO_2

nanocomposite in the bacterial membrane and also cellular internalization of these nanoparticles.

Based on the experimental results, it is proposed that the sharp character of the nanocomposite, along with their oxidative power as well as the electrostatic attraction between the nanocomposite and the biological material are main reasons for the high biocidal activities.

Introduction

This chapter describes a brief introduction to nanotechnology, titanium dioxide (TiO_2), TiO_2 nanocomposite and their applications, which are further explained in the next chapters.

1.1 Nanotechnology

The word nanotechnology is the sum up of two words Nano and technology, Nano is derived from a Greek word “Nanos” which means “Dwarf”. The metric unit of length is a Nanometer (nm), therefore one nanometer means one billionth (10^{-9}) of a meter and written as 1 nm. If we compare the size of nanometer to meter it is the same as the marble to earth (Kahn, Jennifer 2006; Berger M. 2006). The technology is the knowledge and use of systems, techniques, or the organizational methods. The concept of the nanotechnology was given by physicist Richard Feynman. In 1959 his famous talk “There is Plenty of Room at the Bottom” he depicted a process by which the ability is developed to manipulate individual atoms and molecules (Wikipedia). In 1974 Professor Norio Taniguchi (Taniguchi 1974 Tokyo Science university, Japan) also delineated the term nanotechnology as “the process of deformation, consolidation and separation, of materials by one atom or by one molecule”.

The elementary concept of nanotechnology was studied by Dr K Eric Drexler in 1980, which elevated the nanoscale phenomena and devices by various talk and books (Eric Drexler 1991). This is how the term nanotechnology acquired its current sense which is proposed by US National Nanotechnology Initiative (NNI, 2008). NNI defines the nanotechnology as “exploration and growth at the scale of nanometer

range and comprehend the phenomena at this miniature scale to develop new novel applications” (NNI, 2008).

When particles become very small (in the nano range) there are more atoms on the surface than inside the particle, and atoms on the surface may have different properties than those inside the particle (European Commission (EC). 2004). A small word NANO has indeed changed noticeably every facet of the way we think in science and technology (M. Ratner 2003).

1.2 Nanomaterials

A nanoscale material is any solid material that has a nanometer dimension; such as three dimensions (particles); two dimensions (thin films) or one dimension (thin wire) and have morphological features on nanoscale (Cristina et al. 2007; Rodgers 2006). Nanomaterials attracted extraordinary consideration and interest in the last few years from all around the world since the materials at nano scale show special properties as compared to their bulk part because of the larger surface area at the nanoscale (Ratner et al. 2003). Nanomaterials can be classified according to various approaches which are described as follows (Table 1.1)

Table 1.1 Classifications of Nanomaterials

In relation to Dimensions	
3 dimensional < 100nm	Particles, hollow spheres, quantum dots
2 dimensional < 100nm	Platelets, fibers, Tubes, wires,
1 dimension < 100nm	Coatings, Multilayer, Films etc.
According to Phase Composition	
Single phase solids	Amorphous and crystalline particles, and layers
Multi phase solids	Matrix composites, coated particles, etc.
Multi phase systems	Colloids, Ferro Fluids, aerogels
According to Manufacturing Process	
Liquid phase reaction	Sol-gel, hydrothermal processing, precipitation,
Gas phase reaction	Condensation, CVD, Flame synthesis, etc.
Mechanical procedures	Plastic deformation, Ball milling, etc.

Currently most nanomaterials are organized into following four types:

The class of carbon allotropes in which graphene sheets are rolled into spheres or tubes i.e. carbon or silicon nanotubes. Due to their electrical properties and mechanical strength both carbon and silicon nanotubes are of equal interest.

The metal based nanomaterials include metal oxides including nano silver, quantum dots, nano gold, titanium dioxide, zinc oxide. A quantum dot is semiconductor crystal which is closely packed and consists of thousands of atoms. The size of the quantum dot ranges from a few to hundred thousands nanometers.

The dendrimers are nanosized branched particles made up of polymers. The surface of a dendrimer has various chain ends, which can be tailored to achieve precise chemical functions. This characteristic of a dendrimer could also be valuable for catalysis process and drug delivery applications.

Composites are the combination of one type of nanoparticles with another type or with different bulk materials. The composites are being added to various products from biological applications to auto parts and packaging materials. The addition of composites to these products dramatically improves their antimicrobial, photocatalytic thermal and mechanical properties.

1.3 Nanocomposites

Ajayan et al. (Ajayan et al. 2003) defined the nanocomposite as a solid material in which at least one of the phases have any dimensions less than 100 nanometers or the material having nano scale replicated spaces between the different phases that develop them. Nanocomposite materials formed by oxide or metallic particles which are dispersed in polymer, vitreous matrices, or ceramics have significant applications in areas such as antimicrobial, catalysis, solar cell, UV shielding, electronics and others.

1.4 Titanium Dioxide (TiO₂)

Titanium is the world's fourth most abundant metal and ninth most abundant element. William Gregor, in England, discovered it in 1791 (Carp et al. 2004). TiO₂ is an oxide of titanium which occurs naturally. There are three polymorphs of TiO₂ named as Anatase, Brookite and Rutile. TiO₂ is a white powder which is non toxic. Because of its brightness, opacity and high refractive index it is most widely used white pigment in coatings, plastics, toothpaste, paper, food, cosmetics, sun care products, food colouring and medicines (pills ,tablets) (www. wikipedia.com). TiO₂ is an inert compound which has a great potential to create chemical and biological hybrid nanocomposite which can be used as biotracer and also initiate intracellular processes (Paunesku et al. 2003). TiO₂ nanoparticles are attractive for several applications, such as photocatalysis (Hore et al. 2005), solar cells (Hagfeldt et al. 2004), sensor (Palomares et al. 2004), nano ceramics (Winterer et al. 2002) and for degrading environmental hazardous materials (Schattka et al. 2002; Chen et al. 1997). TiO₂ is widely investigated for its Photocatalytic properties since 1972 (Fujishima et al. 1972). It is extensively studied as photocatalyst since that time (Hoffmann et al. 1995; Zhang et al. 1998; Litter et al. 1996; Ranjit et al. 1999; Wang et al. 2000; Dhananjeyan et al. 2000; Wang CY et al. 2000).

1.5 TiO₂ Photocatalysis

Photocatalysis is a term that entails photon assisted production of catalytically active species. In photocatalysis, light energy greater than the band gap of the semiconductor such as TiO₂, excites an electron from the valence to the conduction band (figure 1.3).

Honda and Fujishima extensively use TiO₂ in photocatalysis since the demonstration for photoelectrolysis of water using a TiO₂ electrode under an anodic

bias potential (Fujishima et al. 1972). Since then, photocatalysis, through the use of semiconductor powders, has drawn much attention for its potential in the conversion of light energy into chemical energy. Intensive research has been created a wide range of efficient semiconductor-based photocatalytic materials (Milliset al. 1997; Linsebigler et al. 1995; Fujishima et al. 2000). Several simple oxide and sulfide semiconductors have band gap energies adequate for supporting a broad variety of environmentally concerned chemical reactions (Hoffmann et al. 1995; Grätzel 2001). Among the semiconductors including TiO_2 , SrTiO_3 , $\alpha\text{-Fe}_2\text{O}_3$, ZnO , ZnS (Hoffmann et al. 1995; Grätzel 2001), TiO_2 has demonstrated to be the most appropriate for extensive environmental applications, since it is biologically and chemically stable; it is also inert with respect to photo and chemical corrosion; and it is economical (Xiaobo Chen et al. 2005; Clemens et al. 2005). TiO_2 as a robust photocatalyst has been applied in a range of environmental significance in addition to air and water purification, destruction of microorganisms (Xiaobo Chen et al. 2005; Clemens Burda et al. 2005) inactivation of cancer cells (Xiaobo Chen et al. 2004; Xiaobo et al. 2005) photo splitting of water to produce hydrogen gas (Xiaobo Chen et al 2004) and for the clean up of oil spills (Yongbing et al. 2003; Clemens et al. 2003).

1.6 Synthesis of Titania Nanoparticles

Titanium dioxide (TiO_2) is found in nature as an oxide of Ti. TiO_2 does not exist as a refined structure and therefore frequently fabricate from its leucocene / ilmenite ores. Amongst the different structures of Ti the brookite, anatase, rutile and TiO_2 are the most prevalent structures. Since titania are widely used in the biochemical and chemical industries due to its adaptable nature and various characteristics, therefore the synthesis of the titania is always of a great interest.

platinum or palladium. More accurately, as given in the international noble metal market, the price of silver is only about 1/66, 1/81 and 1/17 of that of gold, platinum and palladium (<http://www.thebulliondesk.com/>) respectively. Silver has an electron accepting region at an energy level just below the conduction band. Hence, subsequent to charge separation and absorption of light, the electron in the conduction band can efficiently be trapped by silver, whereas the hole oxidises H₂O and forms OH[•] radicals, which are devoid of the recombination menace (Kuo et al. 2007). Seery et al. previously showed enhanced visible light photocatalysis with Ag modified TiO₂ (Seery et al. 2007). Ag-TiO₂ nanocomposites used for organic reactions were well documented, including the hydrogenation of aromatic nitro compounds (Cheng et al. 2006; Sweatlock et al. 2005). In addition to serving as heterogeneous catalysts, Ag-TiO₂ nanocomposite has also been utilized as powerful antibacterial agents. The much lower cost of silver than other noble metals and the active performances of nanosized silver in various applications as indicated in the recent literature point out the possibility and significance of developing highly active Ag-TiO₂ nanocomposites.

1.8 Photocatalytic Disinfection of Biological Contaminants and Organic Pollutants

Since the 1980s, antimicrobial treatment has become a prevalent and widely accepted remediation strategy to control harmful organisms (Sommer et al. 1997). Photocatalytic technology of TiO₂ is a striking approach for controlling environmental pollutants. The bactericidal effect of TiO₂ nanoparticles results from inactivating the viability and the destruction of the microorganisms. This feature renders TiO₂ photocatalysts to be applicable to environmental protections (Sunada, Kikuchi et al. 1998). The findings indicate TiO₂ can act as an antibacterial and antiviral agent (Schwietert, Yaghoubi et al. 2001). The antibacterial effect of Ag-TiO₂ on oral

bacteria was evaluated by Yoshinari et al and evaluated that surface modification by means of TiO_2 is useful in providing antibacterial activity of oral bacteria (Yoshinari, Oda et al. 2001). Ag^+ at lower concentration is a potent antibacterial against a wide range of bacteria (Kawashita et al. 2000). Results achieved proved that Ag-TiO_2 nanocomposite is more efficient for antibacterial applications than pure TiO_2 (Sweatlock et al. 2005).

1.9 Objectives of Study

Current study is designed to

- Synthesize TiO_2 nanomaterials by sol-gel method and to study the complete morphology and crystallization behaviour of TiO_2 nanomaterials.
- Synthesize Ag-TiO_2 nanocomposite material and to elicit influence of pH on the synthesis of dispersed Ag-TiO_2 nanocomposite
- Use state of art instruments like Field Emission Gun-Scanning Electron Microscopes (FEGSEM), Transmission Electron Microscope (TEM), and X-ray Diffraction (XRD) etc. for the characterization of nanomaterials.
- Ascertain the antimicrobial activity of Ag-TiO_2 nanocomposite against gram positive bacteria.
- Investigated the contact between the bacteria and as synthesized Ag-TiO_2 nanoparticles exploiting the transmission electron microscopy
- Produce a written report (thesis) and publications summarising findings with recommendations for future work in this area.

1.10 Outline of the Thesis

The outline of the thesis is as follows:

Chapter 1 In the first chapter there is a concise background information and introduction of the basics of nanotechnology, nanomaterials and nanocomposite leading to the research objectives.

Chapter 2 highlights a general literature review on TiO_2 and Ag-TiO_2 nanocomposite and also presents an overview of the antimicrobial and photocatalytic mechanisms. It also recapitulates various synthesis techniques generally, and focuses on sol-gel synthesis by giving step-by-step description of the sol gel process.

Chapter 3 contains materials and experimental set up employed for the synthesis of TiO_2 and Ag-TiO_2 nanocomposite. All characterization techniques used are also presented.

Chapter 4 contains the detailed characterization of TiO_2 and Ag-TiO_2 nanocomposite with emphasis on the effects of pH on the synthesis of Ag-TiO_2 nanocomposite materials.

Chapter 5 reports the antibacterial functions of the Ag-TiO_2 nanocomposite and the basis of the superior performances of synthesized Ag-TiO_2 nanocomposite to the reported counterparts (TiO_2) are discussed in the context of the recent literature. Moreover, the bacterial interaction with Ag-TiO_2 nanocomposite using transmission electron microscope is also described in detail.

Chapter 6 includes the contributions of this thesis work to knowledge and suggestions to the future work.

1.10 Benefits of study

Current study got loads of data, which is of much importance for the bactericidal use of Ag-TiO₂ for cosmetics and other industries working in antibacterial sector. Moreover the subject of the study is of critical importance to the regulatory and safety decision makers and implementers. These findings will provide a bridge to decision making among regulatory authorities in their endeavours to make new regulations for nanomaterials in end user products. The data produced during this study is a base line for the use of Ag-TiO₂ in future remediation technologies.

1.11 Future prospects

This research gives an understanding of the Ag-TiO₂ nanocomposites along with effect of pH on morphology and behaviour of nanomaterials. This is a road mark towards in depth research for the pH characteristics of nanomaterials and their effects on different biocidal and photocatalytic techniques.

Literature Review

In this chapter a literature review of Nanotechnology, Nanoparticles synthesis and applications in general would be described with specific and detailed emphasis on TiO₂, Ag-TiO₂ nanocomposite and their antimicrobial activities against gram positive and gram-negative microorganisms.

The main focus of this research centres on the Photocatalytic abilities of TiO₂, i.e. when light of energy larger than the band gap excites an electron from the valence band to the conduction band, hydroxyl radicals are formed that will oxidise organic materials to H₂O and CO₂. Simple as this process appears, there are many factors, which influence the efficiency of the photocatalytic materials. Many of which are investigated throughout this thesis.

2.1 Nanotechnology

Nanotechnology deals with processes that take place in the range of nanometer scale, i.e. from approximately 1 to 100 nm. At this scale the materials possess unique properties (Klabunde 2001). Nanotechnology is an interdisciplinary science including physics, materials, chemistry, engineering and biology (Rao e al. 2004; Rao et al.2006). It is very crucial to have an interaction between different disciplines of science that lead to the new discoveries. Since the Industrial Revolution, Nanotechnology has been considered “the biggest engineering innovation” (Gwinn et al.2006).

2.1.1 Nanomaterials

According to size the matter can be categorised broadly. We can observe the macroscopic matter with the naked eye. Atoms and molecules are microscopic which

have a dimension less than 1nm. Cells and Bacteria are Mesoscopic particles, which have dimensions in the order of micron(s), and can be observed with the help of optical microscopes (Drexler 1991). There is another class of matter that lies in the gap between macroscopic and mesoscopic matters, which is called nanoscopic particles. The nanoparticle can be compared to the other small objects with respect to size as shown in fig 2.1.

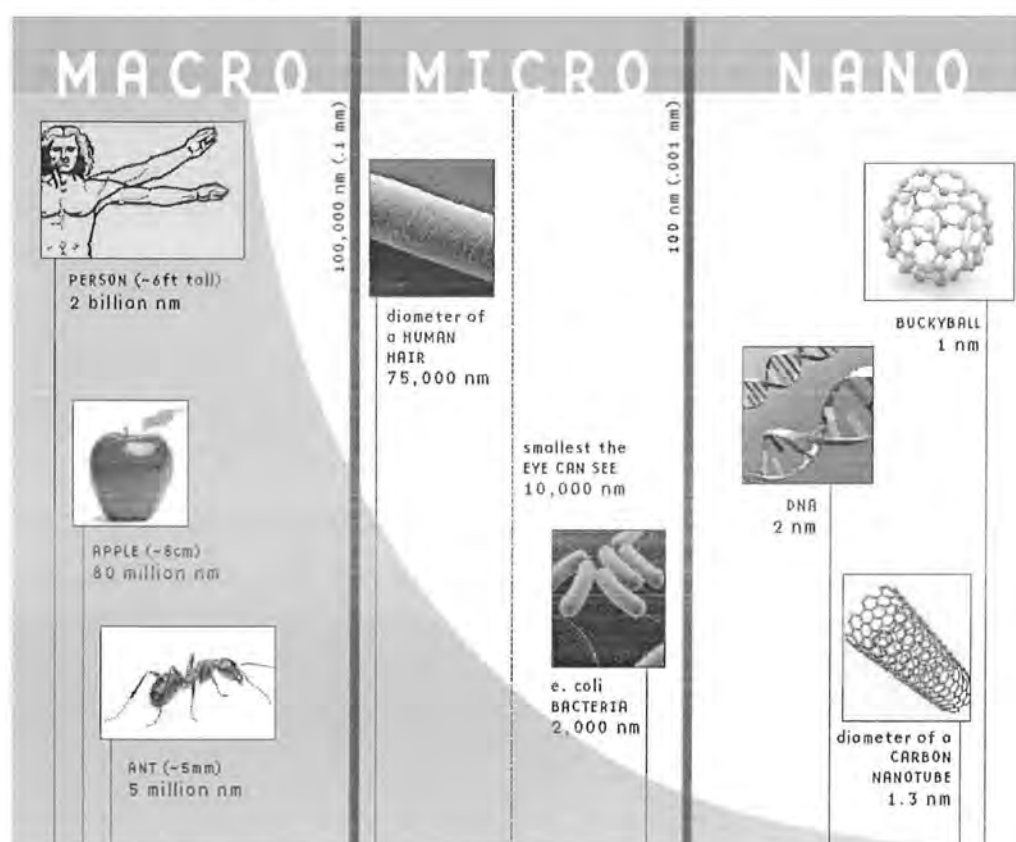


Fig.2.1 The Size of Nanomaterials In Comparison To Other structures On The Length Scale

2.1.2 Nanoparticle

A nanoparticle is defined as a particle, which has all the dimensions in nano scale. Aitken et al. described that nanomaterials may be produced from the assembly of atoms or molecules or by the reduction of the bulk materials to nano scale (Aitken et al .2004). According to Thomas and Syre, 2005 the structures at nano scale exhibit

unique electrical, optical, chemical and mechanical properties, which differ from their bulk counterpart (Thomas and Syre, 2005).

2.1.3 Comparison With Biological Materials

Due to the characteristic size scale, the nanomaterials lie in between atoms and bulk materials as illustrated in Fig 2.1 with biological examples. If we compare the nanoparticles to the living cells then nanoparticles are much smaller than a living cell, which are 10-20 μm in size. The basic unit of nature is an atom, which has a typical size of an angstrom: 10^{-10} m, which is 1/10 of a nanometre (radius of the hydrogen atom). Smallest nanoparticles, like fullerenes, contain about a 100 atoms (Klabunde, 2001).

The closest analogy can possibly be drawn between nanoparticles and large organic molecules, such as proteins. Some proteins reach tens of nanometres in size e.g. molecular motors responsible for DNA transcription, cargo movement in cells etc. (Rao CN et al. 2004). However, mechanisms of action and properties of nanoparticles and complex organic molecules are very different. The matter at the nano scale influence physical and chemical properties of matter to a large extent. It is because of the increased fraction of the surface atoms, which result in the increased catalytic activity and decrease stability, melting and boiling point (Roduner E 2006).

2.2 Titanium Dioxide (TiO_2)

In the periodic table titanium belongs to group IV transition metal with an atomic number 22. It is the 9th most abundant metal in the earth's crust and comprises 0.6% by mass (Zumdahl and Zumdahl, 2003). In 1791 Reverend William Gregor, who reported its occurrence as a novel element in ilmenite, discovered Titanium in

England. After several years it was rediscovered in rutile ore by a German chemist, Heinrich Klaporth.

TiO₂ does not lie in pure form in the nature but found in the mineral form as an oxide like rutile, anatase, brookite and ilmenite (FeTiO₃) (Carp, Huisman and Reller, 2004). TiO₂ is the most broadly studied semiconductor because of its wide applications including biomaterials, ceramics, paints, industries, gas sensors, electronic devices, heterogeneous catalysis, coatings, photocatalysis and solar cell applications (Diebold U 2003). TiO₂ is broadly used as a white pigment. The annual consumption of raw TiO₂ mineral is about one billion metric tons out of which 97% are being used in the pigment industry. The application of TiO₂ as a photo catalyst is increased greatly in the last decade because it is low cost, non-toxic and chemically stable compound. There are three main polymorphs of TiO₂ brookite, anatase. Each of these forms has their own unique optical and structural attributes. All polymorphs of TiO₂ have been studied for their photochemical and photocatalytic characteristics. Rutile ore is the primary source of TiO₂ and is discovered in 1803 in Spain by Werner. Until recently rutile is the most extensively studied while the brookite is not a well studied polymorph of the TiO₂. Anatase and brookite are more stable at lower temperatures but both will be transformed to rutile on high temperatures (M. Howard 1999).

2.2.1 Crystallographic Structure of TiO₂

TiO₂ have three polymorph structures: rutile, anatase and brookite. In polymorphs, titanium (Ti⁴⁺) atoms are co-ordinated to six oxygen (O²⁻) atoms, forming TiO₆ octahedra (S. Mo 1995). Rutile, Anatase and Brookite differ only in the arrangement of these octahedra. The structure of anatase is made up of corner (vertice) sharing octahedral (figure 2.2a) resulting in a tetragonal structure (S.D.Mo

and W. Y. Ching, 1995) while in rutile the octahedra share edges to give a tetragonal structure (figure 2.2b) (R. Asahi et al. 2000; W.Luo et al. 2005) and in brookite both edges and corners are shared to give an orthorhombic structure (figure 2.2c) (S. Mo 1995; Feng et al. 2001).

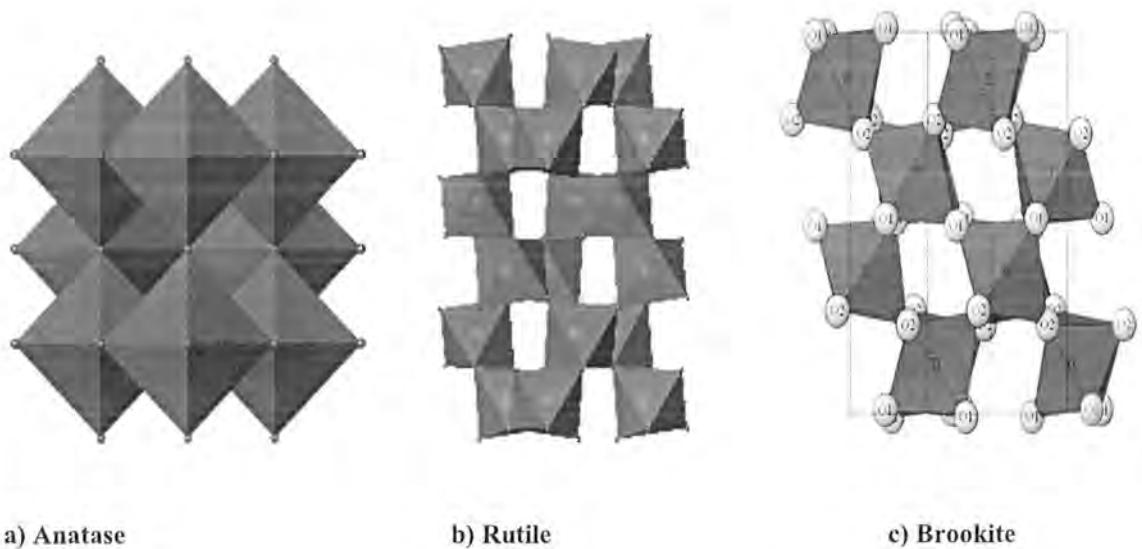


Fig. 2.2 Crystallographic Structure of TiO_2

There are three well known polymorphs of TiO_2 are rutile, anatase both having tetragonal crystal structure, and brookite having rhombohedral crystal system (Nie XL et al. 2009). These three polymorphs can exist as bulk materials and as nanomaterials. Each titanium ion is at the centre of an oxygen octahedron in all of these three structures. The oxygen ions form a slightly distorted hexagonal compact lattice in rutile while in anatase, the oxygen form a CFC lattice (S.D.Mo and W Y Ching, 1995). Each oxygen has three coplanar near neighbour titanium cations in both rutile and anatase structures. In rutile, the three $\text{Ti}-\text{O}-\text{Ti}$ angles are roughly equals to 120° but one of angles in anatase is about 180° while the other two are close to 90° . The structures of TiO_2 (Figure 2.2) and the physical properties are shown in Table 2.1 (D. Reyes-Coronado et al. 2008). Rutile and brookite are structurally similar as

polyhedron chains form as both are linked by three unlike corners of the unit cell except in brookite the polyhedron bridge are joined from end to end the cis bridges and its unit cells dimensions are unequal (J. K. Burdett et al.1987). As Brookite has an orthorhombic crystal system and space group Pbc_a, Therefore, the brookite structure is of lower symmetry as compare to the other polymorphs of TiO₂ (M. Howard et al. 1999). Furthermore, the Ti-O bond lengths and O-Ti-O bond angles also varie (S. Mo 1995). (Table 2.1 shows various properties of Physical and structural properties of TiO₂ polymorphs).

Table 2.1 Different properties of TiO₂ polymorphs

Characteristics	Rutile	Anatase	Brookite
Formula Wt. (g/mol)	79.890	79.890	79.890
Crystal system	Tet	Tet	Ortho
Molar Volume	18.693	20.156	19.377
Density (g/cm ³)	4.2743	3.895	4.123
Melting Point (°C)	1825	1825	1825
Specif gravity	4.0	3.9	4.12
Light Absorption(nm)	< 415	< 390	
Refractive index	2.75	2.55	
Lattice constants (Unit Cell)(Å)	a = 4.59 c = 2.96	a = 3.78 c = 9.52	a = 9.184 c = 5.145
Ti-O bond length (Å)	1.95 (4) 1.98 (2)	1.94 (4) 1.97 (2)	

There are very minute differences in the optical properties of each phase and the absorption band gap for the rutile, anatase, and brookite phases were calculated to be 1.78eV, 2.04eV, and 2.20eV, respectively (H. Tang et al. 1994). Hence all the

polymorphs of titanium dioxide are used for different purposes. Such as, the rutile phase owing to its high refractive index is generally used in sun block lotions, plastics, leather, paper, high-grade corrosion-protective white coatings and paint (J. S. Olsen et al. 1999). Due to the electronic structure, the anatase phase has exceptional optical and pigment properties and is used as an optical coating and photocatalyst (R. Asahi et al. 2000). The brookite phase is rare and difficult to synthesize therefore is of limited use (W.Luo et al. 2005). The brookite phase is similar to rutile in general chemistry and physical properties Hence researchers are searching for the ways to synthesize high purity brookite phase of TiO_2 as it is being explored in the recent literature that there it may possess photocatalytic properties but there is still a need to research in depth (R. Buonsanti et al. 2008). It is evident that titanium dioxide industry irrespective of both phases is growing very fast. Various researchers demonstrated that the preparation method (Wilska 1954), concentration of dopant (MacKenzie 1975; Banfield and Bischoff 1993), atmosphere (Gamboa and Pasquevich 1992) and particle size (Kumar 1995; Gribb and Banfield 1997) can influence the anatase to rutile phase transformation.

2.3 Synthesis Techniques

The choice of synthesis technique can be a significant aspect in determining the effectiveness of the photocatalyst as studies have shown that TiO_2 particle size and physical forms are among the most important factors in determining the overall Photocatalytic efficiency (Frank S. N et al. 1977; Keshmiri et al. 2006; Walker et al. 1995). There are many methods of synthesizing titanium dioxide, such as hydrothermal (Cheng et al. 1995) combustion synthesis, gas-phase methods, microwave synthesis and sol-gel processing (Keshmiri et al. 2006). This research

focuses on sol-gel processing techniques, which will be discussed in detail, however, an overview of other much used techniques is also provided.

2.3.1 Hydrothermal synthesis

Hydrothermal synthesis is typically carried out in a pressurised vessel called an autoclave with the reaction in aqueous solution (Chen X 2007). The temperature in the autoclave can be raised higher than the boiling point of H₂O, getting the pressure of vapour saturation. Hydrothermal synthesis is broadly used for the preparation of TiO₂ nanoparticles, which can easily be obtained through hydrothermal treatment of peptised precipitates of a titanium precursor with water (K.Tomita et al. 2008; Chen X 2007). The hydrothermal method can be helpful to control particle structure, crystalline phase, grain size, and surface chemistry through regulation of temperature, solvent properties, the solution composition, reaction, aging time, additives and pressure (M.Hirano et al. 2004; Carp O 2004).

2.3.2 Combustion

Combustion synthesis leads to highly crystalline particles with large surface areas (Y Kitamura et al. 2007; Nagaveni et al. 2004). This process entails a fast heating of a solution upto 650 °C for a very diminutive time of one to two minutes which makes the material crystalline and also inhibit the transition from anatase to rutile because of very short span of time. (Litter et al. 1996; K Nagaveni et al. 2004).

2.3.3 Gas Phase Methods

Gas phase processes are ideal for the fabrication of thin films. Gas phase can be carried out chemically or physically (MK Akhtar et al. 1994). Chemical vapour deposition (CVD) is an extensively utilised industrial practice that can coat larger

surfaces in a very small time (VG Bessergenev et al, 2002). During the procedure, titanium dioxide (TiO_2) is synthesized via precursor chemical reaction in the gas phase (Jones et al. 2003; Wang et al. 2005; Choy K L 2003). There is an additional thin film deposition method called Physical vapour deposition (PVD), in which gas phase is used to synthesize film, however, there is no chemical conversion from precursor to product is involved. Electron Beam evaporation (E-beam) is also used to form the titanium dioxide thin films by using a fixed beam of electrons produced from the heated tungsten wire. Titanium dioxide films deposited with E-beam evaporation are much better and finer quality in terms of conductivity, crystallinity and smoothness as compare to CVD grown films (VG Bessergenev et al. 2002). To focus the electron beam with required conductance, the TiO_2 powder should be heated in a hydrogen atmosphere at at 900 °C (Van de Krol 1997).

2.3.4 Microwave Synthesis

Various TiO_2 materials have been synthesised using microwave radiation. Microwave techniques eliminate the use of high temperature calcination for extended periods of time and allow for fast, reproducible fabrication of crystalline TiO_2 nanomaterials. Corradi et al. prepared colloidal TiO_2 nanoparticle suspensions within 5 minutes using microwave radiation (Corradi et al. 2005). High quality rutile rods were developed combining hydrothermal and microwave synthesis, 157 while TiO_2 hollow, open ended nanotubes were synthesised through reacting anatase and rutile crystals in NaOH solution. (Wu, X.et al. 2005)

2.4 Sol-Gel Processing

In this dissertation, the sol-gel approach is addressed with a specific reference to titanium dioxide nanomaterials. The combination of various types of materials is

used to achieve unique characteristics of the materials as in their basic forms the materials do not reveal the properties required for the special applications. These unique properties obtained after the combination of the materials is of great interest in the technology. The combination between organic and inorganic polymeric materials on nanometer scale depends on methods for synthesizing inorganic polymeric networks appropriate to thermal stability of organic materials. The sol-gel process has been demonstrated a proper tool for building up inorganic network with incorporated organic components (H. Schmidt 1989). So-gel method contains the evolution of a system from a liquid (the colloidal "sol") into a solid (the "gel") phase.

Hydrolysis:



Water Condensation:



Alcohol condensation:



(Where M = Ti, Si, Zr,)

It allows the synthesis of materials with a great array of characteristics: monolithic ceramics (R. J. P. Corriu 1992; Y. Lirong 1988), ultra-fine powders (C. Barbe et al. 2004; X. H. Liu et al. 2000; Y. C.-D. Kobayashi et al. 2001) and glasses, ceramic fibers (Y. Hu et al. 2000; A. Karout et al. 2005) inorganic membranes (C. G. Guizard et al. 1999; C. Guizard et al. 1994) thin film coatings (P. Etienne et al. 1996; N. Carmona 2006) and aerogels. Initially from molecular precursors, an oxide network is obtained through inorganic polymerization reactions which take place in solutions. The term "sol-gel processing" is generally used to illustrate inorganic fabrication of

materials and proposes numerous advantages as compared to the conventional powder route (J. Livage et al. 1989; J. Y. Wen et al. 1996; L. L. Hench et al. 1990).

2.4.1 History of Sol-Gel

The sol-gel method has developed into a wide and increasing research area day by day. In early and mid 1800s, Ebelman and Graham's research on silica gels evoke the interest in the sol gel processing of the glass materials and inorganic ceramics. These early investigators observed that the hydrolysis of tetra ethyl ortho silicate (TEOS) under acidic conditions produced SiO_2 in the form of a "glass-like material". However, exceedingly long drying times of 1 year or more were necessary to avoid the silica gels fracturing into a fine powder, and consequently there was little technological interest. After some experiments, in the 1950s and 1960s, Roy and co-workers documented the potential for achieving very high levels of chemical homogeneity in colloidal gels and synthesized a wide range of novel ceramic composition including Zr, Al, Ti by using the sol gel method which could not be synthesized using the conventional powder methods. After this investigation, especially at the producing ceramic powder enormous and very important proceedings were achieved by chemists (L. L. Hench et al. 1990).

2.4.2 Mechanism Of Sol-Gel Synthesis

The past two decades have shown an increasing interest in the development of Organic/inorganic materials prepared by the sol-gel process (Perrin, F. X et al. 2003; Sanchez et al. 1994 ; Sanchez C et al. 1999; Schubert H et al, 1995; Wen J et al. 1996; Ershad-Langroudi et al.1997). The sol-gel process entails hydrolysis and condensation of the metal alkoxides followed by heat treatment at elevated

temperatures which induce polymerisation, producing a metal oxide network (Barboux-Doeuff et al. 1994).

2.4.2.1 Hydrolysis

The sol-gel reaction involves hydrolysis of the metal alkoxides followed by condensation. Hydrolysis of titanium alkoxides occurs through a nucleophilic substitution (SN) reaction. When a nucleophile, such as water is introduced to titanium alkoxides a rapid exothermic reaction proceeds. The nucleophilic addition (AN) of water involves a proton from the attacking nucleophile (water) being transferred to the alkoxides group. The protonated species is then removed as either alcohol or water (scheme 2.1) (Brinker C. J et al. 1990).



Scheme 2.1 Hydrolysis reaction

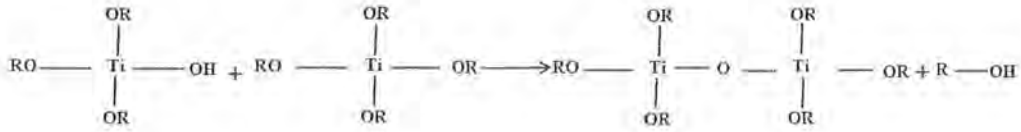
The nucleophilic substitution reaction that occurs during hydrolysis can be described as follows

- Nucleophilic addition of the H₂O onto the +vely charged metal atoms.
- Proton transfer, within the transition state from the entering molecule to the leaving alkoxy group (Sanchez C et al. 1988).

2.4.2.2 Condensation

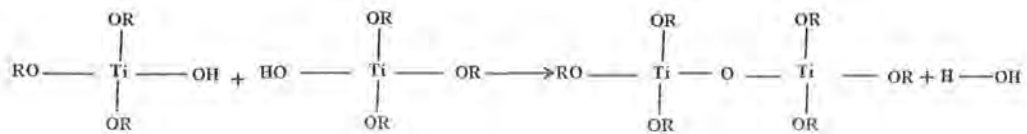
Condensation reactions complete the sol-gel process. Condensation can proceed through either alcoxolation or through oxolation. In both processes an oxo bridge is formed between the metals (M–O–M) but the leaving group differs. During

alcoxolation, two partially hydrolysed metal alkoxides molecules combine and an oxo bridge is formed between the two metals with alcohol departing as the leaving group (scheme 2.2) (Sanchez C 1988; Brinker C J 1990).



Scheme 2.2 Alcoxolation reaction

In oxolation (scheme 2.3) two partially hydrolysed metal alkides combine to form an oxo bridge between the metal centres but water is the leaving group.



Scheme 2.3 Oxolation reaction

Condensation reactions can proceed to form large chains of molecules through polymerisation. The electrophilicity of the metal, the strength of the entering nucleophile and the stability of the leaving group all have an influence over the thermodynamics of the hydrolysis and condensation reactions (Sanderson R T Science 1951; Sanchez et al. 1988; Livage J et al. 1988).

2.4.3 Parameters Affecting Sol-Gel Process

Various parameters are essential to attain a desirable profile of TiO₂. The important parameters include crystalline size, pH, temperature and the choice of appropriate proportions of supplied reagents (TiCl₄, He and O₂) in the inlet gas mixture (Paul et al. 2007).

2.4.3.1 Effect of crystalline size

The control of grain size is also crucial along with controlling the content of a phase. Garvie studied the phase transformations (Garvie 1978) and observed grain size effect on the comparative stability of the monoclinic and tetragonal phases in the ZrO_2 system. Size and shape highly influence the chemical and physical properties of metal nanoparticles (Muller et al. 2004; Brown et al. 2001). The TiO_2 nano scale thin films showed size dependent photo degradation of methylene blue (MB) solution (Chung et al. 2007; Doong et al. 2007) and Chen and co workers studied that the reaction constant is directly proportional to the diameter of particles (Chen et al. 2004). They evaluated the influence of the particle size on the photocatalysis. Testino and his group (2007) suggested correlation between particle morphology and photocatalytic activity is suggested by Testino et al. (2007) and they exhibited that both adsorption at the surface and electron hole recombination can be rate-controlling processes. Thus, both grain sizes and phase content are significant features of TiO_2 nano powders.

2.4.3.2 Effect of temperature on TiO_2

Various calcination temperatures and drying methods of nano-sized TiO_2 have potent effect on energy band structure, optical adsorption property, crystal structure, photocatalytic activity and surface quality and (Ye et al. 2002; Su et al. 2001). Gervais and co-workers (2001) studied that TiO_2 particles heated below $700^\circ C$ are predominantly anatase and above $700^\circ C$ conversion to rutile increases with increasing calcination temperature while in another study Ani and co-workers (2005) described the influence of molar ratio of $H_2O/TiCl_4$ temperature and concentration of precursors on particle size and phase composition. They evaluated that water vapour has a

catalytic role in the enhancement of amorphous to anatase phase transformation at high molar ratio of $\text{H}_2\text{O}/\text{TiCl}_4$ at low drying temperature. Grzmil and co workers (2004) studied that the ratio of anatase-rutile transformation was higher at elevated temperatures and noticed that the process temperature affects the conversion ratio considerably more than the calcination time. The extent of the initial fast hole transfer reaction is correlated with the calcinations temperature (Salmi et al. 2004). Martyanov et al. (2004) observed that annealing at 500°C results in the structure of the anatase phase for TiO_2 on SiO_2 and TiO_2 in the powder form.

2.4.3.3 Effect of pH on TiO_2

Isley and Penn (2006) observed that in sol gel synthesis of TiO_2 at pH3, the addition of HCl resulted in increased amorphous content compared to samples synthesized using HNO_3 . Hu and co-workers (2003) also showed the same results and described that the in the brookite phase volume percentage increases with the decrease of the synthesized pH value and anatase to rutile conversion occurs owing to the presence of Brookite phase. Velikovska and Mikulasek (2007) studied microfiltration of TiO_2 dispersion by changing the surface properties of both the alumina membrane and TiO_2 particles and revealed the effect of pH on TiO_2 dispersion. The acidity has detrimental effect on the crystal structure formation and phase transformation (Luo 2003). In 2005 Zhu et al. (2005) noticed that, the titanate nanofibers transform to anatase and rutile nanoparticles in acidic aqueous titania dispersions via various mechanisms. During adsorption process, Triethanolamine exhibited to improve the pH effect on the nucleation speed of anatase TiO_2 particles, resulting in the wide array of the size control. It was also observed that the Triethanolamine plays shape controller of the TiO_2 anatase particles for synthesizing ellipsoidal particles from $\text{Ti}(\text{OH})_4$ gel at a pH greater than 11 (Sugimoto et al. 2003). In 2001, Feng and co-workers (Feng et

al. 2001) investigated that pH has detrimental effect when layered titanate $H_{1.07}Ti_{1.73}O_4 \cdot H_2O$ treated in a $Ba(OH)_2$ solution or distilled water under mild hydrothermal conditions, transforms the layered titanate to $BaTiO_3$ or anatase. According to the findings of Chu and co-workers (2007) the pH is a sensitive parameter to the rate of degradation under UV/ TiO_2/H_2O_2 and UV/ TiO_2 systems. HO^\bullet affects the photoexcitation and ultimately degradation at basic or acidic pH values since the introduction of H_2O_2 an HO^\bullet scavenger, slowdown the decomposition rate at alkaline medium. By aging the $Ti(OH)_4$ gel at temperature $140^\circ C$ for 72 hours, and increasing the pH from 0.6 to 12 the particle size of anatase (TiO_2) increases from 6 to 30 nm. However, the yield of anatase is observed to decrease with the increase of pH above 9.6 and found to be 65% at pH 12.0 and merely 9% at pH 12.5 (Sugimoto et al. 2003). The pH increase also decreases the nucleation rate of the TiO_2 anatase, as is described by the reduction of the precursor complex concentration, $Ti(OH)^{+3}$ and the adsorption of OH^- onto TiO_2 (Sugimoto et al. 2003). The pH also effects the phase transformation of TiO_2 as the starting and ending temperature of the anatase to rutile transformation increases as the pH increases whereas the brookite phase decreases with the increased pH (Hu et al. 2003). Acidic pH showed a denser film growth, higher refractive index, and a lower surface roughness of TiO_2 multilayer films than the films deposited in different conditions (Kim et al. 2006).

2.4.4 Advantages of Sol-Gel Process

Sol gel has many advantages over the other method of TiO_2 nanoparticles synthesis. In 1999 Wang described sol gel method for its better Better homogeneity from the raw materials used (Wang 1999). Pope and Mackenzie illustrated this process for its better purity from the raw materials and also employed sol gel process to save energy and minimize Lower temperature of preparation and evaporation

losses. It also minimize air pollution (Pope and Mackenzie 1988). Sol Gel process evade reaction with container to ensure purity and by pass phase separation and crystallization (Tillotson, Gash et al. 2001). Special properties of sol gel determines the new crystalline phases from non crystalline solid (Chen and He). The sol gel process also shows the potential to synthesize solids with fixed structure by altering the experimental conditions (Jeon Yi et al. 2003). Nevertheless, sol-gel process has lots of advantages over the conventional methods. Prospective advantage of the sol-gel process can be summarized as follows:

- sol-gel process offers a convenient mode to purify precursors;
- It has a potential to get homogenous distributions of precursors;
- It presents a simple method to initiate trace elements;
- It authorises to employ the chemistry to manage reactions;
- It also permits the development of a pre-inorganic system in solution;
- Sol-gel process permits the modification of appropriate viscosities for coatings;
- It also offers the synthesis of new glass compositions;
- It also allocates the densification to organic solids at moderately decreased temperatures;
- It helps in the synthesis of active ceramic powders (J. Livage and J. Lemerle, 1982). And, Sol-gel process does not allow only for materials to have any

composition, but it also permits the production of new hybrid organic-inorganic materials which do not exist naturally (A. C. Pierre 1998).

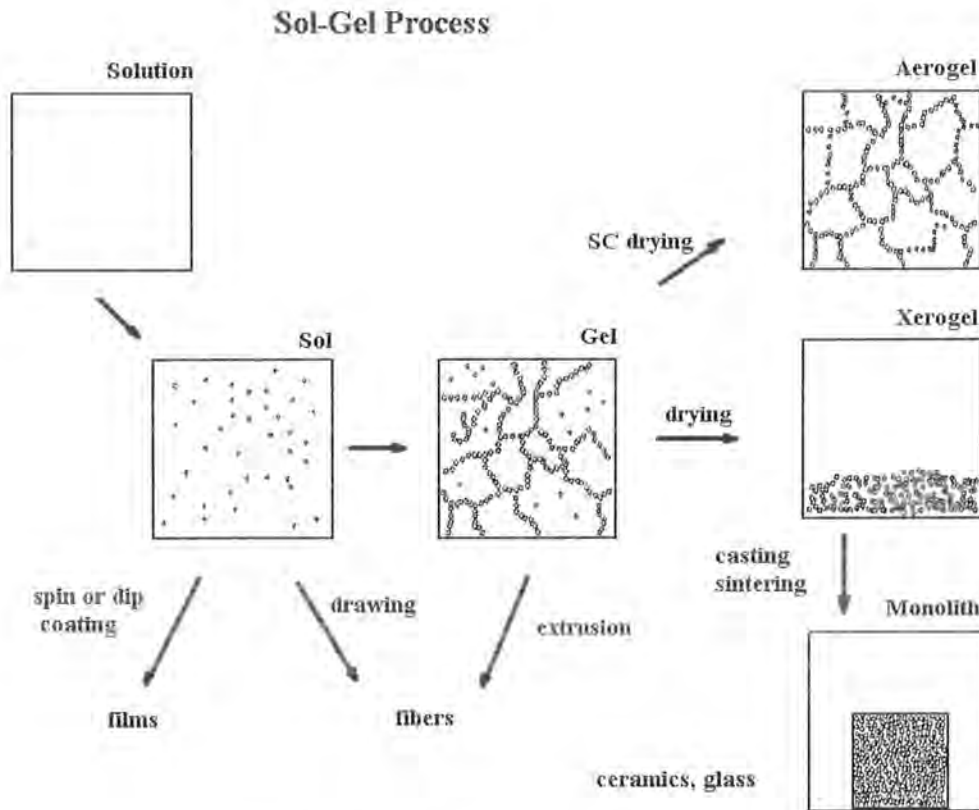


Fig 2.3 Applications of Sol-gel Process

Due to all these reasons the sol-gel process has earned great technological and scientific consideration in the previous decade. Furthermore, sol-gel ceramics structure can be easily controlled as the size of the particles. But the greatest limitation of sol-gel processing for synthesizing ceramic is still the cost of precursors and these are especially alkoxides. Most of these alkoxides are nonetheless quite easy to make; especially if they do not tend to polymerize. A few of them such as Zr and Ti are even used industrially for coating applications by the Schott Company (H.

Dislich1983). It is possible to produce countless materials with sol-gel method such as powders, films, monoliths and coatings, nanocomposite/nanoparticles. In this connection, sol-gel method opened new research area as shown in fig 2.3 for improving properties of materials such as in optic (for example; transparent hard coatings, LC displays, colour coatings, reflecting coatings, antireflective coatings, etc), electrical coatings (for example; dielectric, electrochromic, etc.), thermal (for example; thermally resistant coatings, IR reflective glazing, thermally resistant paints, etc.), passivation (for example; passivation of semiconductors, protective coatings on polymer and metals), release/wetting (for example; biomedical applications, slow release of materials/drugs, anti stick coatings, easy-to-clean coatings, anti graffiti coatings, anti fouling coatings, etc.), sensors (for example; pH sensors, gas sensors, fibre sensors, etc), catalyst (aerogel catalyst, catalyst supports, micro filters, controlled pore materials, liquid chromatographic elements, etc.), membranes, filters, selective adsorbents, coloured thin coatings, etc (D. R. Uhlmann et al. 1998; M S W Vong et al. 1997; M. Serwaczak et al. 2006; M. Crisan et al. 2004) .

2.5 Analytical Techniques For Nanomaterials Characterization

Researchers have used various techniques for the characterization of nanomaterials including Scanning Electron Microscope (SEM), X-ray Diffraction (XRD), and Transmission Electron Microscope (TEM). There are various approaches to characterize nanomaterials, which rely on the nature of studies and the characteristics of materials. Here few of the techniques are described in relation to the research work done by different researcher. Cheng and co-workers (2006) characterized and modified nanomaterials by a combination of X-ray photoelectron spectroscopy (XPS), transmission electron microscopy (TEM) , thermo gravimetric analysis (TGA), fourier-transform infrared spectroscopy (FT-IR), and they measured

the thickness of the surface layer by using Auger electron spectroscopy (AES). Bojinova and co-workers (2007) used only X-ray diffraction (XRD) to characterize anatase TiO₂ nanoparticles. In another study Armelao and co-workers (2007) evaluated significant information on nanoparticle distribution, shape and size by the collective use of field emission-scanning electron microscopy (FE-SEM) and glancing incidence X-ray diffraction (GIXRD). Their results exhibited significant dependence of the functional performances on the system's morphological, structural, and compositional characteristics. Ki et al. (2008) synthesized a novel photocatalyst WO₃/TiO₂ nanocomposite by hydrothermal process by using cetyl trimethyl ammonium bromide (CTAB) as surfactant.

The as obtained WO₃/TiO₂ nanocomposite was characterized by X-ray diffraction (XRD), field emission scanning electron microscope (FESEM), transmission electron microscope (TEM), and diffused reflectance spectroscopy (DRS). Byun et al. (2008) characterized ZnO and ZnO-coated TiO₂ nanoparticles by XRD, UV-vis spectrophotometer and HR-TEM whereas X-ray powder diffraction (XRD), transmission electron microscopy (TEM), X-ray photoelectron spectroscopy (XPS), specific surface area (BET), scanning electron microscopy (SEM), Fourier transformed infrared (FT-IR), UV-visible diffuse reflectance spectra (DRS) were used to characterize N-doped TiO₂ microtubes by Xu et al. (2008). Auger electron spectroscopy (AES) along with X-ray diffraction (XRD), field emission scanning electron microscopy (FE-SEM), and water contact angle measurement were used by Chan et al. in 2007 (2007) to characterize Cr-doped TiO₂ thin films. Zhang et al. (2007) characterized the highly ordered TiO₂ nanotube array (HOTDNA) electrodes by SEM microscopy, X-ray diffraction (XRD), and UV-vis spectra (Li et al. 2007). Doong et al. (2007) used Scanning electron microscopy (SEM), X-ray diffraction

(XRD), differential scanning calorimetry (DSC), thermogravimetry (TGA) and specific surface area analyzer to examine properties of highly ordered TiO₂ porous films while Rengaraj et al. (2007) used XRD, Raman spectroscopy, Transmission Electron Microscopy (TEM), Scanning Electron Microscopy (SEM), EDX, EDS, FT-IR, BET and XPS spectroscopy for the characterization of TiO₂ nanocomposite. Overschelde and co workers (2007) examined irradiated thin films by X-ray diffraction, profilometry and scanning electron microscopy and evaluated deposited and irradiated films concluding that the deposited films are amorphous whilst the irradiated films are anatase structure. They also concluded that the crystallinity greatly vary in different films.

Different spectroscopic techniques were used for the characterization of phenyl porphyrin, H₂Pp and their consequent copper (II) complexes by Chen et al. (2007). Oliveira et al. (2003) synthesized Novel titanium-tin mixed oxide (Ti,Sn)O₂ with anatase structure by Raman spectroscopy, X-ray photoelectron spectroscopy (XPS) and transmission electron microscopy (TEM) and concluded that absorption edge of the carbon incorporated titania thin films is directly dependent on the carbon content and shifted from ultraviolet to visible region. In the verification process of the continuation of paramagnetic species such as OH and H₂O radicals on UV-irradiated TiO₂-based photocatalysts, Electron spin resonance (ESR) studies have also been carried out by Kim et al. (2005) and showed that hydroxyl radicals could decompose organic pollutants into nontoxic products due to their elevated oxidizing ability.

2.6 Silver Nanoparticles

It was generally believed that the catalytic activity of silver cannot, in most reaction systems, compete with other noble metals for instance platinum, palladium

and gold (J. G. Yu, 2005). Yet the lower cost of silver than these metals makes the development of novel Ag-based catalysts a very attractive topic. As an example, the deposition of Ag nanoparticles onto semiconductor photocatalysts (such as TiO₂) has been broadly adopted to enhance the photocatalytic activities of such materials (J.X.He et al. 2004; H M S Suh et al. 2004).

Silver is among the extensively used metal in the world as it is a very good conductor due to its enhanced metallic properties. Silver has excellent antimicrobial properties and is being used in various applications and products. At the nano size scale the metal is highly effective and used in technology and medicine. The silver (Ag) nanoparticles are typically ~20nm in diameter, and are currently being exploited in numerous technological applications and also in advance recognition as a form of counter measures against several illnesses that cannot be treated through traditional methods.

Silver nanoparticles have some highly distinguishable properties which make it the most extensively used nanoparticles in the industry (Alt et al. 2004; Son et al. 2004; Morones et al. 2005). One extremely valuable quality is its antimicrobial property. The use of Silver in its pure form dates back to the ancient Greeks where it was used for the sterilization purposes to keep the germs away. Fabricating the Silver metal at nano scale extensively increases its antimicrobial property making it more practical in the elimination of all kinds of microbes including viruses, fungus and bacteria.

Current research has recognized the use of silver nanoparticles in the field of medicine and also improving the medical applications of silver nanoparticles. Research suggested that the use of silver nanoparticles can help to prevail over the infection commencement and also support the more rapid wound healing (Braydich et

al. 2005). There was a considerable antibacterial activity was examined with very low concentrations of the silver nanoparticles (Rao CNR et al. 1992). The silver nanoparticles directly deteriorate the plasma membrane and bacterial enzymes thus inhibiting the growth of bacteria. This leads to a morphological distortion of the bacterial cells, resulting in the escape of cytoplasmic substance to the surroundings and destruction of bacterial metabolism (Morones et al. 2005). Silver Bandages are available over the counter with nanosilver woven into the “wound pad” as an antibacterial agent. For acne prone conditions, Ag-NP, approximately ~10nm in diameter, is being incorporated in therapeutic cosmetics and skin care products (Muller-Goymann, 2004). Several studies have demonstrated the importance of nanosilver as an antibacterial agent (Alt et al. 2004; Son et al. 2004). Braydich and co-workers (2005) found silver to be toxic in germ line stem cells. In general, silver is considered as a natural material with very insignificant or no allergic reactions when tried for curing different diseases and is also regarded as safe for the use of human being.

2.7 Ag-TiO₂ Nanocomposite

Ag doped Titania nanoparticles have been broadly utilised as a filler in the fabrication of antibacterial coatings, antibacterial plastics, dishware and medical facilities and functional fibers, for the reason that Ag⁺ even at a smaller concentration has a strong antibacterial activity against numerous kinds of bacteria (Kawashita et al. 2000). Silver ions doping made enhancement of the photocatalytic activity of TiO₂ because it changed lattice parameters of TiO₂, which should attribute to the O vacancies produced by the substitutional silver ion at lattice site (Liu et al. 2003). Silver containing Titania coatings were found to be considerably more photocatalytically and antimicrobially dynamic than bare titania (Page et al. 2007),

furthermore the antimicrobial activity in the dark was not noteworthy, demonstrating that silver ion diffusion was not the method for antimicrobial action. The Silver doped titania coating is a potentially valuable coating for hard surfaces in a hospital environment due to its healthiness, strength to cleaning and reprocess, and its outstanding antimicrobial reaction (Page et al. 2007).

2.7.1 Ag Nanoparticle Enhanced Photocatalysis-A Special Case of Application of Ag-TiO₂ Nanocomposite

The photocatalytic reaction is a process of energy transfer from light energy of photon to electrochemical energy via catalysis. The term photocatalysis implies when semi-conductor materials for instance TiO₂ undergo irradiation by light of a certain wavelength, it produces photon assisted production of catalytically active species (Suppan P 1994; Mills A et al. 1997). In the process of photocatalysis, when a semiconductor is irradiated by beam energy higher than a semiconductor band gap, it stimulates an electron from valence to the conduction band as described in figure 2.4.

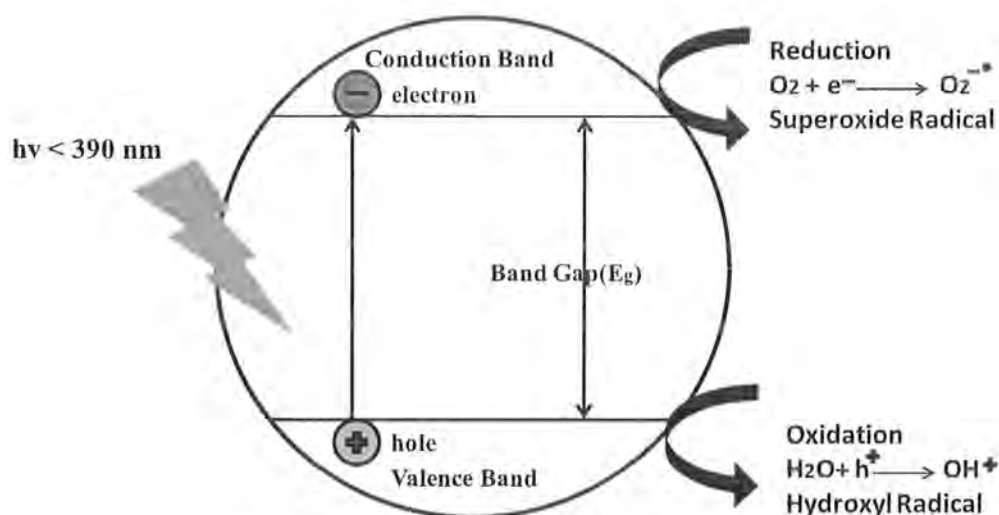


Fig. 2.4 Photocatalytic mechanism

2.7.1.1 Basics of Photocatalytic Processes

Titanium dioxide (TiO_2) is a white substance in which titanium exists in IV oxidation state. TiO_2 have various several polymorphs but the most important and noticeable are rutile and anatase. Since TiO_2 is a semiconductor, its Light absorption property efficiently results in a charge transfer to a ligand from a metal, therefore O_2 electrons are transported to the d-orbitals of unfilled titanium. For rutile (3.0 eV) and anatase (3.2 eV), this conversion is in the UVA region leading to a quick absorption band at 390 to 400 nm.

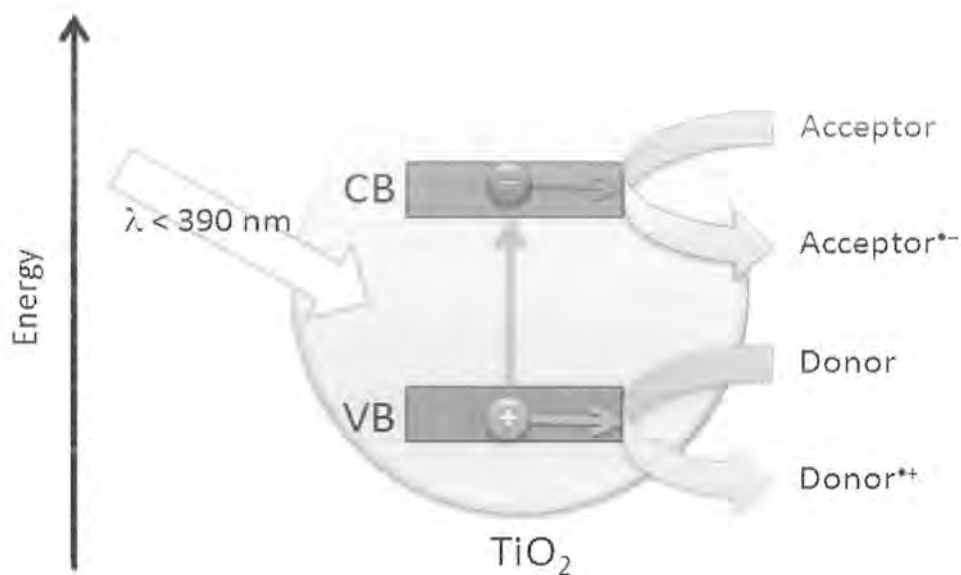
2.7.1.2 General Mechanism of Photocatalysis

For a better understanding of photocatalysis it will be essential to elucidate a few elementary definitions that are mainly significant to the perspective of photocatalytic processes. As an indication we take an electron energy level in a vacuum and as the highest level, the higher band is termed as the conduction band, and the lower band is termed as the valence band. In expressions of energy, the variation among the upper boundary of the valence band and the lower boundary of the conduction band is called the bandgap (E_g) of the semiconductor. The bandgap is one of the main essential factors for the semiconductor optical characteristics (A. Wood. et al. 2001).

In the electronic processes, on illumination by UV light electrons promote to a conduction band, leading to a hole in the valence band which is basically a disadvantage of the electron density that was focused on that orbital, and generally allocated a positive charge to denote the loss of negative electron (J. G. Yu et al. 2000). The hole is strongly oxidizing as the orbital extremely needs to regain electron density which is lost after light illumination. It can regain this basically by recombining the electron in the conduction and valence band since the recombination

is a sum of non radiative and radiative processes (B. F. Xin, et al 2005). According to the law of energy gap, the closer rutile energy levels leads to the non radiative process which is more capable, and therefore recombination is well-organized.

Alternative pathways to recombination are possible, which concludes that these materials can be used as photocatalyst. The hole has a capability to oxidise water which is present on the surface of the material ensuing in the development of hydroxyl radicals (OH^\cdot) (V. Subramanian et al. 2004). These hydroxyl radicals are very potent oxidisers, and can simply oxidise any organic species that come about, eventually to water (H_2O) and carbon dioxide (CO_2). In the meantime, the electron present in the conduction band has no hole to recombine with, because it has oxidised surface bound (H_2O) (J. G. et al. 2000). It rapidly looks for a substitute to decrease, and speedily decreases O_2 to form the superoxide anion which consequently react with water forming the hydroxyl radical (OH^\cdot) again. This entire process can be sum up as below in fig 2.5.



Process	Name
$\text{TiO}_2 + h\nu \rightarrow h_{\text{VB}}^+ + e_{\text{CB}}^-$	Charge Separation
$h_{\text{VB}}^+ + \text{H}_2\text{O} \rightarrow \text{OH}^*$	OH*Generation (VB)
$e_{\text{CB}}^- + \text{O}_2 \rightarrow \text{O}_2^{\bullet-} + \text{H}_2\text{O} \rightarrow \text{OH}^*$	OH*Generation (CB)

Fig 2.5 Light energy greater than band gap leads to separation of a charge, with electron reducing a donor (generally O_2) and hole oxidising a donor (generally H_2O); bottom: review of processes occurring (Image based on Bahnemann 2004).

At TiO_2 surface, the prerequisites for proficient photocatalysis can be inferred from the reaction of the electrons. There should be H_2O bounded at surface which permit proficient oxidation; and after aeration give O_2 to the solution (B. F. Xin et al. 2005). Furthermore, the degradation of the pollutant by the catalyst involves the pollutant to be adsorbed onto the surface of the material, and consequently more pollutant can adsorb on the greater surface area. Thus, nanoparticle materials are favoured as they hugely boost the surface area for the pollutants.

2.7.1.3 Limitations of TiO₂ Photocatalysis

The main constraint of TiO₂ photocatalyst is that the materials absorb UV light only; as a result the excitation via sunlight is justified only by the 5% of sunlight which is present in the UV region. There is ample evidence in the literature to improve the approaches to enhance the visible light performance of the materials. An additional drawback is the fact that recombination is and therefore it is less effective with anatase. It is usually accepted that anatase is a preferred photocatalyst to rutile. Therefore, incorporation of metal nanoparticles like Ag increases the capability of visible light absorption and also enhances the effectiveness of consequent reactivity in comparison to the recombination process (M. R. Hoffmann et al. 1995).

2.7.1.4 Enhanced Photocatalysis efficiency by incorporation of Ag metal nanoparticles

A variety of methods have been applied to enhance the activities of photocatalysts, including, for example, doping (both cationic and anionic), coupling of semiconductors with different band structures, and deposition of noble metal nanoparticles for instance Ag/Au on the surface of TiO₂ (Y. Zhang et al. 2009).

For instance, inclusion of a little quantity of Ag (1–5%) enhanced the photocatalysis process as the Ag has the electron accepting region lies at energy just below the conduction band. (D. F. Ollis et al. 1991).

Thus, subsequent to charge separation and light absorption, Ag trap the electrons in the conduction band efficiently, whereas the hole oxidises H₂O and forms OH[•] radicals devoid of the chance of recombination (A. L. Linsebigler et al. 1995). There is an optimal amount of silver to add to the titanium as a result the silver regions are isolated through out the material and make regions to entrap electrons however not in a larger quantity since it would then cover the surface of the titanium

dioxide and prevent light absorption (H. Gerischer 1995). Besides, the large quantity of Ag may perform as a recombination site itself and make possible link among electron and a hole (P. Pichat 1987).

The discharge of TiO_2 (and of linked literature with ZnO) can be inferred as an evaluation of the recombination effectiveness. The research observing the discharge of metal oxide verified that the emission intensity decreases with the increasing amount of Ag (P. Pichat 1987; B. Ohtani et al. 1993). It specifies that the silver efficiently traps electrons and decreases the recombination of electron-hole, as shown in the following illustration:

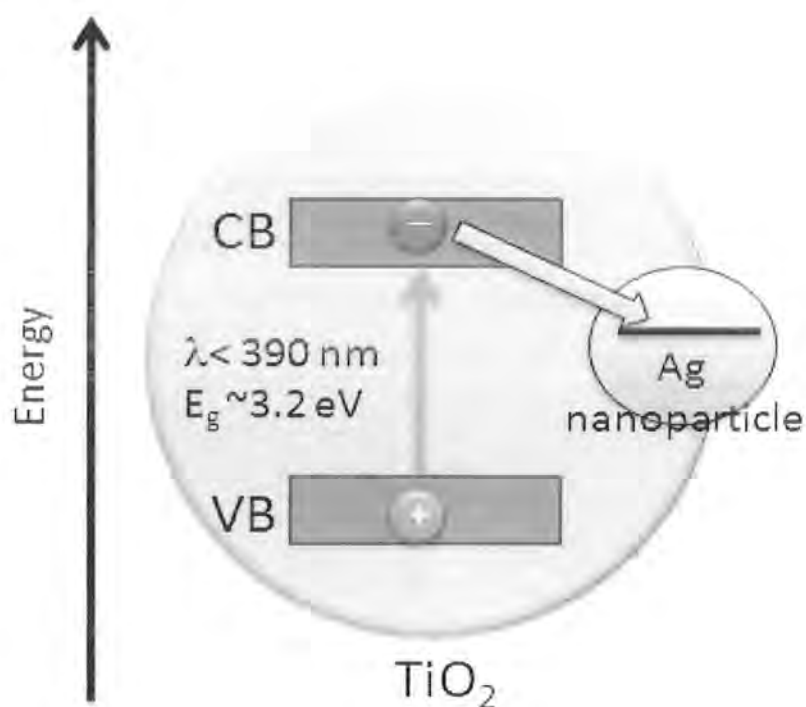


Fig 2.6 Integration of silver nanoparticles traps photo generated electrons and assists longer charge separation

The synthesis of Ag and TiO_2 can be attained by various methods such as, silver nanoparticles can be doped on the TiO_2 surface by photo-assisted reduction of

Ag^+ ions in aqueous solutions under UV illumination (A. Sclafani et al. 1991; D. Friedmann et al. 2007). In addition Ag-TiO₂ nanocomposite structures can also be obtained, for instance, by initially reducing Ag^+ ions to form an Ag core and then hydrolyzing titanium-(triethanolamino) isopropoxide to form a TiO₂ shell around the Ag particles (T. Hirakawa and P. V. Kamat, 2004; T. Hirakawa and P. V. Kamat, 2005).

When there are no electron scavengers are present, these materials revealed the potential to stock up the photo generated electrons which are transferred from TiO₂ to silver core leading UV excitation as exhibited in figure 2.6. The transfer of electron carry on until a Fermi level stability is set up between Ag and TiO₂. There are approximately 66 electrons per Ag/ TiO₂ core/shell structure stored in the Ag core as measured by the surface plasmon resonance band shift. This electron storage capability is very important in in photon energy conversion as it stores the electrons in the excitation process and delivers them again in the dark (T. Hirakawa 2005). Noble metals nanocomposites with ZnO also indicate the same electron transfer and equilibration of Fermi level as studied by A.Wood (A. Wood 2001).

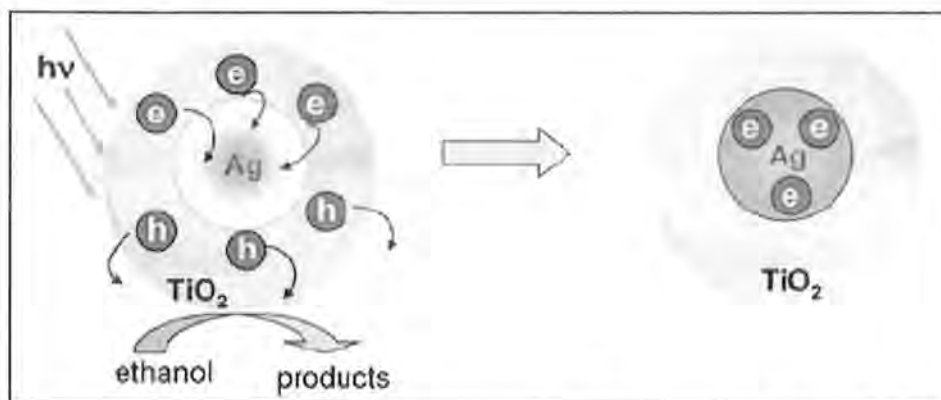


Fig 2.7 Electron accumulation in core-shell Ag/ TiO₂ in UV irradiation (Hirakawa and P. V. Kamat 2004)

Au and Pt nanoparticles when incorporated in to photocatalysts like TiO_2 , also have the ability to augment photocatalytic reactions however the high cost of Au and Pt represents the major limitation (as compared with Ag) of using them in photocatalysts (G. R. Bamwenda et al. 1995; J. G. Highfield et al. 1989; J. S. Lee et al. 2004; T. A. Egerton et al. 2008).

2.7.2 Potent Antibacterial activity of TiO_2 -Ag Nanocomposite:

The most frequently used noble metals in antimicrobial applications are silver and gold. For example, gold - capped TiO_2 nanocomposites have a strong oxidizing ability and showed a 60-100% killing efficacy of *Escherichia coli* (Fu G F et al. 2005, Guo et al. 2011, Watts et al. 1995). Likewise, silver has long been studied and recognized for its potential as an antimicrobial agent, with silver ions and nanoparticles having been shown capable of killing bacteria, viruses, and fungi. Recently, Ag- TiO_2 nanocomposite powders, Ag- TiO_2 nanofilms, Ag-deposited Ag- TiO_2 nanocomposite films were all shown to exhibit enhanced photocatalytic activities and bactericidal activities compared to TiO_2 nanoparticles or TiO_2 nanofilms. Such as, when Zhang et al. used a one - pot sol – gel approach to produce 10 nm TiO_2 nanocomposites with a high Ag - loading ability, the nanocomposites showed a complete inhibition of *E. coli* growth at silver concentrations of only $2.4\mu\text{g ml}^{-1}$ (Zhang H.J. et al. 2009).

The compositing of Ag into TiO_2 films has been met with similar success; as an example, Liu et al. used the Ag doping of a TiO_2 nano film to kill silver - resistant *E. coli* when the nanocomposite films were UV light - irradiated (Liu Y et al. 2008). In this case, the bacterial survival rate on the nanocomposite was only 7%, compared to 53.7% on UV light - irradiated pure TiO_2 nanofilms (Liu Y et al. 2008) Similarly, silicon catheters coated with Ag- TiO_2 nano films with embedded nanocomposites

demonstrated a self - sterilizing effect, with a 99% sterilization of *E. coli*, *Pseudomonas aeruginosa* and *Staphylococcus aureus* after UV illumination (Yao Y et al. 2008). A similar doping of Ag-TiO₂ nanofilms with Ag-TiO₂ nanocomposite particles led (in solar light conditions) to a photocatalytic killing of *E. coli* that was 6.9 - fold further efficient than with TiO₂ nanofilms, and 1.35 - fold more effective than with Ag-TiO₂ nanofilms (Akhavan O 2009). Finally, UV-illuminated platinum nanoparticles embedded in a TiO₂ nanofilm demonstrated an increase in the photocatalysis - driven killing of *Micrococcus lylae* cells, compared to UV-illuminated pure TiO₂ nano films (Wang X C et al. 2005). The prevention of bacterial contamination in our daily activities is an interesting challenge for scientists and engineers.

The research and development studies have resulted in better understanding on the contamination pathways and also the development of novel or new antimicrobial materials. Although there are many well-known antibacterial materials used against a spectrum of bacteria nowadays, research studies on new or novel materials with better textural and biocidal properties have been increasing each year. Wilks et al. investigated infection risk of *E. coli* O158:H6 which is a severe pathogen causing haemorrhagic colitis from contaminated metal surfaces, including stainless steel because it is one of the most common construction materials used in abattoirs, food processing and handling industries, domestic premises, public transit systems, hospital settings, large drinking water systems and, also the places where bacterial contamination could pose an imperative health threat (Wilks et al. 2005).

They reported that in a desiccated state, *E. coli* O157 was found to be able to continue to exist on stainless steel surface at refrigeration and room temperatures for more than 28 days. Although some reduction in bacteria concentration occurred

during 28 days, the remaining population density stayed constant at 10⁴ CFU, which shows a potentially serious health risk (Wilks et al. 2005). Physical methods, such as heat and radiation could be used to achieve sterilization through destroying microbes but they are not as adequate as the prevention of contamination. In fact, the effectiveness of the physical methods would not last for a long time. Thus, the usage of antibacterial materials seems to be better solution against bacterial contamination. Antibacterial materials could be classified into two groups; organic and inorganic materials. Organics are phenols, halogenated compounds, quaternary ammonium salts and in recent years, studies about antibacterial materials have been focused on natural materials, such as chitosan and chitin. For inorganic agents, metals, metal oxides and metal phosphates are known common antibacterial materials. Among inorganic materials, nano size metals and metal oxide were found to show high antibacterial efficacy against bacteria (Stoimenov et al. 2002, Sondi et al. 2004) and also the oxide materials could substitute the conventional organic antibacterial agents (Yamashita et al. 2001).

Ahmadi et al. studied morphological effects of Ag- TiO₂ nanocomposite and evaluated this against gram positive bacteria and found it very beneficial for the bactericidal effect of gram positive bacteria (Ahmadi et al. 2009; Davis et al. 2011) Besides, Akhavan et al. observed the Ag-TiO₂ nanocomposite antibacterial effect in visible and solar light irradiations and found that antibacterial activity of Ag- TiO₂ nanocomposite against e-coli is 5.1 times enhanced as compared to the TiO₂ nanoparticles in dark (Akhavan 2009). The antibacterial ability of Ag-TiO₂ was because of the generation of hydrogen peroxide (H₂O₂), which was very effective in the inhibition of bacterial cell growth (Sawai J et al.1998.). As studied by Trapalis et

al, hydrogen peroxide was found to denature the cell proteins in bacteria (Trapalis C. C2003).

In the study of Yamashita et al. heat was applied to ZnO powders at different temperatures (Yamashita et al. 2001). Antibacterial activities of the powders were tested against *E. coli* as a function of lattice constant of hexagonal structure and its effectiveness on the H₂O₂ production. It was established that generation of H₂O₂ occurred in all samples. However, samples heated at 800°C possessed a higher antibacterial activity than those heated at 1400°C (Yamashita et al. 2001). Stoimenov et al. studied the antibacterial and sporicidal activities of MgO nanoparticles and its halogenated derivatives synthesized by an aerogel procedure (Stoimenov et al. 2002). They reported that the materials had an excellent activity against *E. coli* and *B. megaterium*, and fairly good activity against spores of *B. subtilis*. These materials possessed the high surface area, hence bringing about the enhanced surface reactivity that increased the adsorption capacity for active halogens. Owing to the minute particle size, the total contact surface area increases, thus resulting in a high antibacterial activity. This study showed that metal nanoparticles exhibited the excellent bacterial activity against bacterial population (Stoimenov et al. 2002).

Similarly, Sondi et al. examined the antibacterial efficacy of silver nanocrystallites on *E. coli* by developing a simple preparation method to synthesize low-cost and non-toxic materials, such as stable silver hydrosols with high concentration (Sondi et al. 2004). Determining optical density of *E. coli* bacterial cultures in liquid medium was performed for antibacterial activity tests and also as a second method agar plates were used. In the liquid medium, silver nanoparticles delayed the bacteria growth whereas they completely inhibited the growth on agar plates, thus proving that silver nanoparticles could be used as antibacterial materials.

Kumar et al. prepared a polyamide composite material containing silver. In their study, silver was added to the melted polyamide directly (Kumar et al. 2004). They reported that the silver doped polymers showed antibacterial activity by the release of silver ions. Antibacterial activity tests of the polyamide/silver composites were applied against *E. coli* and *Staphylococcus aureus* bacterium. These tests demonstrated that the composites were effective against pathogens (Kumar et al. 2004).

It is generally preferable to prepare antibacterial materials in a supported antibacterial agent form. There are several reasons to use a support material. A support material enables to prepare materials in such a way that it makes them more convenient for handling than unsupported antibacterial materials. For instance, a solid oxide supported metal ions, such as silver on silica, are more convenient for handling and applying than unsupported antibacterial solution, such as silver nitrate solution (Lin Y et al. 2011; Tanimato et al. 2000).

Another advantage of using a support is that the effectiveness of the antibacterial material is increased because the support material enlarges the active surface area of an antibacterial material and subsequently, the contact area between the antibacterial agent and the medium will increase. However, the support material could also control the release rate of the agent to the medium that provides a long-term antibacterial effect. In the cases where no support is used, the agglomeration of the antibacterial agent could occur; hence resulting in loss of surface area, i.e. contact area (an undesired condition for the performance of the antibacterial material). In addition, a more uniform and narrow dispersion of the antibacterial agents could be obtained using an appropriate support material. For instance, a metal ion doped solid supported polymers are more effective than unsupported metal colloids because of the

uniform dispersion that could be inhibited by adjusting the particle size of the support (Hagiwara 1998).

2.8 Applications of TiO₂

2.8.1 Photocatalytic splitting of water

Ever since 1972 when Fujishima and Honda carried out the photocatalytic splitting of H₂O using TiO₂ much work has been done into maximising the potential of the process as it can provide clean renewable energy from sustainable sources (Chen et al. 2007).

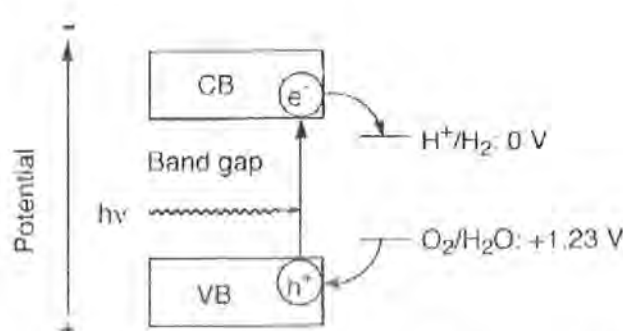


Figure 2.8 TiO₂ photocatalytic splitting of water (Chen et al. 2007)

Figure 2.8 shows a diagrammatic presentation of the principle of TiO₂ photocatalyst water splitting. An electron can be stimulated from valence to the conduction band by the light energy greater than the band gap. The photo-generated electron-hole pair causes redox reactions where H₂O molecules are reduced by excited electrons to form H₂ and oxidised by holes to form O₂ leading to H₂O splitting (Nicholls, D1974; Wisitsoraat, A 2009).

2.8.2 Self-Cleaning Surfaces

TiO₂ technology has been utilised by Pilkington Glass to develop a range of self-cleaning windows known as Pilkington Active self-cleaning and super-hydrophilic glass displays the properties of TiO₂ (Figure 2.9).



Figure 2.9 Self cleaning windows from Pilkington Activ10
(<http://www.pilkingtonselfcleaningglass.co.uk/trade/>; 28-May-2010)

Photocatalyst-modified cement (Sawai et al.1996) can also be produced by incorporated TiO_2 into concrete. It is used to coat hospital surfaces and provide antimicrobial protection against harmful bacteria such as MRSA and *E. coli* (Block et al. 1997) .The surfaces of partitions and lights and road side can be kept clean by applying TiO_2 which also provide the advantage of reducing harmful exhaust gases such as VOCS and NO_x . Despite the great promise shown by the self-cleaning abilities of TiO_2 surfaces, there are certain limitations. Since TiO_2 is a semiconductor material with wide band gap of (3.2 eV), the self-cleaning process can only be initiated by light of wavelength ~ 390 nm or less. This cause's substantial reduction in the efficiency of the product as light of such energy, ultraviolet light (UV), only makes up 3 – 5 % of the solar spectrum. Therefore, in order to develop the efficiency of these materials it is essential to either reduce the band gap or to introduce mid-band gap energy levels that act as a steppingstone between the energy levels, facilitating visible light absorption.

2.8.3 The dye sensitised solar cell

The dye sensitised solar cell (DSSC) has shown great potential as the next generation of solar cells (Kato et al. 2010). The DSSC has several advantages over current photovoltaic cells such as; low production costs, more consistent energy production from diffuse and direct sunlight, colour choice and transparency (figure 2.10). Also, because the DSSC utilises TiO_2 nanoparticles, solar cells of much smaller sizes can be produced and they can even be flexible.



Figure 2.10 DSSC (Dye sensitised solar cell)

(<http://media.hbmedia.co.nz/celsias/uploads/admin/dssc.jpg>)

As TiO_2 synthesis reactions are better understood it may become possible to design synthesis techniques that will produce TiO_2 materials capable of enhanced electron capture properties.

2.8.4 Photocatalytic degradation of pollutants

Due to the environmental applications such as air purification and water remediation (Fujishima et al. 1972; Mi et al. 2008; Wisitsoraat A et al. 2009) TiO_2 has attracted great interest in the past decade. The photocatalytic mechanism is activated by light energy superior than semiconductor band gap. Upon photo-activation, an electron-hole pair is produced that reacts with adsorbed species to produce radical species. These radicals are powerful oxidising agents and will oxidise organic contaminants to carbon dioxide and water.

2.9 Conclusion

The above literature review presents some of the cutting-edge research achievements in the field of TiO_2 , Ag and TiO_2 -Ag nanocomposite. In addition, the recent literature has also been actively updated by the new findings of TiO_2 , Ag and TiO_2 -Ag nanocomposite activities in different environments. These arguments therefore strongly justify the importance of the research on the synthesis and applications of TiO_2 and nanosized silver-containing titania materials.

Deposition of Ag nanoparticles onto a solid supporting material provides an effective means to achieve a high degree of Ag dispersion. Titanium dioxide, owing to its low-priced, safety and exceptional constancy, has been widely used as the support material for noble metal nanocatalysts. In addition, TiO_2 is a semiconductor photocatalyst with a wide band gap that has studied extensively during the past decades. The combination between Ag and TiO_2 photocatalysts has also led to some interesting special effects on the photocatalytic and antibacterial characteristics of TiO_2 . Therefore, TiO_2 and Ag supported TiO_2 nanoparticles were chosen as the target material to be synthesized in this thesis work.

Consequently, the effect of pH on the synthesis of Ag-TiO₂ nanocomposite and its application for antibacterial activity is studied. Moreover, successfully synthesised Ag-TiO₂ nanocomposite is also investigated for interaction with bacteria which should be of great scientific value and are worthy of in-depth investigations.

Experimental Procedures and Characterisation Techniques

Introduction

This chapter describes experimental details of TiO_2 and Ag-TiO_2 nanocomposite synthesis and characterization and techniques used. It also explains methods used for the applications of synthesized TiO_2 , Ag-TiO_2 nanocomposite for antimicrobial and dye degradation studies.

3.1 Synthesis of Nanomaterials

3.1.1 Synthesis of Titanium Dioxide (TiO_2)

Materials: Titanium isopropoxide (TIP, 97%, Aldrich) was used as the precursor.

Different kinds of precursors can be used to synthesize TiO_2 through Sol-Gel technique, for example, tetra-n-butyl-titanate, TiCl_4 , etc. In our experiment, we chose titanium isopropoxide $\text{Ti}(\text{OC}_3\text{H}_7)_4$ (also noted as TIP) as the precursor to start with. This solution is 0.96 g/cm^3 in density, with a sensitive nature to moisture. The chemical structure of Titanium isopropoxide described in Figure 3.1

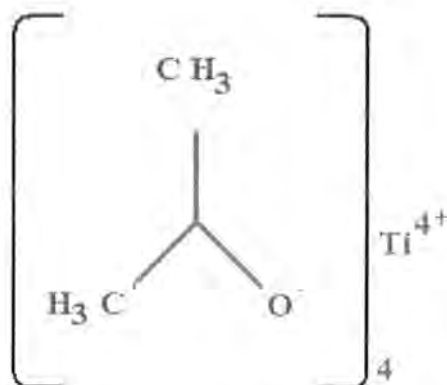


Fig 3.1 Chemical structure of Titanium iso propoxide

Absolute ethanol (analytical reagent grade, Aldrich) served as a stabiliser for titanium isopropoxide (TIP). All reagents were used exclusive of any additional purification. Doubly distilled water was used to initiate the hydrolysis and the condensation process. Table 3.1 shows the materials used for the preparation of TiO₂ nanopowder.

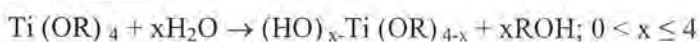
Table 3.1 Chemicals used in the experiment

Chemical Name	Molecular Formula	Purity	Company
Titanium Isopropoxide	Ti(OC ₃ H ₇) ₄	97%	Sigma Aldrich, UK
Hydrochloric Acid	HCl	37%	Fisher, UK
Absolute Ethanol	CH ₃ CH ₂ OH		Sigma Aldrich, UK
Deionised water	H ₂ O	-	

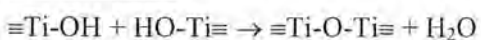
3.1.2 Sol-gel Method

In the sol-gel process, an organic medium is used to hydrolyze titanium alkoxides with the addition of H₂O which results in the polymerization of the hydrolyzed alkoxide during condensation of hydroxyl or alkoxy groups. This can be illustrated by the equations as follows, (R= an alkyl group).

Hydrolysis



Condensation



Therefore, an oxide polymer complex is produced via hydrolysis and polycondensation chain reactions and their comparative rates establish the degree of the oxide polymer branching. On the whole, rapid condensation rate will assist in the creation of long, branched polymeric chains ensuing in TiO₂ films which are highly porous (Xu et al. 2008). Additionally along with the molar ratios of alcohol and water to the titanium alkoxides, pH is also a vital aspect which influences the rates of hydrolysis and condensation. At low pH, the charge-charge repulsion between protonated titanium cations reduces the condensation rate and makes the less porous oxide film (D C Hague 1993). Nevertheless, the titanium alkoxides hydrolytic polycondensation in standard conditions results in the precipitation of particulate materials and synthesize the unstable sol. Consequently, some amount of inorganic acid for instance HNO₃ and HCl can be used to bar the initiation of the precipitate formation.

3.1.3 Synthesis of Nano-sized TiO₂ nanopowder by sol-Gel process

Nano-sized TiO₂ powder was synthesized by means of a Sol-Gel method with titanium isopropoxide (TIP), absolute ethanol and deionised water as preparatory materials. A predetermined quantity of ethanol and deionised water (M Ethanol: MTIP: MH₂O = 1:2:12) mixture was added dropwise into TIP solution whereas magnetic stirring was also applied consequently. As soon as the titration process completed, HCl was added into the aqueous solution while maintaining the pH of the solution at 2.0. The acid HCl was used in the process to control the process of hydrolysis and as a result to control the grain growth (B R Li 2002). The high stirring speed was used for the solution for one more hour and then peptized overnight. Subsequent to peptization, formation of a two layer solution was observed with upper

layer of organic by-product of the hydrolysis, and the bottom layer a gel of a titanate acid. Afterwards the filtration process was used to collect the gel. The gel was dried for several hours at 110°C until the yellow colour crystals become visible which were crushed into a fine powder by using pestle and mortar.

Annealing

Annealing process was carried out at 150 °C for 1h, followed by the increase in temperature to 600 °C for 2 hrs with 5 °C /min heating rate. White crystalline TiO₂ powder was obtained after the annealing process. Synthesis of nanocrystalline TiO₂ can be shown by a process flow chart as described in Figure 3.2 while the hydrolysis reaction which lead to the formation of TiO₂ can be illustrated by the subsequent reaction.

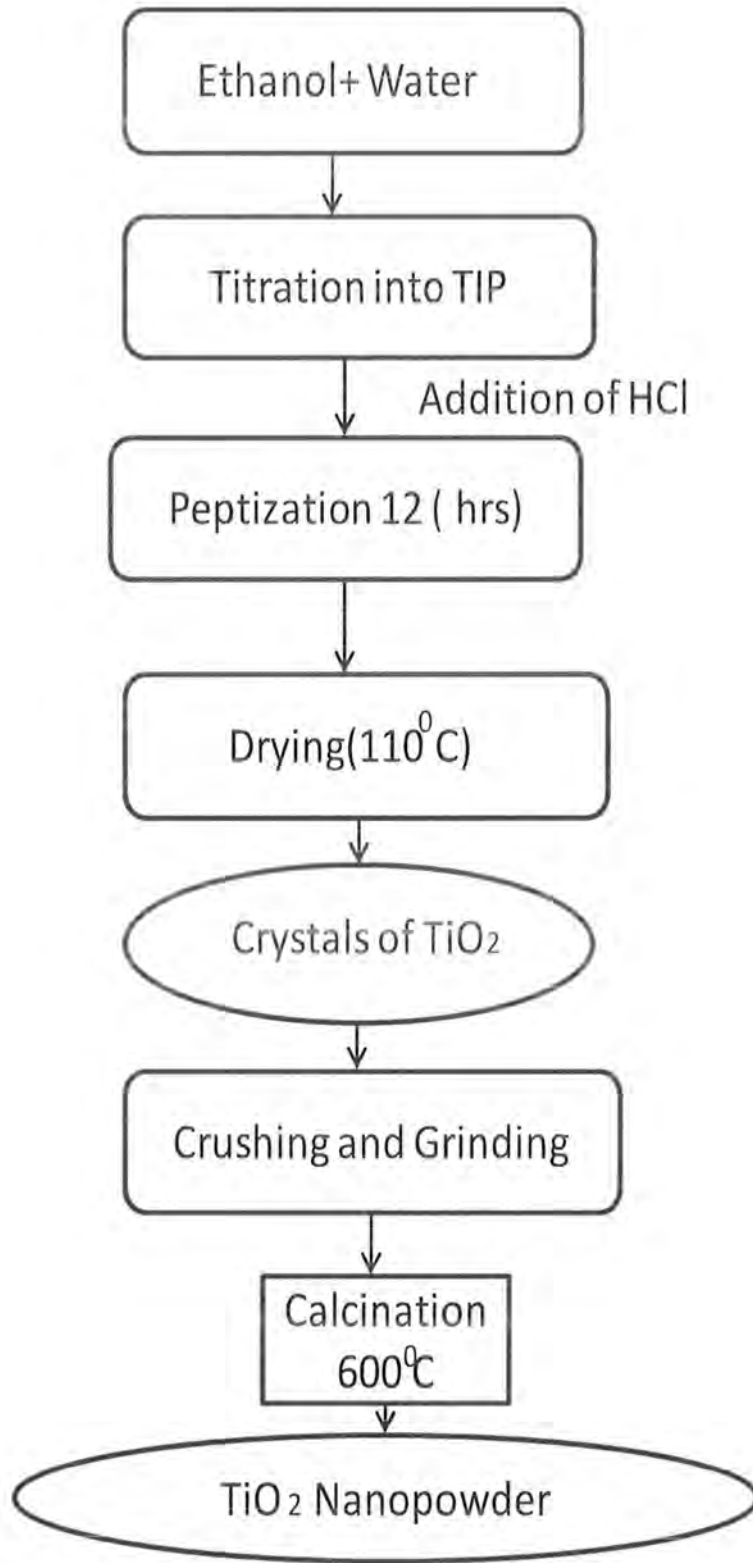


Fig 3.2. Flow chart showing synthesis of TiO₂ nanopowder via Sol-Gel process.

The advantages of TiO₂ synthesis by means of conventional sol-gel processing are high purity and good control over the microstructure and morphology, beginning at room temperature and completed by a heat treatment process at a temperature often reaching several hundred degrees Celsius. While it is possible to achieve a wide variety of morphologies and grain sizes, in order to control these, extensive chemical modifications must be made to the metal oxide system under investigation. In the sol-gel process, TiO₂ particles evolve into various morphologies at different stages depending on the hydrolysis/condensation conditions.

Generating from the hydrolysis/condensation, (Ti-O-Ti)_n molecular clusters (dimers, oligomers...) grow into denser solid particles in the solution. The sol particles (primary particles) can evolve into either discrete particles or three-dimensional gel networks according to the experimental conditions. Influence of temperature is studied on the microstructure and morphology of TiO₂ Nanoparticles.

3.1.3 Characterizations of TiO₂

X-ray Diffraction (XRD) was used to study the crystalline structure of synthesised TiO₂ nanopowder. The crystal size of TiO₂ was estimated by FWHM according to Scherrer's principle.

$$D = 0.9 \lambda / \beta \cos \theta$$

Where D is the average grain size,

λ is the wavelength of Cu K α (= 1.5405 Å),

β is the FWHM (full width at half maximum), and

θ is the diffraction angle.

The surface morphology was investigated by JEOL 5600, FEGSEM 6400. It was found that fine structure on the sample surface may not appear under high voltages of the electron beam that might be due to organic emission from the sample surface caused by high energy electrons. To observe the surface morphology of TiO₂ particles, the alignment of the electron beam was carried out at a low electronic voltage, e.g. 5 keV with a smaller spot size.

3.2 Synthesis of Ag-TiO₂ Nanocomposite

3.2.1 Materials

All chemicals were analytical grade and used without further purification. Deionised water was used as the dispersing agent through all the experiments.

Chemicals used in the synthesis of Ag-TiO₂ nanocomposite as shown in the Table 3.2 were titanium isopropoxide (TIP) with a purity of 97% (Aldrich, UK) as a precursor, analytical grade hydrochloric acid (HCl, 37%, Fisher, UK) as a catalyst for the peptisation and deionised water as dispersing media, Polyethylene glycol (PEG) with an average molecular weight of 6 Kg mol⁻¹ (Fluka, Germany) and AgNO₃, 99.99%(Sigma Aldrich, UK) (All the chemicals used in the synthesis of Ag-TiO₂ nanocomposite are described in Table 3.2).

TABLE 3.2 Chemicals used in synthesis of Ag-TiO₂ Nanocomposite

Chemical Name	Molecular Formula	Purity	Company
Titanium Isopropoxide	Ti(OC ₃ H ₇) ₄	97%	Sigma Aldrich, UK
Hydrochloric Acid	HCl	37%	Fisher, UK
Polyethylene glycol	H(OCH ₂ CH ₂) _n OH	-	Fluka, Germany
Silver Nitrate	AgNO ₃	99.99%	Sigma Aldrich, UK
Deionised water	H ₂ O	-	

3.2.2 Method

The Ag-TiO₂ nanoparticles were prepared by a photo deposition process. TiO₂ used in this experiment were synthesised by sol-gel process by hydrolysis of titanium isopropoxide (Ti (OC₃H₇)₄, Sigma Aldrich) followed by calcination at 450 C° for 2 h. 1g of TiO₂ powders were dispersed in desired volume of deionised water under ultrasonic stirring for 15 min. The oxide slurry was illuminated with UV (A) light for 20 minutes to oxidize any possible organic carbon impurities on the TiO₂ surface.

Photo deposition was carried out by adding a calculated volume of 0.05 M aqueous AgNO₃ into the TiO₂ nanopowder sol, so as to attain an eventual 1.25 wt % loading of Ag. This amount was found to be the optimum value based on synthesis with varying Ag loading in order to obtain a nanocomposite morphology containing on average one Ag nanoparticle anchored on the surface of one titania nanoparticle. After the AgNO₃ was uniformly dispersed and dissolved, a 15 W UV lamp with a

central wavelength of 365 nm was powered on to illuminate the sol along a normal direction for 3 h while the sol was magnetically stirred. In order to vary the pH value of the solution from 1 to 10, the pH was adjusted by adding either NaOH or HCl. The suspension was centrifuged at 12000 rpm for 10 min and then washed with distilled water several times to remove any impurities. Lastly, the suspensions were dried at 100C° to obtain the sample for characterization.

The formation of colloidal Ag metal nanoparticles on TiO₂ was confirmed by XRD. A series of Ag-TiO₂ nanocomposite with a constant Ag loading of 1.25 wt % at varying pH values were prepared. The samples were labeled as pH1, pH2 pH3..... pH10, denoting the relevant pH value used during photo deposition of Ag on titania nano particles.

3.2.3 Characterization

X-ray diffraction (XRD) pattern for the structure of powder was recorded on a Philips X'pert Diffractometer equipped with a CuK α radiation source (λ 1.541 80 Å°). The process of Ag-TiO₂ nanoparticles impregnation was accurately monitored by a Perkin Elmer Lambda25 UV spectrophotometer at different pH values ranging from 1 to 10. TEM images were recorded on the JEOL 200CX, which is a 200kV analytical TEM/STEM. For TEM studies the samples were prepared by placing a drop of aqueous Ag-TiO₂ nanoparticles dispersion on a piece of carbon-coated copper grid under ambient conditions.

Sample Powders were also characterized for their specific surface area by using N₂ adsorption/desorption method at liquid nitrogen temperature (-196 C) from Brunauer-Emmett-Teller equation (BET) at 77.3K using a Micromeritics Tristar 3000 analyzer. Prior to BET measurement, powders were degassed for 24 h at 90 °C under

a pressure of 0.1 Pa. To prevent any possible crystallization during outgassing, higher drying temperature was avoided.

3.3 Inactivation of bacteria using Ag-TiO₂ nanocomposite


There are many types of microorganisms of interest that could be studied, such as bacteria, spores, viruses, fungi and so on. Our attention was focused on common bacteria that represent different bacterial classes. The organism studied in this study was *Escherichia coli* (*E. coli*), a Gram-negative rod-shaped bacterium.

The purpose of selecting bacteria was to see the interaction with the nanoparticles were the same for the two different groups of bacteria.

3.3.1 Preparation of Bacterial Culture

Luria bertani (LB) medium was purchased from Difco which contain tryptone, yeast extract and NaCl (composition of LB Broth is given in Table 3.3). Agar powder was purchased from Sigma Aldrich. Luria Bertani (LB) agar consisted of LB medium and 15g/L agar. Saline solution used was 0.85 % (w/v) sodium chloride in water. Media, saline solution and 50% glycerol (w/v) were autoclaved at 121 °C for 15 minutes for sterilization.

Table 3.3 Composition of Luria Bertani (LB) Broth

Composition of LB Broth		(Fig 3.3) Luria Bertani (LB) Broth
Tryptone	10 g	
Yeast Extract	5 g	
NaCl	10 g	

E. coli (either a small amount of previously prepared liquid bacterial culture or a single colony from a Petri dish) were added to a sterile flask, containing 25-100 mL Luria Broth (LB) nutrient. The solution was typically agitated under aerobic conditions for 12-24 hrs on a shaker at 37°C. At that moment the flask contained a turbid suspension of bacteria cells with a concentration between 10⁶-10⁹ Colony Forming Units (CFU)/ mL. For some of the experiments a more precise concentration was desired, in order to use the same concentration for several experiments. Further, this attempt included the use of the cells in their log phase, versus stationary phase. At those times, 100 µL of previously prepared culture was inoculated in 100 mL LB broth and left over night. Next day, 50 µL of the previously grown overnight culture was extracted and added to 50 mL of fresh Luria Bertani broth and agitated at 37°C on a shaker thermostat. At certain time intervals, samples were extracted, and their optical density (OD) was measured at 600 nm. During these time intervals, aliquots were also plated to determine CFU/mL at each time interval. Graphs were prepared, including an OD versus Time (hrs) graph and CFUs versus Time (hrs). To prevent any contamination, special care was taken for all culture preparations and handling by using sterile glass ware, needles and syringes throughout all experiments. The used glassware was autoclaved before use at 121 °C for 20 minutes to ensure that all microorganisms were dead. Syringes and needles were purchased pre-sterilized and used as received. In all experiments, analysis of the bacterial cells was performed using serial dilutions and viable colony counting technique on the Agar plates. These are standard techniques to assess the viable cells as the numbers of cells are very large (Madigan et al. 2006). Figure 3.4 provide an overview of the viable colony counting method through serial dilution.

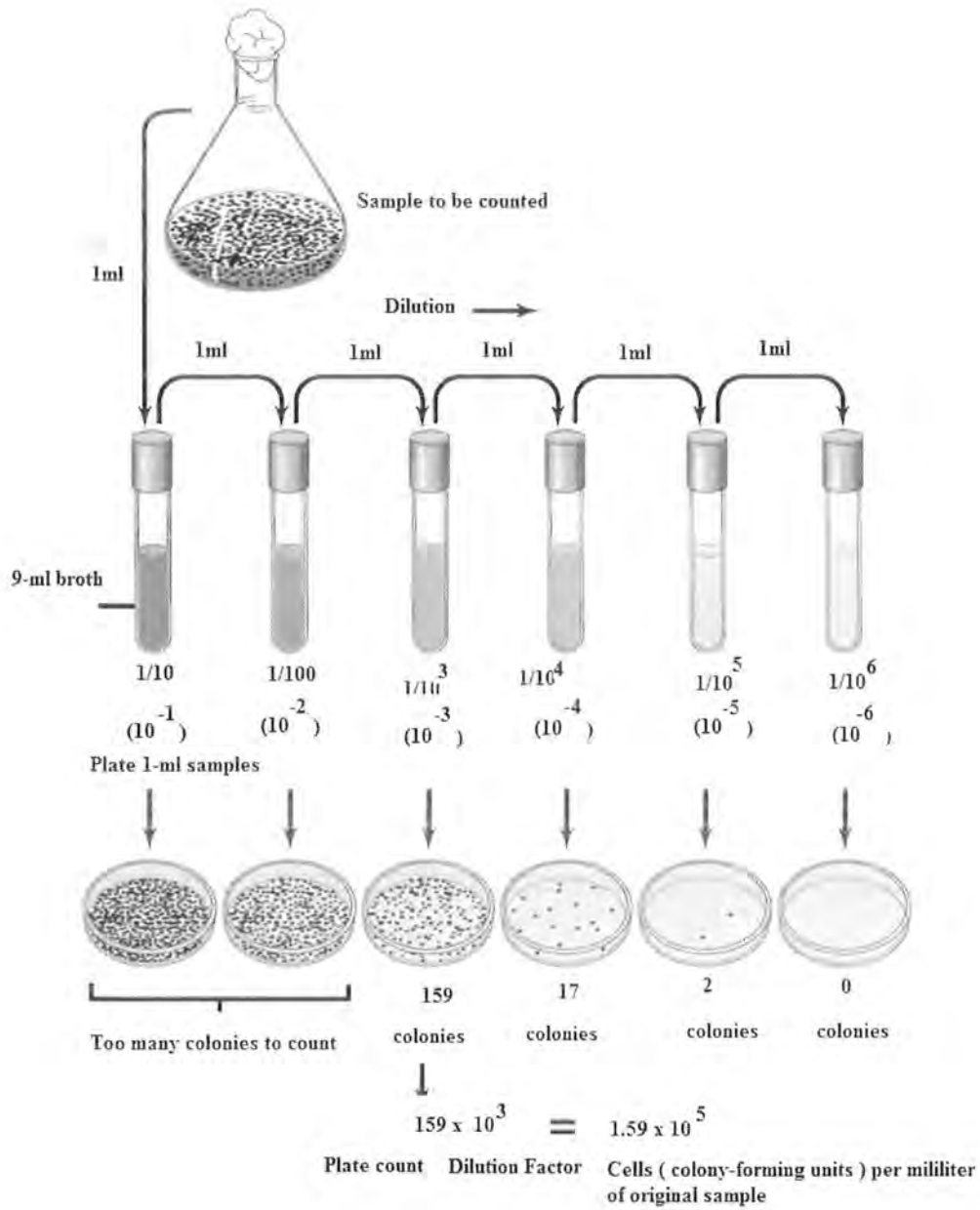


Fig. 3.4 Viable Colony Counting Method by Serial Dilution

For the purpose of understanding the experiments and results obtained, several variables were used which are given in Table 3.4

Table 3.4 Variables used in the experiment

Variables	Meaning
TiO ₂ +UV	Samples with TiO ₂ nanoparticles and UV light
Ag-TiO ₂ +UV	Samples with Ag-TiO ₂ nanoparticles and UV light
TiO ₂ (dark)	Samples with TiO ₂ nanoparticles in the absence of UV light
Ag-TiO ₂ (dark)	Samples with Ag-TiO ₂ nanoparticles in the absence of UV light
Control	Bacterial cells without nanoparticles and UV light

3.5 Characterisation Techniques

3.5.1 X-ray Diffraction:

The X-ray diffraction method is useful method for phase characterization and identification in polycrystalline materials (Lifshin 1999). The International centre diffraction data (ICDD), which is also called (JCPDS) Joint committee on Powder Diffraction Standard, is the organization maintaining the database of organic and inorganic spectra. The database is available either directly from ICDD or from the diffraction equipment manufacturer.

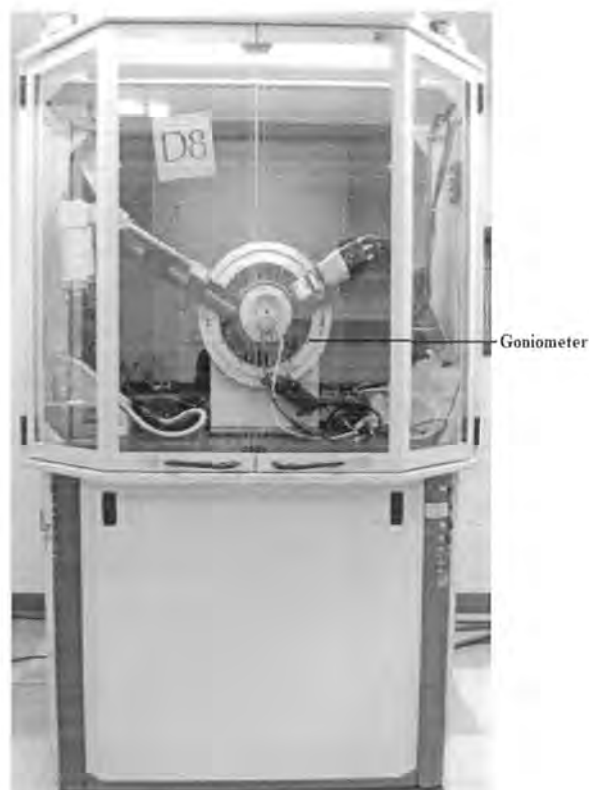


Fig 3.5 PANalytical vertical X-ray Diffractometer

The X-ray diffraction outline of substance is similar to a fingerprint of the substance. This technique is preferably appropriate for description and recognition of polycrystalline phases of materials (H. Shimakawa et al. 1993). Whilst X-rays interrelate with a crystalline material, a diffraction outline is attained. Each crystalline material provides a specific pattern and that pattern is always same for the material (Stanjek and Hausler 2004). The mechanical assembly consists of a associated gearing called a goniometer, a sample holder and a detector arm (Figure 3.5). The X-ray diffractometer works on the principle of Bragg's law as demonstrated in Figure 3.6. The Bragg's law describes that for X-rays scattered from a crystalline solid (Washingtonedu),

$$n\lambda = 2d \sin \theta \quad (1)$$

Where, θ = angle of incidence of X-ray beam, (degrees)

d = the distance between atomic layers in a crystal, (\AA)

λ = the wavelength of the incident X-ray beam, (\AA)

n = an integer

In the goniometer there is an equal distance between the X-ray focal spot to the sample and between the sample and the detector. The sample is fixed in a horizontal position in a θ : θ goniometer. The detector and X-ray tube both move about concurrently above the angular range (θ Theta).

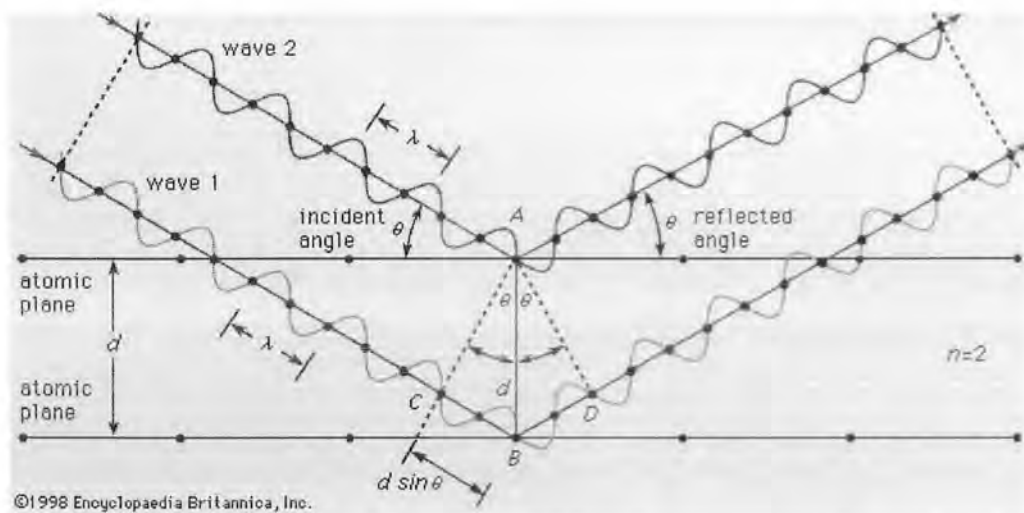


Fig 3.6 Bragg's Law (bmcu Washington.edu)

The model of XRD equipment used for the research work was PANalytical vertical X-ray Diffractometer with PANalytical data collection software, X'Pert High Score. The results obtained experimentally were compared with the existing database ICDD. During this study XRD patterns were collected using a $\text{Cu } K \alpha$ ($\lambda = 1.5418 \text{ \AA}$ (angstroms) radiation source with a nickel filter over a 2θ range of $5-90^\circ$ with a collection time of 4 seconds and a step size of 0.1. This Diffractometer collects with high angular resolution (down to 0.008 degrees in 2θ) powder X-ray diffraction

patterns of polycrystalline samples. For analysis the (101) peak ($2\theta = 25.28^\circ$) of anatase and the (110) peak ($2\theta = 27.42^\circ$) of rutile were used. Grain size can be estimated from an XRD line broadening analysis using the Scherrer equation (Li *et al.* 2003).

$$D = k\lambda/\beta\cos(\theta)$$

Where

D is diameter of nano crystals,

λ is the full width at half maximum length of the diffraction peak on a 2θ scale,

θ is the radiation wavelength (1.54180Å or 15.418 nm)

and

k is a constant value (k=0.9).

The value of D was calculated from the (101) diffraction peak that was best resolved in the diffractograms. The grain sizes illustrated in this research were measured by XRD analysis and the X'Pert High Score software associated with the Bruker D800 Advance diffractometer. The High Score Plus software was used to estimate the grain size by a variation of the Scherer equation that accounts for instrumental broadening. The grain sizes described in this research are of 101 and 110 peaks only. The range of measured 2-theta angle was 10-80 and the source of X-ray was Cu K- α . The generator settings were 40 kV voltages and 40 mA current.

3.5.1.1 Sample Preparation

For all the experiments it is very crucial to have smooth and flat surface samples. The sample is pressed into a sample holder as follows:

- Attach the glass slide to one side of sample holder by using the sticky tape.
- Spread the sample uniformly onto a glass slide obtaining a flat upper surface.

- Cover the sample holder by another glass slit and attach it using the sticky tape.
- Insert the sample holder with sample to the Diffractometer.

In the current project the samples investigated by XRD were TiO₂ nanopowder and Ag-TiO₂ nanocomposite. The main objectives were:

- Phase identification by diffraction of the XRD peaks characteristics for crystals of particular components. The obtained patterns were compared with International Centre Diffraction Data (ISDD), which is also known as (JCPDS).
- X'Pert Highscore Plus determined the Phase identification and crystallite size.

3.5.2 Electron Microscopy

In electron microscopy the analysis is done by irradiation of samples with the focused beam of electrons at 1-30 KV, collecting and analysing the radiations emitted. ("Electron Microscopes", House Ear Institute, Advance Hearing Science, 2001. <http://www.hei.org/research/aemi/emt.htm>). Electron microscopes operate in either transmission (TEM) or reflection scanning (SEM) mode. The basic principles and setup of each working mode are briefly described in this section.

3.5.3 Scanning Electron Microscopy (SEM)

There are two main types of images formed during operation of scanning electron microscope: Secondary electron images (SEI), and back scattered electron images, (BEI) (S. Qourzal et al. 2004). The secondary electron images are commonly used to study the surface topography of sample, while backscattered electron images are used for showing the compositional differences in the material or specimen.

3.5.3.1 SEM/EDX Analysis

The emission for the particular x ray radiation is initiated by sample with the beam of electrons. The SEM/EDX spectrum of the energy (KeV) versus relative counts of the detected x-ray is obtained for qualitative and quantitative determination of the elements present in the sample.

Recording the map showing intensity of characteristics X ray radiation reveals the spatial distribution of selected elements within the sample. This normally takes place when the beam of electron is scanned in rectangular raster through the sample (Sasaki and Kato 2004). The obtained map has a dot format, where each recorded X-ray photon produce a bright dot on the display at a point corresponding to the position of the beam on the sample (C N R Rao et al. 2004). The density of dots shows concentration of selected elements at particular place.

3.5.3.1 Sample Preparation

Collected sample for SEM may contain some impurities, which have to be removed by cleaning with distilled water or hydrochloric acid HCl. Some friable material requires impregnation with low viscosity epoxy resins to improve their mechanical strength. For compositional imaging a polishing of the specimen is needed to minimize a interference of topographic effects.

Commonly, the specimen for electron scanning is mounted to the disc shaped "stub" which is about 2 cm in diameter made of aluminium or copper. Sample is normally attached to the stub by carbon tape and coated with layer of conductive material (sputtering, if the specimen has an insulating nature).

In this project the TiO_2 and Ag- TiO_2 powder samples were deposited on the stub and thinned by a glass rod. The stub is tapped after each roll till there is a uniform thin layer of powder over the tape surface. After that the TiO_2 samples were

sputtered by Ag plasma to have a uniform layer to avoid charging of sample. Copper sputtered Ag-TiO₂ samples.

The topographic SEM images were taken by use of secondary electrons while compositional images were taken by use of backscattered electrons. The SEM/EDX techniques show concentration of elements; Ti, O₂, Ag or other elements in particular point of interest of the sample. The SEM images were analysed with use of the INCA software. The high resolution FEG SEM 6400 was used to show detailed morphology of the as synthesized TiO₂ and Ag-TiO₂ nanocomposite.

3.5.4 Transmission Electron Microscope (TEM)

The transmission electron microscope (TEM) was the first type of electron microscope to be developed and is composed precisely on the light transmission microscope except that a focused beam of electrons is used as a replacement for light to “see through” the sample. A more technical explanation of how TEM works is as follows (Figure 3.7) (Edington 1975).

Transmission Electron Microscopy measures the transmitted electrons through the sample to study. Therefore, only very thin samples can be looked at, and usually, TEM requires preparation techniques to make the sample thin enough to be transparent to the electrons (Edington 1975). Conventional transmission electron microscopy studies were executed on a TEM JEOL 2000FX working with an acceleration voltage of 200 kV. Electron diffraction patterns and high-resolution images were also recorded.

3.5.4.1 Sample Preparation

Sample thinning is crucial in getting good TEM image. To prepare a sample for TEM analysis powder sample is mixed with high purity acetone (99.9%) and

sonicated for 15-20 minutes. Carbon coated grids were dipped into the resultant mixture, dried and preserved carefully.

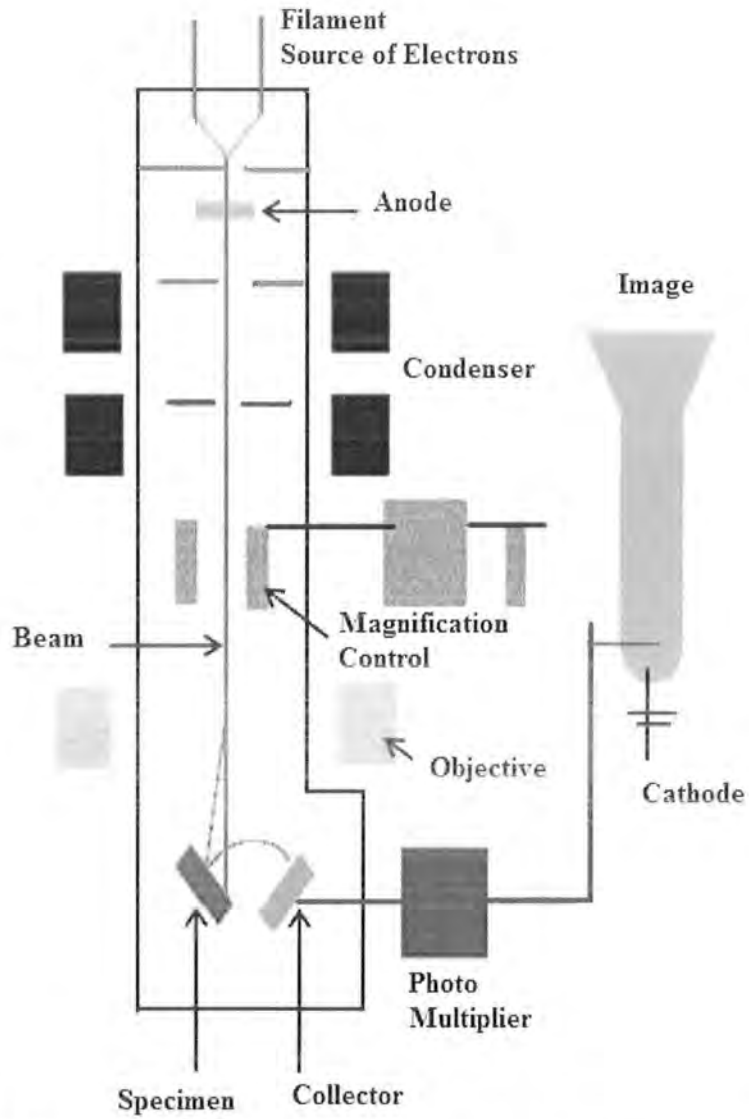


Fig 3.7 Transmission Electron Microscope (TEM) Mechanism

3.5.5 Field Emission Gun Scanning Electron Microscopy (FEGSEM)

Powders morphology was studied by JEOL 6340F FEGSEM. Secondary electron images (SEI) were taken at accelerating voltage of 5-10 KV and a working distance of 6mm. The powder samples were directly deposited onto a double faced conductive carbon tape, which was earlier mounted on a SEM stub.

In Scanning Electron Microscopy (SEM), the sample surface is scanned with a fixed electron beam. Backscattered electrons from the surface or secondary electrons can be measured with two different detectors (Yang et al. 1998).

Secondary electrons are due to ejection of electrons by ionization of the sample atoms under the primary electron beam. As the secondary electrons come from close to the surface, they give a high-resolution image. Backscattered electrons are electrons from the primary beam that come out of the sample after losing some of their energy in it. They come from deeper in the sample, so the surface image resolution they give is lower than with the secondary electrons, but "chemical contrast" images due to variation of the atomic number in the sample can be obtained (Yang et al. 1998).

3.5.5.1 Sample Preparation

To prepare sample for FEGSEM a conductive carbon double face tape is fixed on a stub used for SEM. Powder samples were deposited and thinned by rolling a glass rod. The stub is tapped after each roll till there is a uniform thin layer of powder on the surface of tape. The samples were then sputtered in Ag plasma to have a uniform layer to avoid charging of sample. Ag-TiO₂ samples were sputtered by gold.

3.6.2 UV-vis Spectroscopy

Ultraviolet visible (UV Vis) spectroscopy exploits light in the visible and adjoining near infrared (NIR) and near ultraviolet (UV) ranges (S J Gregg 1997). Molecules go through electronic transition in this region of the electromagnetic spectrum. This method is corresponding to fluorescence spectroscopy, in which fluorescence deals with transitions from the excited state to the ground state, whereas absorption measures transitions from the ground state to a higher energy level state.

An illustration of the mechanism of a typical UV vis spectroscopy is revealed in Figure 3.8 which exhibits that the functioning of this instrument is relatively straightforward.

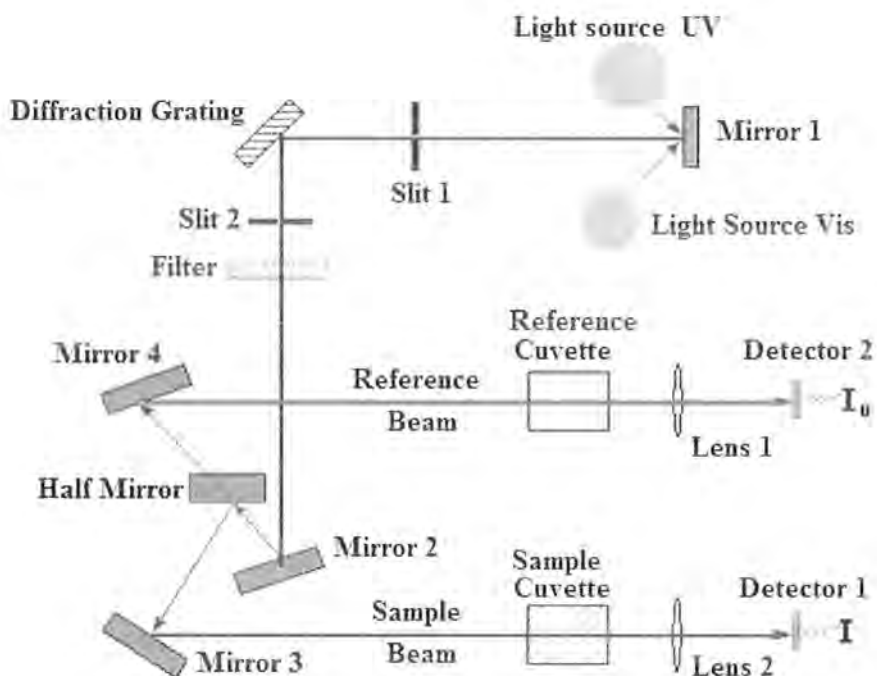


Figure 3.8 Components Of a Typical UV Vis Spectroscopy

A prism or diffraction grating is used to separate a beam of light (from visible or UV light source) into its constituent wavelengths. As a result every monochromatic beam having single wavelength is split into two equal intensity beams by a half r

mirrored device. One beam, the sample beam (colored magenta), go through a small transparent container (cuvette) containing a solution of the compound being studied in a transparent solvent. The other beam, the reference (colored blue), passes through an identical cuvette containing only the solvent. Consequently electronic detectors are used to calculate and compare the intensities of these light beams. The intensity of the sample beam is defined as I , while the reference beam, which should have suffered little or no light absorption, is called as I_0 . Over a short span of time, the spectrometer automatically scans all the component wavelengths in the mentioned way. The ultraviolet region scanned is normally from 200 to 400 nm, and the visible portion is from 400 to 800 nm. A UV-Vis spectroscopy (Perkin Elmer Lambda25 UV spectrophotometer) was employed to characterize the formation of Ag-TiO₂ nanoparticles and photo degradation of dyes.

3.7 BET-BJH method for determination of specific area and porosity.

The BET theory of multilayer gas adsorption is an extension of theory related to Langmuir monolayer adsorption after introduction of simplifying assumptions. Molecules of the first layer act as the sites for multilayer adsorption that leads to development of an unlimited number of layers at saturation pressure, p_0 . Under equilibrium pressure, p , the rates of condensation and evaporation of gas phase are equated for each layer. The summation of amount of gas adsorbed in all layer, Q , gives BET equation. The plot of BET isotherm is a curve of quantity of adsorbed gas ($\text{cm}^3 \text{g}^{-1}$) versus relative pressure (p/p_0). The gas adsorption isotherms at temperatures not far from their condensation points show two regions for most adsorbents. The isotherm is concave for range of low pressure while at the higher-pressure isotherm in convex.

Two stages have been implicated in the estimation of the surface area by BET method from isotherm. The first, the linear plot of $1/[Q(p/p_0-1)]$ versus p/p_0 needs to be constructed over approximate array of relative pressure $p/p_0 = 0.05-0.35$ to obtain the monolayer capacity Q_m . The second stage is to calculate the specific surface area S_{BET} . This entails understanding of average area, taken by each molecule of adsorptive gas. The gas used in this research was nitrogen at 77 K.

3.7.1 The pore size distribution by Barret, Joyner and Halenda (BJH)

Barret, Joyner and Halenda (BJH) proposed the derivation of pore size distribution from nitrogen adsorption isotherm. The assumptions made in BJH method include: the pores are of distinct form, the allocation is restrained to mesopore range, and the meniscus curvature is guarded by pore morphology and size. The computation of BJH method is generally based on the gradual elimination of condensed gas phase by stepwise lowering relative pressure P/P_0 during Desorption process. The pore volume and pore dimensions relation is presented graphically either in the form of cumulative plot of pore volume v ($\text{cm}^3 \text{g}^{-1}$) versus pore size D (nm) or as dv/dD versus D (nm).

3.7.2 Sample Preparation

Generally the preparation of samples for BET-BJH experiments requires degassing of investigated material before the experiment. The method of degassing strictly depends on the characteristics of samples.

The BET surface area and porosity of samples was investigated by means of BET-BJH method. The tested samples were: TiO_2 synthesized by sol gel method and Ag- TiO_2 nanocomposite which were degassed by nitrogen flow and heating up to the 100 C for 24 hours before the experiments. The degassing instrument used was

Flowprep 060 Micrometrics Degasser, with nitrogen flow up to $50 \text{ cm}^3 \text{ min}^{-1}$. The adsorptive gas in the experiments was N_2 at 77K temperature.

3.8 Zetasizer Malvern 3000 HAS

The zetasizer Malvern 3000 HAS instruments have two main functions. This can either work as a particle sizer using a cuvette as sample holder or measure the zeta potential (mV) of colloid in the cell between cathode and anode (Fig 3.9).

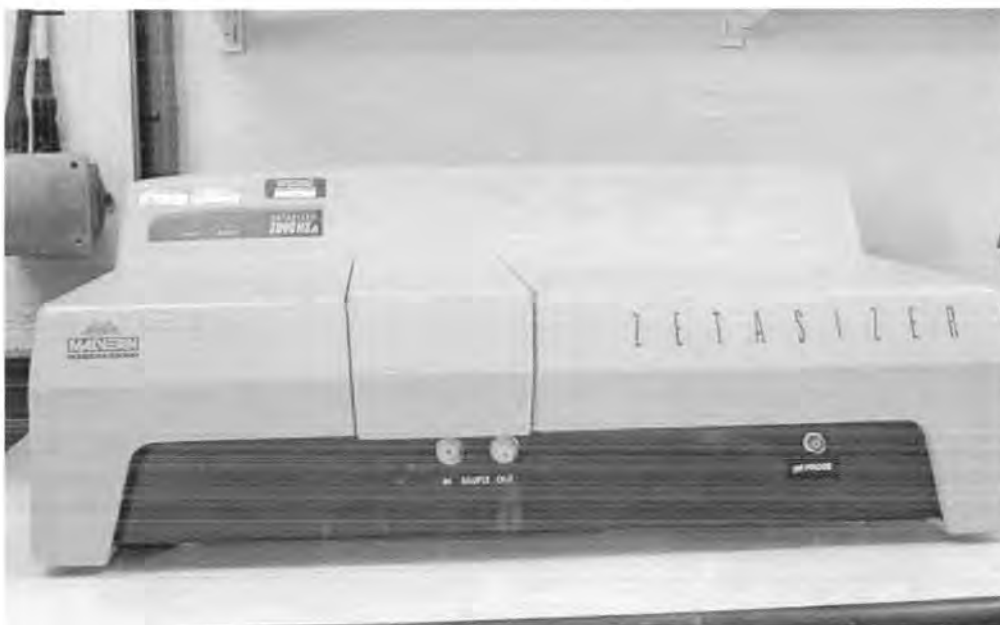


Fig 3.9 Zetasizer Malvern 3000 HAS

3.8.1 Measuring particle size:

The zetasizer Malvern 3000 HAS works according to the principles of Photon association Spectroscopy, which is the system for measuring the size of particles in range of nanometre. PCS uses monochromatic laser to measure the random movement of particles, Brownian motion, due to physical interactions with solvent molecules, which surrounds particles. The measured diameter referred how a particle diffuses within liquid; therefore it is described as hydrodynamic diameter. The size of particle

is calculated from the translational diffusion coefficient by use of Stokes-Einstein equation, which envisages that diffusion is inversely concurrent with viscosity of the medium, assuming diffusion of spherical model particles through liquid.

$$D = k_B T / 6 \pi \eta r$$

Where:

D is the translational diffusion coefficient ($\text{m}^2 \text{s}^{-1}$),

k_B is Boltzmann constant JK^{-1} ,

T is the absolute temperature (K),

η is viscosity (Pa s),

r is the hydrodynamic diameter of the spherical particle.

The translational diffusion coefficient is based on the size of particle core, concentration, surface structure and nature of ions in the medium.

In the PCS instrument the intensity fluctuations of scattered light arise from particles. In PCS the light source of monochromatic He-Ne laser with preset wavelength of 633 nm is used. Photo multiplier detects the scattered light. Fluctuations in the intensity of scattered light are converted into electrical pulses and passed to a correlator, which applies appropriate functions and data analysis are performed by the computer. The results are displayed in both graphical and tabular forms.

3.8.2 Measurement of zeta potential:

The firmness of particle dispersion is based on the equilibrium of the repulsive and attractive forces which exist between particles as they move towards one another in the suspension. If the particles have modest or no repulsion force, then aggregation, flocculation and aggregation or coalescence will eventually happen. The zeta potential value (mV) of the particles is an evaluation of interface between particles. The dividing line among stable and unstable suspension is usually taken at either +30 mV

or -30 mV. Generally the particles with zeta potential more than $+30$ mV or more negative than -30 mV are measured as stable. Zeta potential is size independent parameter. When the measurement sequence is completed by Zetasizer Malvern 3000 HAS instrument the values of zeta potential are displayed in both graphical and tabular form, similarly to the particle size measurement.

3.8.3 Sample Preparation

The samples for measurements by Zetasizer Malvern 3000 HAS instrument need to be much diluted. Choosing the correct concentration and dilution medium is important. The solvent must be clean with known refractive index and viscosity. The ultra sonification can be used for some types of samples to enhance dispersion in medium.

The samples tested for zeta potential were TiO_2 and Ag-TiO_2 nanocomposite. All specimen prior to zetasizer measurements were dispersed in distilled water (refractive index 1.33) with Triton X-100 surfactant ($\rho = 1.067 \text{ g cm}^{-3}$, Aldrich, Germany). The concentration of surfactant was 1.3×10^{-5} . The mixture was agitated in an ultrasonic bath at 50°C for 40 minutes and the resulting suspension was diluted before the measurement taken at room temperature. The concentration of TiO_2 powder in water was optimised to obtain higher value of Zeta Potential than ± 30 (mV).

Summary:

The main purpose of the project was to obtain the information about structure of TiO_2 , Ag-TiO_2 nanocomposite and to study applications of nanocomposites. Therefore the methods describes above were a source of qualitative and quantitative information. The selected methods used in the research were: TGA-DSC, SEM/EDX,

TEM, XRD, BET, UV Vis spectroscopy and particle sizer. The obtained results by the use of techniques described above are essential in making conclusions for the morphology and structure of the prepared TiO₂ and Ag-TiO₂ nanocomposite.

Results and Discussion

TiO₂ and Ag-TiO₂ Nanocomposite Synthesis

Introduction

In this chapter the results of the titania synthesized by sol gel method, morphology and microstructure of titania is discussed. Additionally the deposition of Ag onto the Titania is also described. In oxidative compound conversion photocatalyst have very low quantum efficiency which is particularly limited by the small range of solar spectrum usable for excitation. Therefore, Photocatalytic efficiency can be improved by the reduction of the particle size, doping or using co-catalyst, increasing the surface area, enhancing the photo generated electron-hole pairs and the use of a semiconductor etc.

In the current study sol gel was used to synthesise TiO₂ nanoparticles. In sol gel method the hydrolysis/condensation of a titanium alkoxide in water takes place which is very fast thus a modification of titanium alkoxides by alcohols has been used to alter the reaction reactivity of titanium alkoxides. Thus, a typical sol-gel processing of TiO₂ NPs includes the modification of an alkoxide by an alcohol (chemical modification), the hydrolysis/condensation of the alkoxide by water (generation of sols), the aging of the sols (generation of gel polymer network or gelation), and an annealing of the gels (crystallisation).

TiO₂ nanoparticles were synthesized by sol gel method and characterized by X-ray diffraction (XRD) and SEM to investigate evolution of the structure and morphology of the primary and secondary particles during the annealing process.

4.1 Synthesis of TiO₂ NPs by general sol-gel method

Dried TiO₂ samples (gels) synthesized by hydrolysis of the TIP (titanium isopropoxide) has no crystallinity before heat treatment showing that TiO₂ crystallites would not nucleate and grow without a post heat treatment, as shown in Figure 4.1 (a), however annealing the samples at 600 °C for two hours exhibited crystalline phases of TiO₂ as illustrated in Figure 4.1 (b).

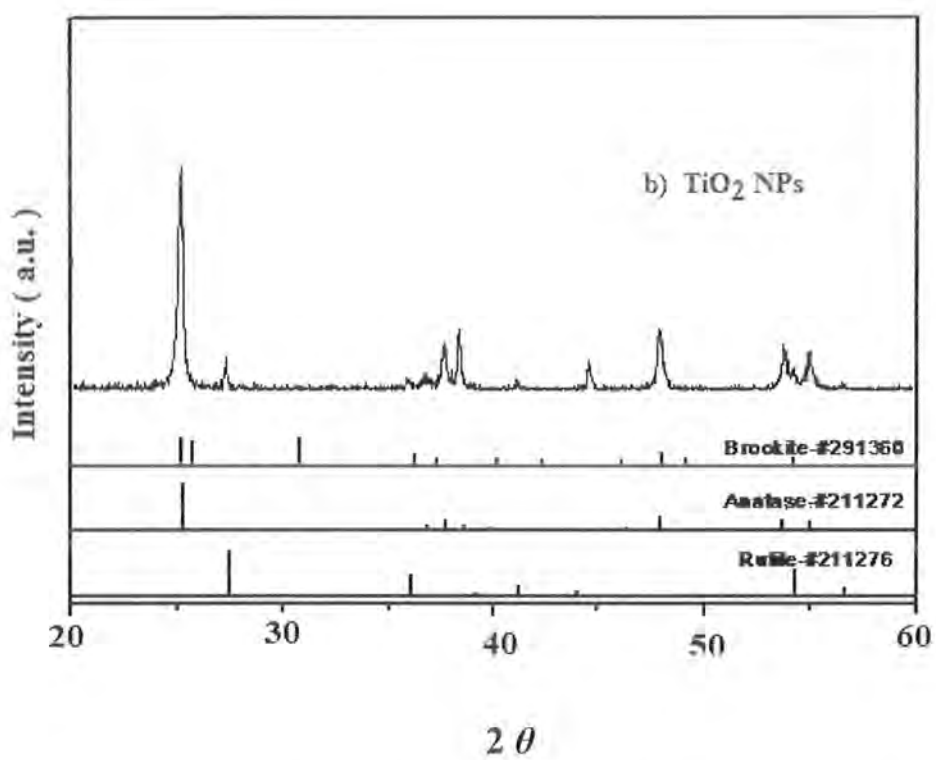
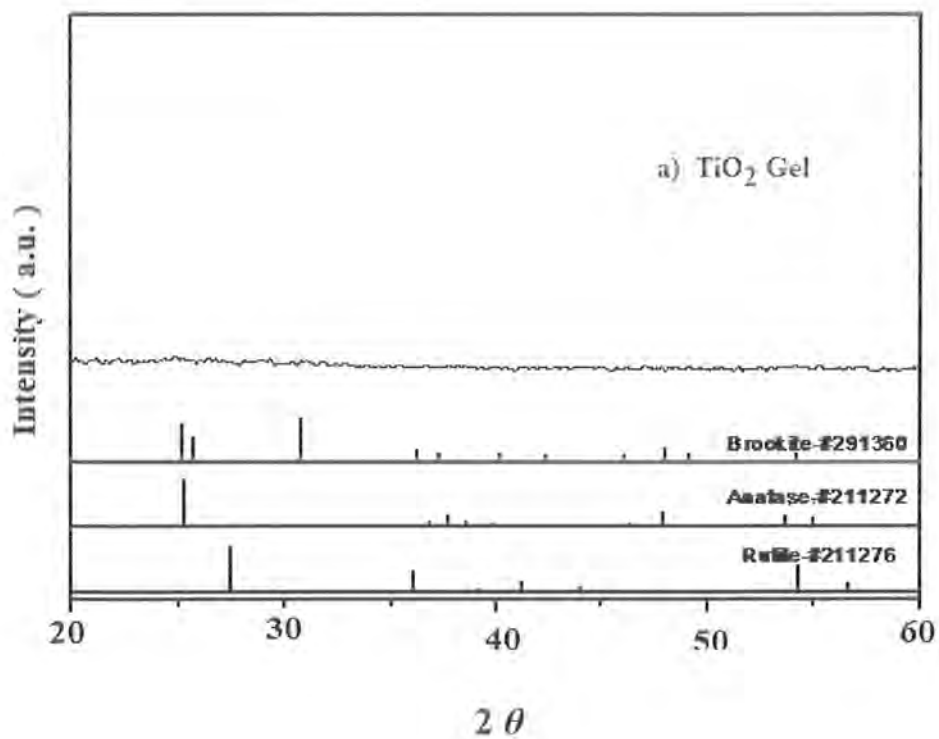


Figure 4.1 (a,b) XRD of TiO₂ synthesized via standard sol-gel method (volume ratio TIP: ethanol: water = 1:1:1)

The XRD pattern specifies that TiO₂ has mainly the anatase phase and very small amount of rutile phase with an average grain size of 10 to 20 nm which was calculated by using the full width at half maximum (FWHM) of the XRD diffraction peak using Scherrer's equation

$$L = k\lambda / \beta \cos \theta$$

where L is the particle's diameter,

λ is the X-ray wavelength, θ is the diffraction angle,

β is the FWHM of the (101) diffraction peak and

k is the Scherrer's constant

(k = 0.89 for FWHM).

Scanning Electron Microscopy (SEM) images exhibited near spherical TiO₂ particles which are adhered and have a mean size about 1.02 $\mu\text{m} \pm 36$ (Figure 4.2a). High magnification image (90,000X) indicates TiO₂ secondary particles are composed of primary nanoparticles with a size of 18 \pm 6 nm (Figure 4.2b). It is imperative to note that the primary particle size is close to the average grain size estimated from XRD which implies the majority of the primary particles are nearly single crystalline.

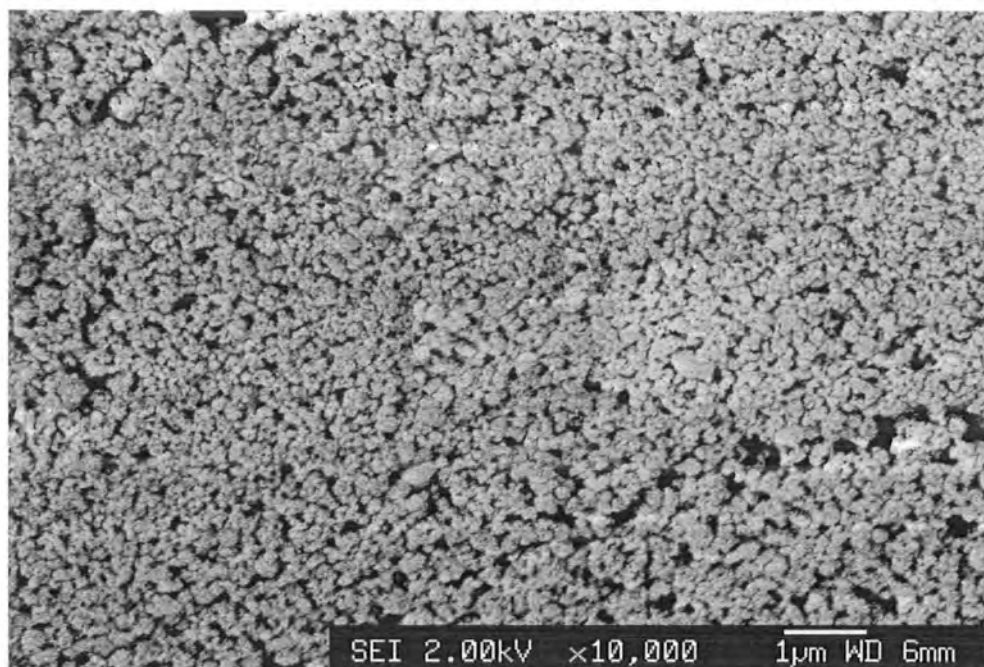


Figure 4.2 (a)

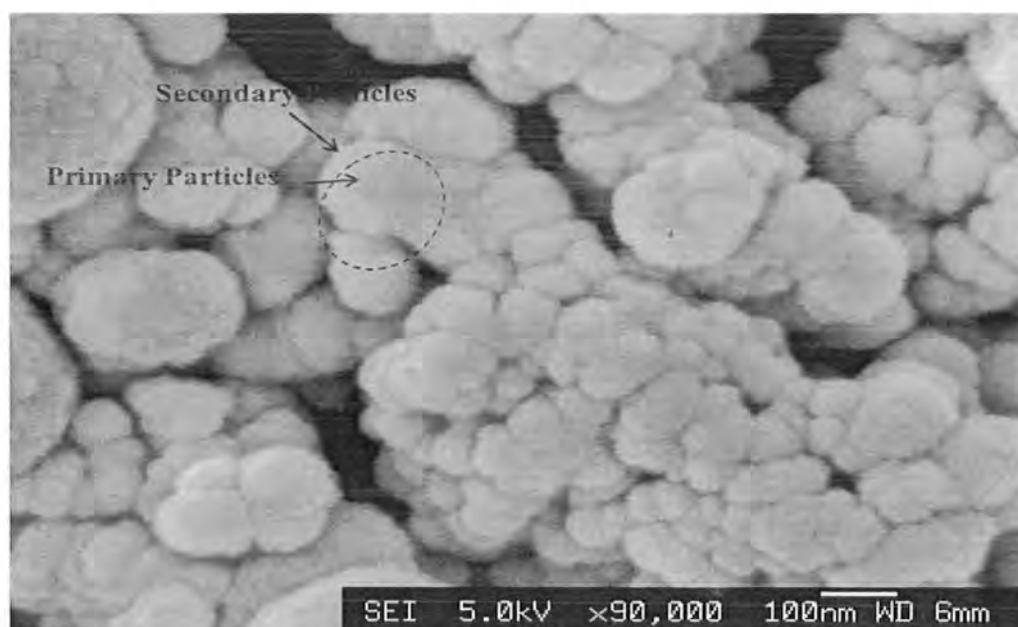


Figure 4.2 (b)

Figure 4.2 SEM images of TiO_2 NPs synthesised by standard sol-gel method (volume ratio TIP: ethanol: water = 1:1:1) at pH=7 (a) 10,000X (b) 90,000X.

The result from SEM and XRD infers that the sol gel method synthesised amorphous primary particles which aggregate into secondary particles. The TiO₂ crystallites or grains appear at around 100 °C and crystallisation of TiO₂ arises at the amorphous primary particles. In this study the amorphous TiO₂ gel particles (bigger sol particles) were composed of (Ti-O-Ti-OR)_n molecules which are generated from the hydrolysis/condensation process.

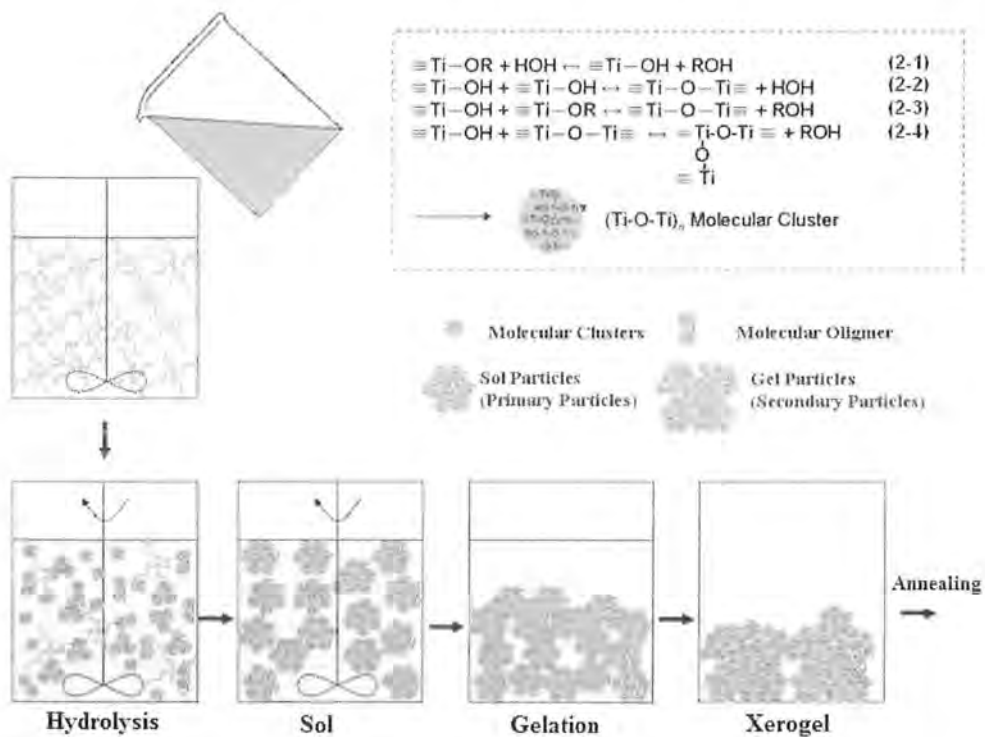


Figure 4.3 Standard Sol-Gel Synthesis of TiO₂ NPs

Figure 4.3 exhibits the schematic synthesis of TiO₂ by general sol-gel process. When water is added into TIP, (Ti-O-Ti-OR)_n molecular clusters are first generated through the hydrolysis/condensation process and form particulate sols and gels

(equation 2-4 in Figure 4.3). The primary particles are formed from the annealed sol particles that are generated from the union of molecular clusters and the primary particle size is dependent on the hydrolysis/condensation and chemistry of the solution. The size of the secondary particles, which are formed from the union of primary particles relates to the dimension of gel particles that is determined by the parameters in the gelation stage and interaction between colloidal particles (D.Vorkapic et al. 1998). In the sol gel procedure the hydrolysis and condensation occur at the near surface region where $(\text{Ti-O-Ti-OR})_n$ monomers were generated and diffuse into the TIP phase, as shown in Figure 4.3. Thus, the sol formation and gelation processes are based on the random collision of the molecular clusters and primary particles respectively. Figure 4.4 gives FEGSEM images of a TiO_2 sample prepared by hydrolyzing pure TIP (Titanium isopropoxide) via the sol gel method. The sample dried at room temperature shows that TiO_2 presents secondary particles which are composed of primary particles.



Figure 4.4 TiO_2 gel particles dried at room temperature

4.1.1 XRD and FEGSEM Analysis

Microstructure and morphology of the primary and secondary particles during the annealing process was studied by XRD and FEGSEM analysis. FEGSEM analysis of TiO₂ particles is displayed in Figure 4.5 which exhibits the microstructure of the particles during the annealing process. This analysis shows that TiO₂ secondary particles have irregular shape and no significant changes in the morphology have taken place throughout the annealing process.

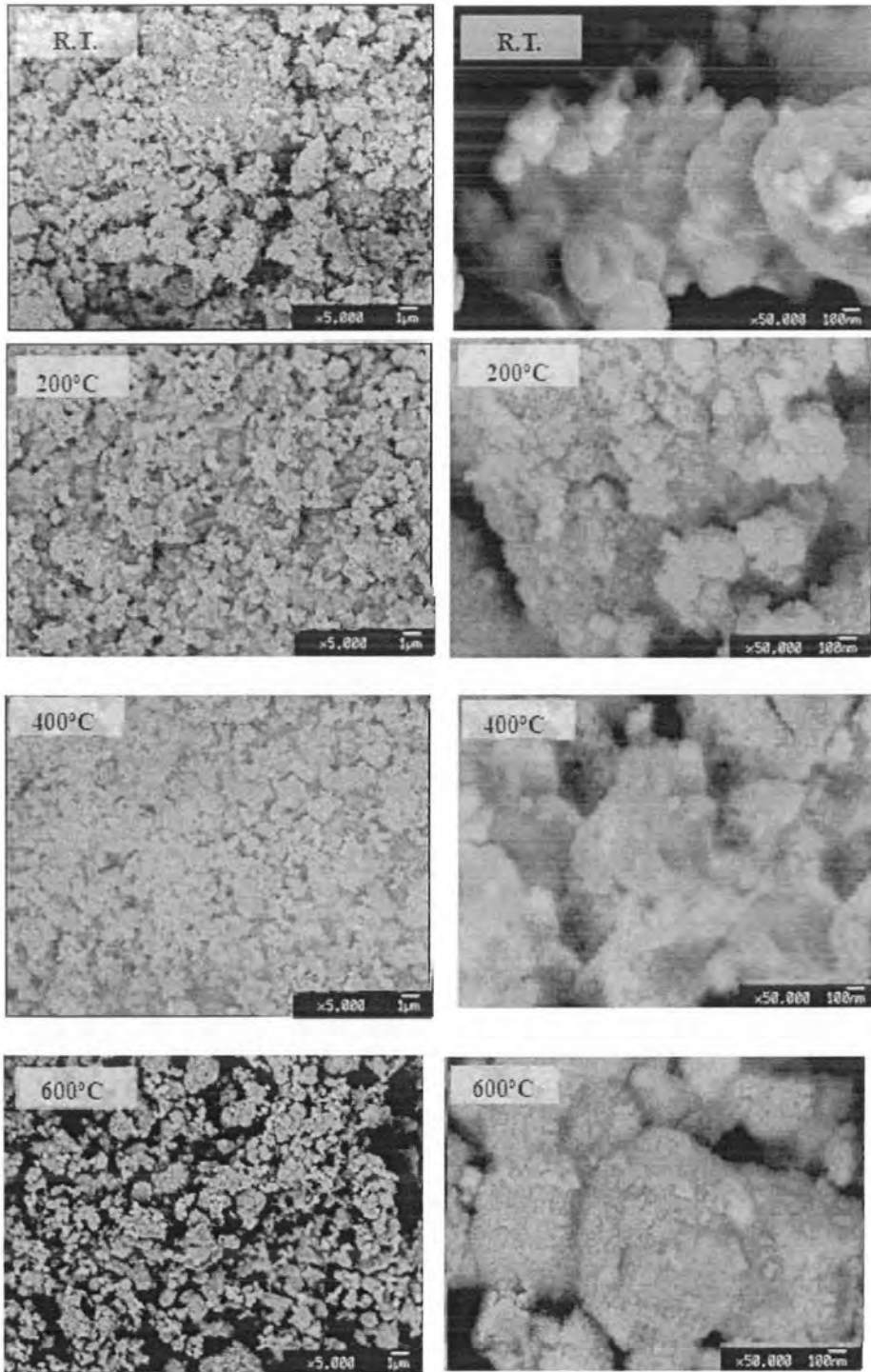


Figure 4.5 FEGSEM analysis of TiO_2 synthesized by pure TIP.

The primary and secondary particles at room temperature showed uniformity and are $14 \text{ nm} \pm 14 \%$ and $1.3 \text{ }\mu\text{m} \pm 28 \%$ respectively. Additionally, there is no significant change in the size up to the temperature $500 \text{ }^\circ\text{C}$ which is most probably due to no sintering event of TiO_2 at $400 \text{ }^\circ\text{C}$. Therefore these particles are able to keep their original size. However, at $600 \text{ }^\circ\text{C}$ both primary and secondary particles enlarge rapidly since the sintering event can cause grain growth. There is a minor decrease in size at $100 \text{ }^\circ\text{C}$ which might be attributed to the elimination of organic compounds. It also resulted in the smaller particle due to shrinkage or cleavage of large particles (Figure 4.5).

XRD data illustrates that no crystalline phase is observed before the annealing process while the anatase appears at $100 \text{ }^\circ\text{C}$ (Figure 4.6). After heat treatment at $600 \text{ }^\circ\text{C}$ for a period of 10 hours it is partly transformed into rutile. Therefore, the final result is a mixture of rutile and anatase.

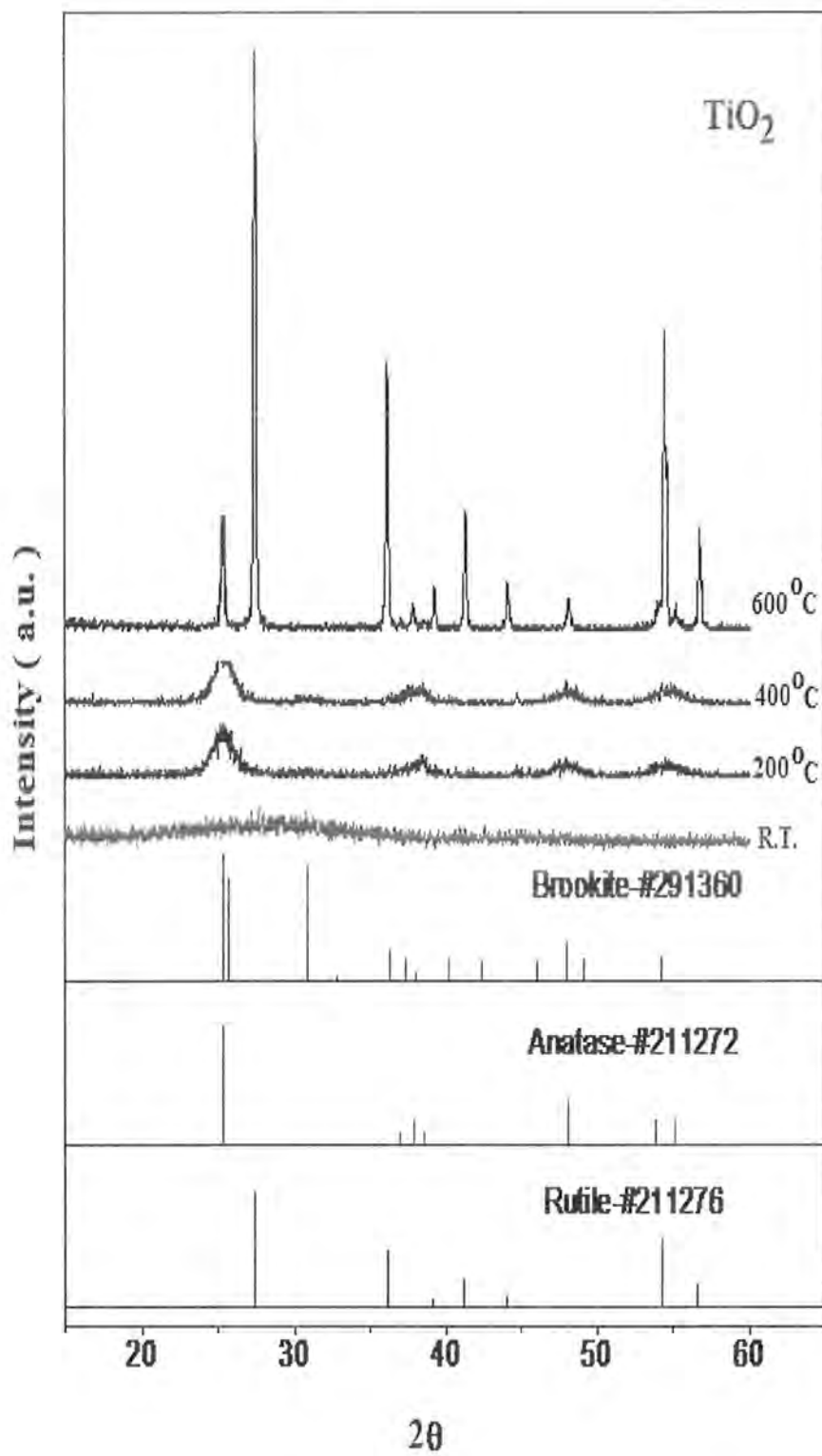


Figure 4.6 XRD of TiO₂ prepared by sol gel

Conversely, TiO_2 grain size, do not match to the size of primary particles which was 5nm and then gradually increased to 8nm at 500 °C. It is worth noting that 8 nm is still smaller than that of primary particles so the grain growth observed in XRD below 400 °C is ascribed to the crystallisation of TiO_2 rather than sintering. At 600 °C, the grain size (calculated by X-ray diffraction) is approximately same as the primary particles size (estimated by FEGSEM), entailing the primary particles become nearly single crystals (Figure 4.6). Hence further heat treatment would result in the grain growth or coarsening between primary particles via the sintering process and the primary particles disappears after annealing at 600 °C. XRD data (Figure 4.7 a, b), revealed that the grain growth above 600 °C is caused by the inter particle coalescence of the primary particles.

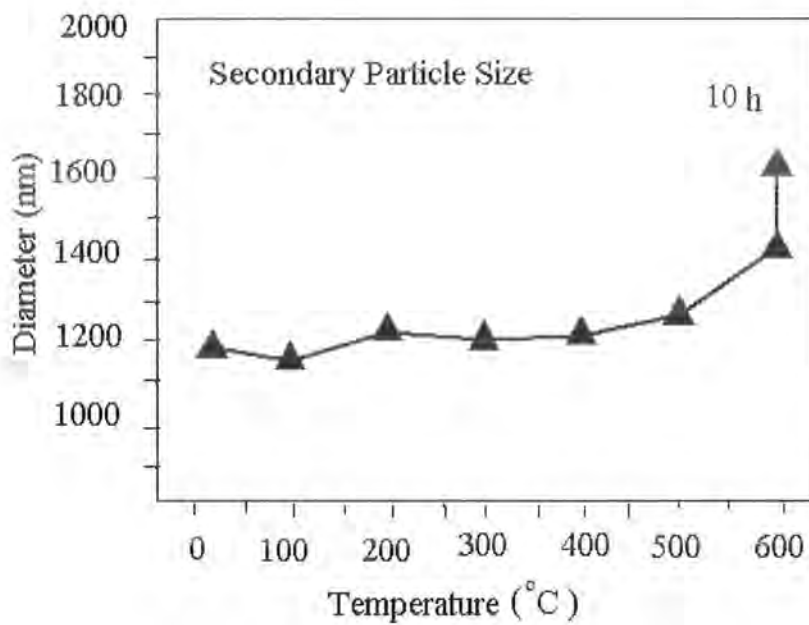
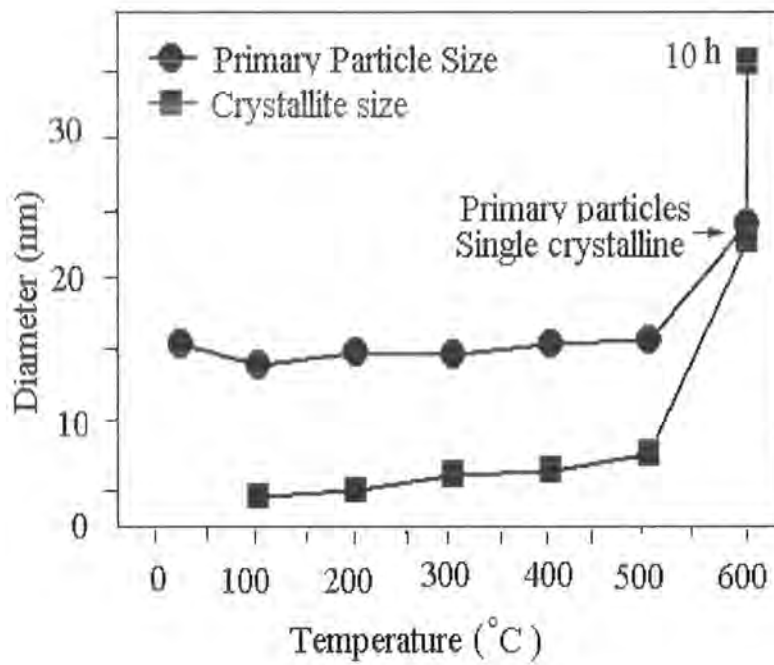


Figure 4.7 (a) Size variations of primary particles (estimated from FEGSEM) and crystallites (estimated from XRD) (b) Secondary particles (estimated from FEGSEM)

In the light of the above results, the growth of TiO₂ could be illustrated graphically by Figure 4.8 which describes that TiO₂ crystallites nucleate at the primary particles, which are generated from the hydrolysis/condensation process, and further develop with increasing temperature. When the temperature is high enough, the primary particles become a single crystal and the grain growth would continue via sintering by the normal process with further heat treatment.

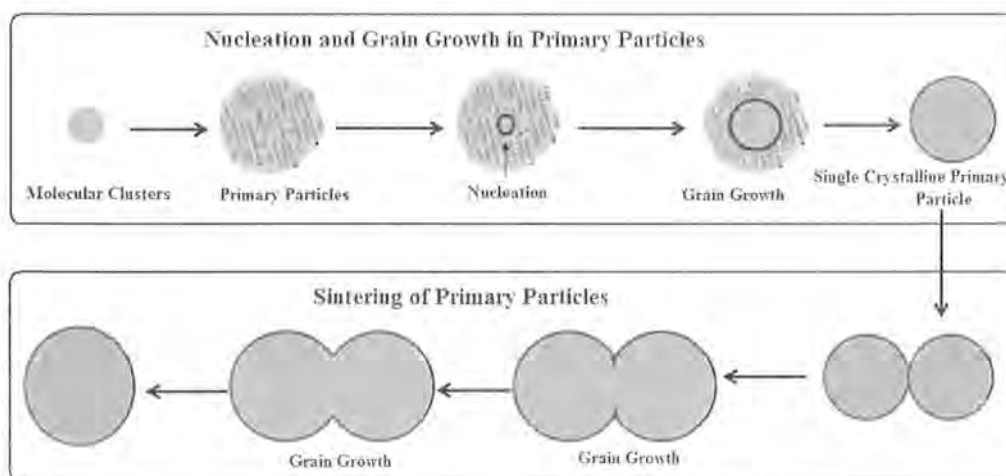


Figure 4.8 Nucleation and growth of TiO₂ in primary particles

In the current study, the aggregation of the primary particles and growth contribute the size enlargement of the secondary particles. An increase in the temperature improve the morphology of the TiO₂ nanoparticles which become more spherical, smaller and denser (Fig 4.8) which might be because of the inward force of the alcohol and is increased by the increase amount of alcohol which induces the chemical bonding.

Variation of the TiO₂ secondary particles is given in Figure 4.6. The TiO₂ secondary particles size has no significant change at the lower temperatures in the annealing process, but readily increases as the temperature is above 500 °C. This

implies the sintering process plays a more important role for the enlargement of the secondary particles.

4.1.2 Influence of ethanol on the microstructure and morphology of TiO₂ NPs

Generally alcohols such as ethanol is used to dilute TIP for reducing the hydrolysis rate, though, it has been observed that alcohols can affect the morphology and size of TiO₂ secondary particles. Influence of ethanol on the NPs morphology is examined in this study. The formation of TiO₂ NPs is based on the interaction between colloids. Hence, effect of ethanol on the aggregation of the primary particles can be exclusively examined.

The morphology of the TiO₂ is notably changed by the addition of the ethanol (Figure 4.9). The size of TiO₂ secondary particles increase from $1.2 \mu\text{m} \pm 42 \%$ to about $1.7 \mu\text{m} \pm 38 \%$ with the addition of volume ratio TIP/ethanol = 5/1. The alcohols cause an aggregation of the primary particles into large secondary particles. It has been recommended that alcohols destabilise the colloidal solution and enhance the rate of re-aggregation because alcohols decreases the dielectric constant of the solvent that correlate with the zeta potential of TiO₂ (H K Park et al. 1997).

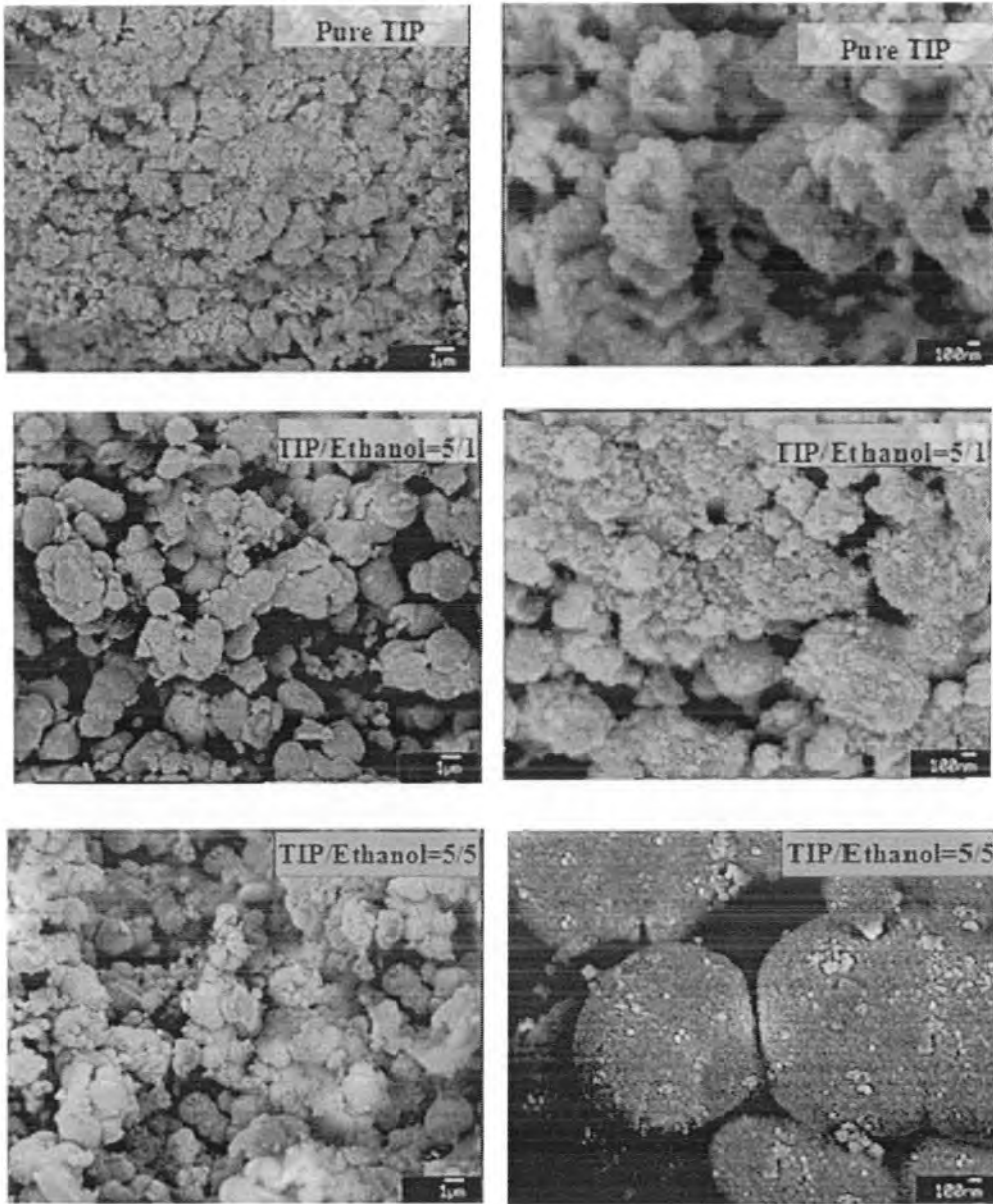


Figure 4.9 FEGSEM images of TiO₂ NPs synthesised by ethanol-stabilised TIP (volume ratio TIP/ethanol = 5/0, 5/1, and 5/5). The samples are annealed at 150 °C/1h, 400 °C/1 hour with heating rate of 10 °C/min.

Furthermore, with increasing the concentration of ethanol the primary particles become denser on the secondary surface (Figure 4.9). The secondary particles steadily become spherical hence suggesting that alcohol aid merging of the primary particles. Therefore, this event is coupled with an enhancement in the secondary particles surface tension, and hence leads to the reduction of surface area. This inward force may relate to the inter-particles pull between the primary particles, which could be attracted to each other and pull inwards the secondary particles. At higher TIP/ethanol = 5/5, the ethanol molecules induced physical or chemical bonding thus the secondary particles have smaller size ($1.28 \mu\text{m} \pm 28 \%$) (Figure 4.9).

Figure 4.10 gives a temporal analysis of FEGSEM images of the TiO_2 secondary particles from ethanol-stabilised TIP (volume ratio TIP/ethanol = 5/1). TiO_2 is amorphous before an annealing process is carried out and at 100°C the TiO_2 crystallites appear as ethanol molecules offer coordinative binding to the anatase TiO_2 surface which might lead toward the crystallisation. Ethanol is removed at a higher temperature (200°C) by vaporisation (Figure 4.10) so the crystallites grow rapidly. The surface details of the secondary particles can be clearly seen in Figure 4.10, which demonstrate that due to the aggregation of the primary particles the sinter-like structure has already appeared at room temperature. This is comprehensible because the heat flow is transported via the surface and thus the sintering would undergo through the surface region. This event eliminates the solid-gas interface associated with the surface energy and therefore reduces the surface energy of the particles.

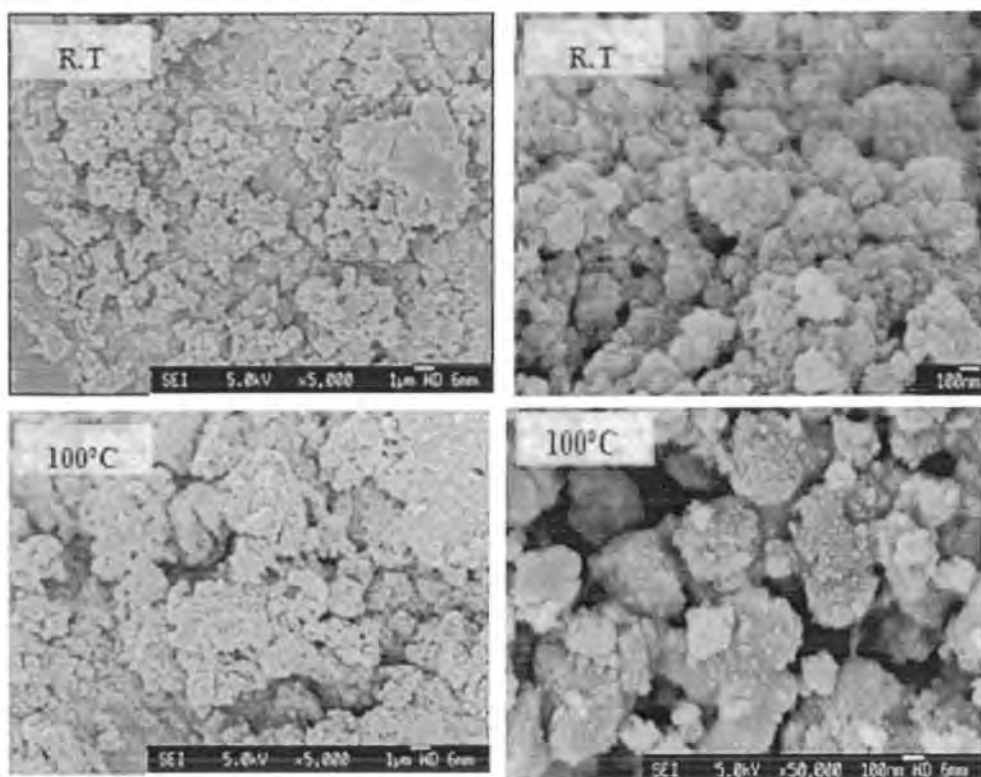


Figure 4.10 Analysis of FEGSEM of TiO₂ synthesised by ethanol-stabilised TIP

The sintering process plays a critical part in the enlargement of the secondary particles as there is no significant change at the lower temperatures in the annealing process but above 500 °C there is a rapid increase in the secondary particle size. The primary particles from ethanol-stabilised TIP become nearly single crystalline at around 600 °C. The sintering event at the near surface region may cause a rapid increase in size if the particles have dense packing thus sintering event at the contact between the primary particles can lead to coalescence of the primary particles as well as the secondary particles. This surface sintering may be the result of the size enlargement above 500 °C, as shown in Figure 4.11 and implies that the TiO₂ particles size is dominated by the packing of the primary particles, which is determined prior to the sintering process, is conducted.

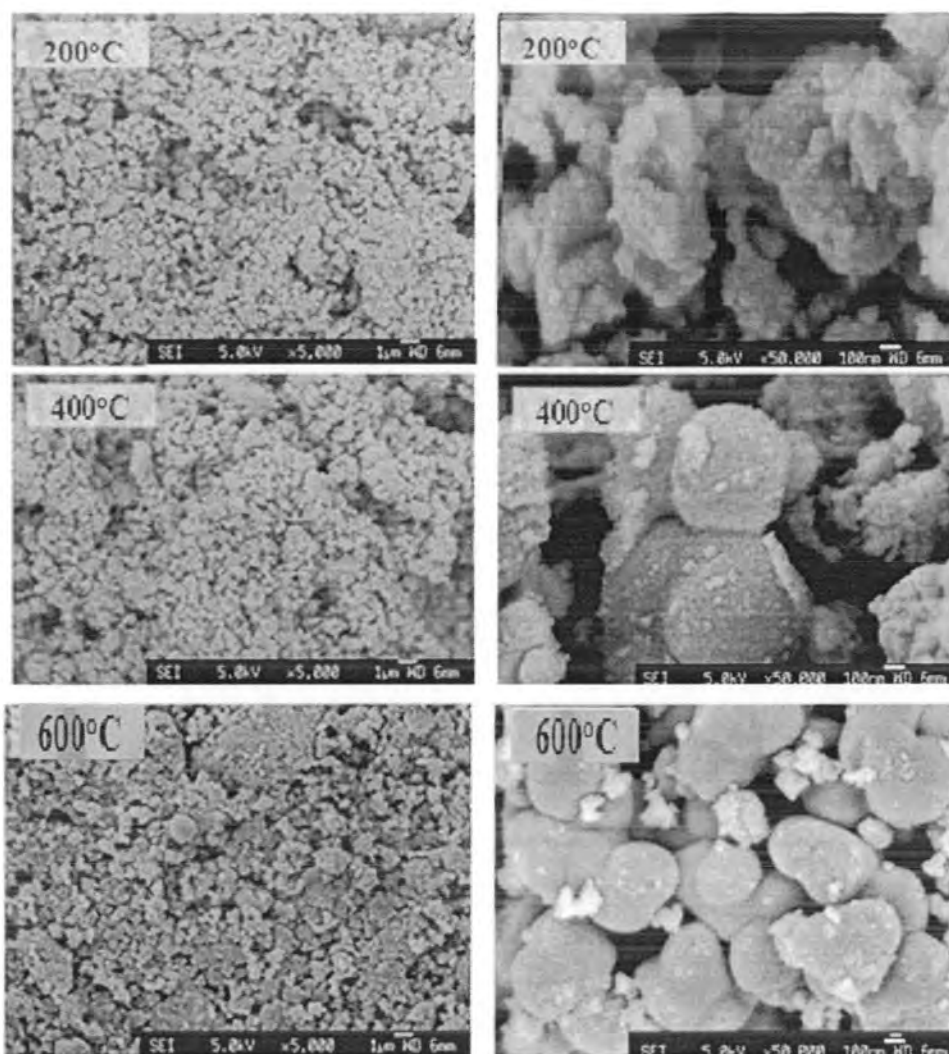


Figure 4.11 Analysis of FEGSEM of TiO_2 synthesised by ethanol-stabilised TIP.

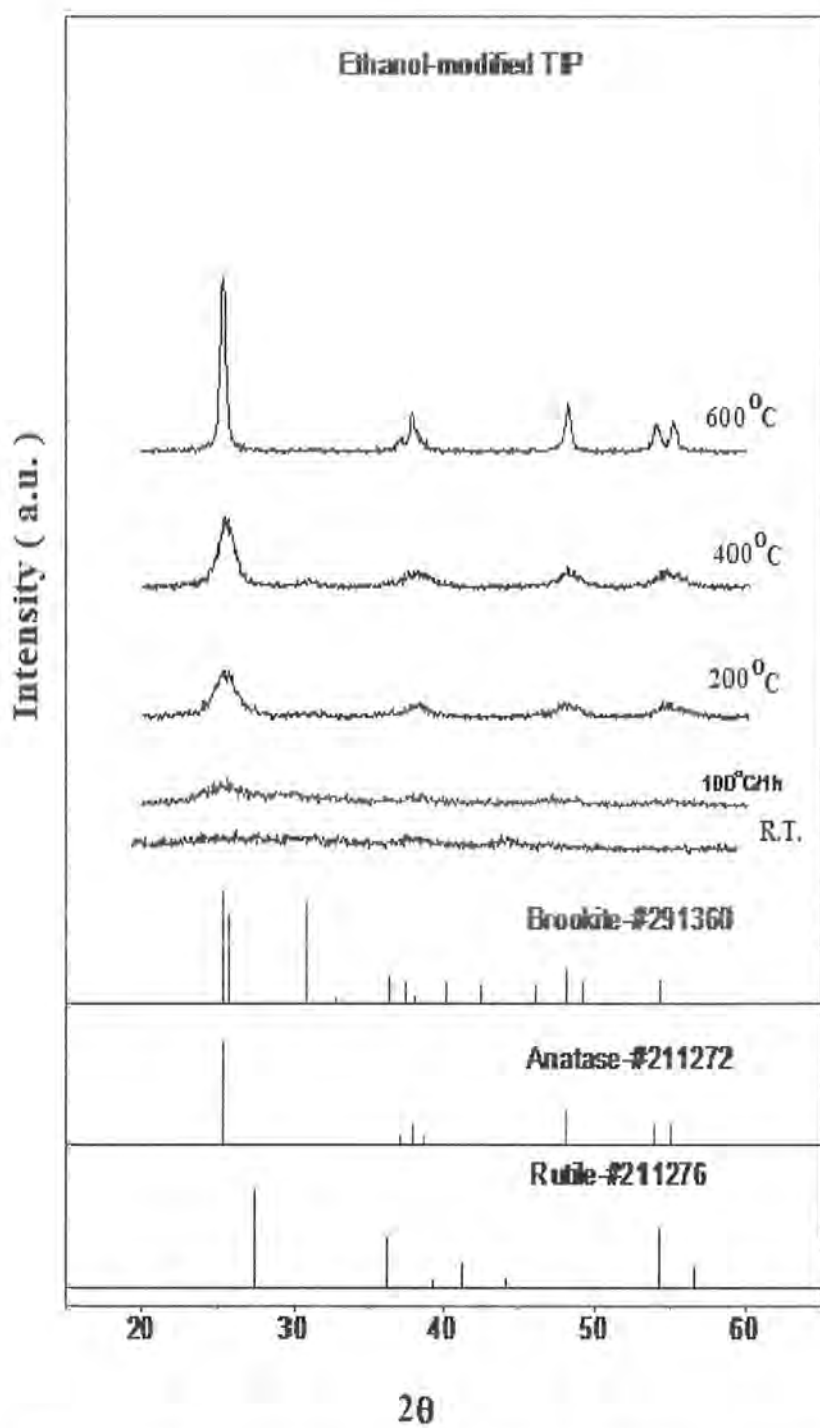


Figure 4.12 Temporal analysis of XRD for TiO₂ NPs prepared by ethanol-stabilised TIP. (Volume ratio TIP/methanol = 1/0.1, aged 8 hours).

Therefore, the experimental results proposed that TiO₂ Nanoparticles are secondary particles composed of primary particles, which are amorphous before an annealing process is performed. At 100 °C Crystalline phase of TiO₂ appears and have a similar size to the primary particles at 600 °C in the annealing process, entailing primary particles become single crystalline particles. The addition of alcohol exhibited to aid aggregation and packing of the primary particles which result in a rapid size enlargement at a high temperature.

4.2 Preparation of Ag-TiO₂ Nanocomposite

Introduction:

To improve the photocatalytic response of TiO₂ by enhancing the separation of electron-hole pairs, numerous methods including doped and composite structures, such as transition metal based NiO, Fe³⁺ and Ni²⁺ (Li XZ et al. 2001; Yu JG et al. 2000; Ihara et al. 2003) or non-metal based nitrogen, PEG, n-TiO₂, sulphur and carbon (Nakamura et al. 2005; Bura et al. 2003; Khan Sum et al. 2002; Ohno T et al. 2004) doped TiO₂ and dye (methyl orange, formaldehyde, rhodamineB (RhB) (Liu G et al. 2000; Zhang et al. 1998) or metal complex (2,2'-bipyridine, 4,4'-diethylester-2, 2'-biquinoline) (Hoertz et al. 2002) sensitized TiO₂ have been developed. So far, it has been shown by many researchers that the modifications of TiO₂ nanoparticles by surface impregnation with noble metals such as Au, Pt and Ag is one successful way to improve the photo catalytic activity of TiO₂ (Chan S et al. 2005; Keller et al. 2003; Kumar et al. 2009) . A noble metal deposited on TiO₂ can play the role of mediating some of the electrons away from TiO₂ surface and preclude them from recombination with holes. Noble metal nanoparticles promote electron transfer processes and provide a way to enhance the photo efficiency of the semiconductor (Toshima et al. 200).

Among the noble metals, TiO₂ nanocomposite, Ag-TiO₂ is well known because it has strong catalytic and antibacterial abilities (Kumar et al. 2009). Surface modification of TiO₂ with noble metal like Ag has been reported to decrease the electron-hole recombination problem (Schmid et al. 1994). Ag-doped or Ag-based nanocomposites have been reported to extend photo absorption in the visible range when present in sufficient amounts.

Previous studies have also shown that the addition of silver can enhance photocatalytic activity of TiO₂. For example Kato et al. (Kato et al. 2005) reported that photo-deposition of Ag on a TiO₂ film enhanced photo catalytic degradation of gaseous sulphur compounds and suggested that Ag acted as a co-catalyst. Hu et al. synthesized Ag/AgBr/ TiO₂ by the deposition-precipitation method and found that it can photo degrade azodyes effectively. They also demonstrated that Ag⁰ species probably enhance the electron-hole separation and interfacial charge transfer on the surface of the catalyst (Chun et al. 2006). Sokmen et al. (Sokeman et al. 2001) revealed that addition of AgNO₃ to anatase TiO₂ enhanced the photocatalytic activity and enhanced the killing of *E. coli* in suspension. Kumar et al. demonstrated the synthesis of Ag-TiO₂ nanocomposite by solution impregnation method (Kumar et al. 2009) and at 4 % loading the nanocomposite had enhanced photokilling ability in water. Hirakawa et al. synthesized Ag-TiO₂ clusters and demonstrated that the photo induced electrons on TiO₂ can be injected into Ag core accompanying the Ag surface plasmon peak blue-shift (Hirakawa et al. 2005). Ag-TiO₂ particles are typically prepared by solution impregnation, deposition-precipitation, (Brook et al. 2007) sol-gel or photodeposition method.

There has been no systematic study reporting on the effect of synthesis technique on the morphological development of Ag and TiO₂ nanoparticles. In this

work, we prepared TiO₂ nanoparticles using simple sol-gel method using procedures described earlier (Kumar et al. 2009), followed by photo deposition of Ag nanoparticles from aqueous AgNO₃ maintained at different pH values in the sol. An appropriate amount of NaOH or HCl was added in order to control the pH value of the AgNO₃ solution containing the titania sol. It is also aimed to find the conditions for anchoring Ag nanoparticle to TiO₂ nanoparticle and evaluate the size ratio between Ag and TiO₂ nanoparticles and the number of Ag particles per titania particle. This knowledge can be exploited for optimizing the Ag-TiO₂ nanocomposite morphology for a given photocatalytic application.

Microstructure and morphology of the nanocomposite samples were investigated by using a series of techniques such as X-ray diffraction (XRD), scanning electron microscopy (SEM), Brunauer-Emmett-Teller (BET) surface area measurements and UV-Vis spectroscopy. The influence of pH on the morphology and properties is discussed.

TiO₂ nanoparticles prepared by sol gel method were coated with Ag by photo deposition from an aqueous solution of AgNO₃ at various pH levels ranging from 1 to 10 in a titania sol, under UV light. The as-prepared nanocomposite particles were characterized by UV-Vis absorption spectroscopy, transmission electron microscopy (TEM), X-ray diffraction (XRD) and N₂ adsorption/desorption method at liquid nitrogen temperature (-196° C) from Brunauer-Emmett-Teller (BET) measurements. It is shown that at a Ag loading of 1.25 wt% on TiO₂ a high surface area nanocomposite morphology corresponding to an average of one Ag nanoparticle per titania nanoparticle was achieved. The diameter of the titania crystallites / particles were in the range of 10 - 20 nm while the size of Ag particles attached to the larger titania particles were 3±1 nm as deduced from crystallite size by XRD and particle

size by TEM. Ag recovery by photo harvesting from the solution was nearly 100 %. TEM micrographs revealed that Ag-coated TiO₂ nanoparticles showed a sharp increase in the degree of agglomeration for nanocomposites prepared at basic pH values, with a corresponding sharp decrease in BET surface area especially at pH > 9. The BET surface area of the Ag-TiO₂ nanoparticles was nearly constant at around a value of 140 m² g⁻¹ at all pH from 1 - 8 with an anomalous maximum of 164 m² g⁻¹ when prepared from a sol at pH of 4, and a sharp decrease to 78 m² g⁻¹ at pH of 10.

4.2.1 CHARACTERIZATIONS

Energy Dispersive X-ray spectroscopy (EDX) analysis was done for the elemental composition of the nanocomposite. X-ray diffraction (XRD) pattern for the structure of powder was recorded on a Philips X'pert diffractometer equipped with a CuK α radiation source (λ 1.541 80 Å). The process of Ag-TiO₂ nanoparticles impregnation was accurately monitored by a Perkin Elmer Lambda25 UV spectrophotometer at different pH values ranging from 1 to 10. TEM images were recorded on the JEOL 200CX, which is a 200kV analytical TEM/STEM (Transmission Electron Microscope/ Scanning Electron Microscope. For TEM studies the samples were prepared by placing a drop of aqueous Ag-TiO₂ nanoparticles dispersion on a piece of carbon-coated copper grid under ambient conditions.

Sample powders were also characterized for their specific surface area by using N₂ adsorption/desorption method at liquid nitrogen temperature (-196 °C) from Brunauer–Emmett–Teller equation (BET) at 77.3K using a Micromeritics Tristar 3000 analyzer. Prior to BET measurement, powders were degassed for 24 h at 90 °C under a pressure of 0.1 Pa. To prevent any possible crystallization during outgassing, higher drying temperature was avoided.

4.2.2 X-ray Diffraction (XRD)

Figure 4.13 shows the X-ray diffraction (XRD) of pure TiO₂ nanoparticles and the (1.25-wt %) silver loaded TiO₂ nanocomposites. In the XRD pattern, a peak at $2\theta = 25.3^\circ$ matching with the (101) peak and $2\theta = 55^\circ$ corresponding to (211) peak of anatase can be observed (ICSD Reference code: 03-065-5714). After photodeposition of Ag, an additional peak at 2θ near 38° arises, this can be assigned to Ag (111) planes. This Ag peak which is subsumed within the TiO₂ peaks at $2\theta = 37.8^\circ$, 38.1° and 38.6° (Pettibone et al. 2008; Rupa et al. 2007) gives evidence for successful photoreduction of Ag ions into metallic form. The ratio of peak intensity between the 38.1 and 38.6 reflections are higher in the Ag-TiO₂ nano-composite material in comparison with the pure single phase TiO₂ peaks. Despite the relatively low concentration of Ag at 1.25 wt % (corresponding to only 0.57 volume % arising from density difference), it is quite surprising to be able to detect the presence of Ag by XRD, suggesting presence of clusters of Ag on surface increasing XRD reflections from Ag. No others peaks of secondary phases containing Ag were detected (Figure. 1). The average crystallite sizes of titania and Ag in the sample were evaluated by the Scherer equation applied to the XRD data: $d = k\lambda / \beta \cos\theta$, where λ is 1.54 \AA corresponding to irradiation wavelength, k is a coefficient 0.9, β is the full width at half maximum (FWHM) of strongest line and θ is the Bragg diffraction angle at the peak maximum. Surface area measurements were made for the composites synthesized at different pH values. Both the crystallite sizes (d) and surface areas corresponding to varying pH values are shown in Table 4.1. The results indicate that at all pH values of photo reduction, Ag particles are crystallized and formed in the nanometer range. The calculated crystallite sizes of TiO₂ and Ag were found to be in the range of $13 \pm 6 \text{ nm}$ and $3 \pm 1 \text{ nm}$ respectively.

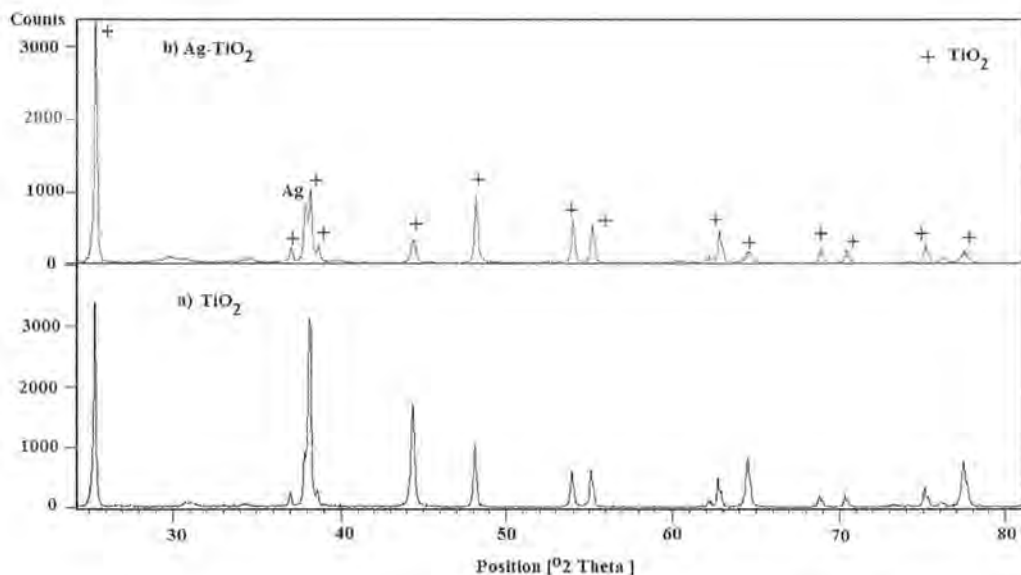


Figure 4.13 XRD Patterns of a) TiO₂ b) Ag-TiO₂ nanocomposite

4.2.3 Brunauer–Emmett–Teller (BET) Surface Area:

Table 4.1 shows the BET surface area data for the Ag-TiO₂ nanocomposites corresponding to the different pH values. It can be observed that the BET surface area of Ag-TiO₂ is mostly constant with increasing pH values at around 140 m² g⁻¹ with an anomalous peak of 164 m² g⁻¹ at pH 4 and then as we move towards higher pH the BET surface area decreased to 135 m² g⁻¹ at pH 9 and then at the highly alkaline pH of 10, the surface area decreased sharply to a much lower value of 78 m² g⁻¹.

It was observed that while the calculated crystallize size of TiO₂ (from XRD) did not change much with pH, the surface area decreased with increasing pH (Li et al. 2004; Riboh et al. 2003). The trend of decreasing surface area is due to the agglomeration of the nanoparticles as can be seen by imaging. At pH 10, a relatively steep drop in surface area shows the highest degree of agglomeration of the nanoparticles. As shown in Figure. 4.14, the nano pore size is more or less constant at all pH values and not affected by agglomeration.

Table 4.1 BET Surface Area, Crystallite size (XRD) of Ag-TiO₂ nanocomposite

Sample pH	BET Surface Area (m ² g ⁻¹)	Crystallite Size (nm)
pH 1	142	10
pH2	145	12
pH3	147	14
pH4	164	11
pH5	137	13
pH6	137	12
pH7	145	10
pH8	134	11
pH9	135	10
pH10	78	15

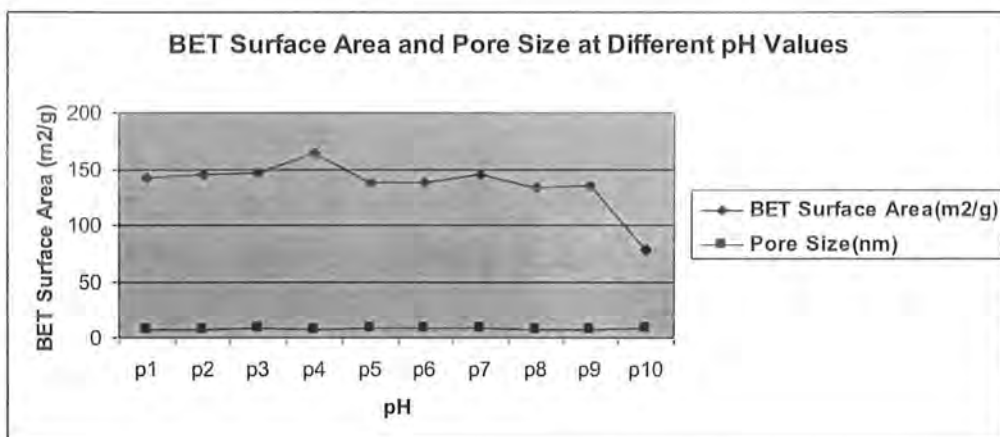


Figure 4.14 BET Surface area and pore size of Ag-TiO₂ nanocomposite

4.2.3 UV Visible Spectroscopy

UV-Visible absorption spectroscopy data of Ag-TiO₂ nanocomposite is displayed in Figure. 4.15. In this study as the concentration of Ag in the nanocomposite was very low (1.25 wt %) and the particle size was very small and did not display any visible absorption (Kumar et al. 2009; Sugimoto et al. 2002). At the

1.25 wt % loading and for the morphology observed, there was no sign of any Ag plasmon resonance. The Ag-TiO₂ nanocomposite did not show any change in the UV-vis spectra when compared with pure TiO₂ (Figure. 4.15). Due to the small crystallite size (3±1nm) and the lower Ag concentration this is possibly insignificant in effect (Kumar et al. 2009). It is also obvious from the literature (Sugimoto et al. 2002; Brook et al. 2007) that the UV-vis absorption spectra density depends on the starting AgNO₃ concentration and absorption intensity in the visible range of the synthesized Ag-TiO₂ nanocomposite increases with the increasing AgNO₃ concentration.

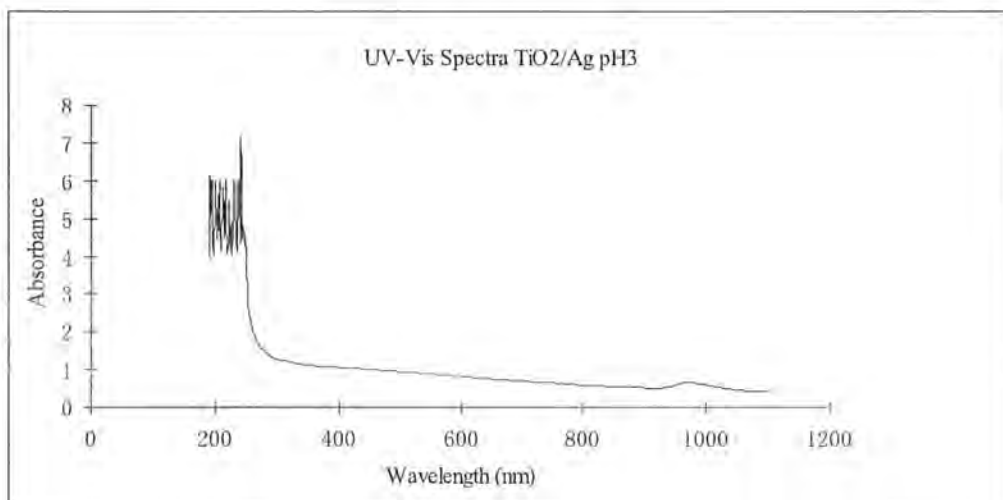


Figure 4.15 UV-Vis Spectra of Ag-TiO₂ photosynthesised at pH=3

4.2.4. Transmission Electron Microscope (TEM):

Transmission electron microscope (TEM) pattern of the Ag-TiO₂ prepared at pH 3 is presented in Figure.4.16, and the corresponding EDX spectrum from TEM is shown in Figure 4.17. The TEM result indicates that mono-dispersive and highly crystalline Ag-TiO₂ nanocomposite was obtained. The particles are near spherical with relatively narrow size distribution. The average particle size of primary TiO₂ and Ag nanoparticles as calculated from the TEM correspond 18±6 nm and 3±1nm

respectively which is very close to the results for the crystallite size calculated from the X-ray diffraction (XRD) patterns using the Scherer equation, with the TEM image indicating a slightly larger average primary particle size. The much smaller spherical Ag nanoparticle is anchored on the surface TiO₂ nanoparticles which are 6 times larger in size. The Ag nanoparticles did not coat the TiO₂ on the whole surface but are adhered at some locations in nanoclusters such that on average we observe one Ag nanoparticle for each TiO₂ nanoparticle. From calculations based on the stoichiometry, and average particle size as observed, the ratio of Ag to TiO₂ is estimated at 1:1 (i.e. 1 Ag particles of 3 nm diameter for every 18 nm titania particle), in good agreement with the results from the TEM images. These results show that Ag recovery by photo harvesting is nearly 100 %. Many of the TiO₂ crystals are also seen as loosely agglomerated into large particles of 40 - 100 nm typically, the degree of this agglomeration relating to the value of BET surface area of a given sample. The value of pH used during photosynthesis of the composite can clearly affect the degree of agglomeration of the composite nanoparticles.

The results of EDX studies are shown in Figure 4.17, which provide additional confirmation for the presence of Ag on the surface of a TiO₂ nanoparticle. With consideration to Ag peaks which are observed in EDX pattern of Ag-TiO₂ (Figure 4.18. a, b) and a very small peak which was detected in XRD pattern of Ag-TiO₂ (Figure.1), suggested the reduction to metallic silver phase on TiO₂ surface has taken place. It is clear that Ag particles with size of 3±1nm were successfully photo deposited on the surface of TiO₂ nanoparticles (18±2 nm). The photo deposition method has led to a finer structure when compared with solution impregnation / calcinations method (Kumar et al. 2009), which showed larger primary particles of Ag (≈ 10 nm) and TiO₂ (≈ 60 nm).

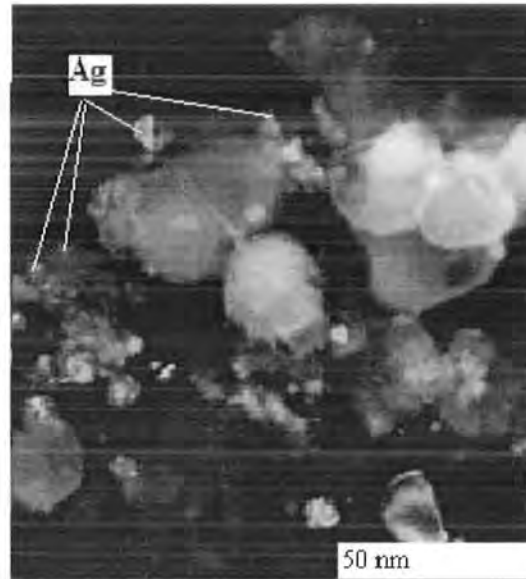


Figure 4.16 TEM Image of Ag-TiO₂ showing the deposits of Ag on TiO₂ Nanoparticles at pH 3

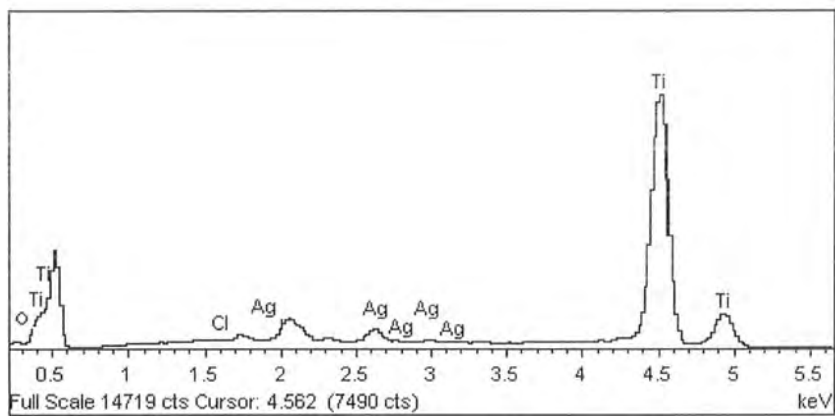


Figure 4.17 The Corresponding EDX Spectrum of Ag-TiO₂ nanocomposite at pH3

4.2.5. Scanning Electron Microscope (SEM):

Scanning electron microscope (SEM) analysis of the Ag-TiO₂ nanocomposite was carried out with the aim to examine morphological changes. In SEM, the samples presented remarkable differences concerning degree of agglomeration between samples from pH 3 and pH 9, as can be observed in Fig. 4.18a and b.

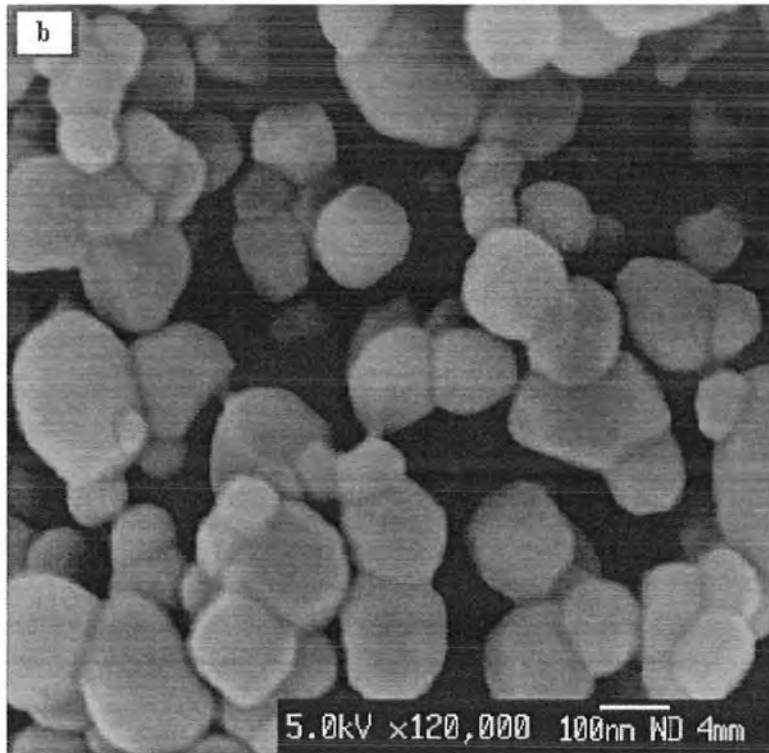
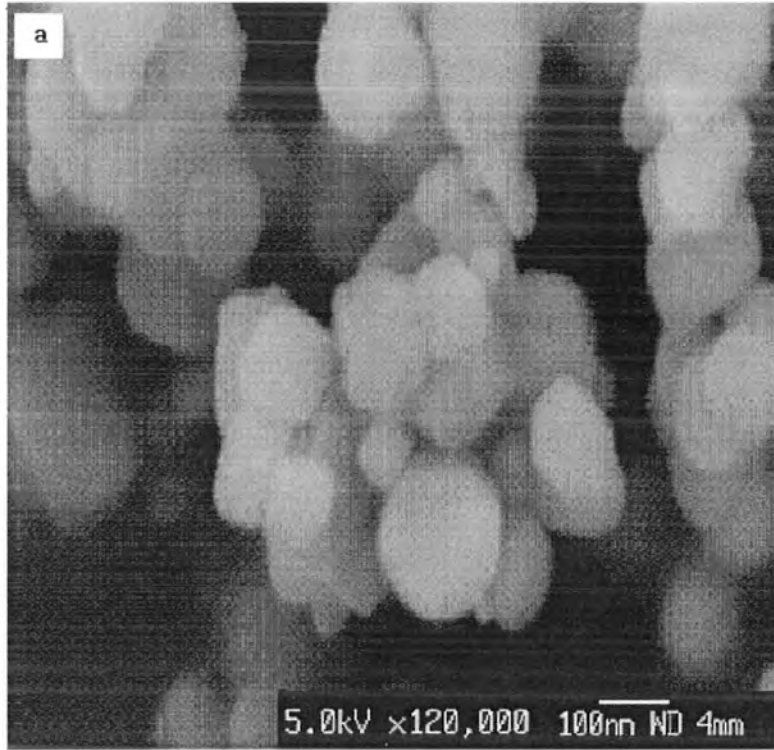
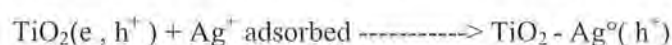


Figure 4.18 (a, b) The SEM images of Ag-TiO₂ nanocomposite at pH 3 and pH 9

The nanocomposite produced at alkaline pH was agglomerated to a greater extent, as shown in Fig. 4.18b while the nanocomposites from the acidic pH, however are less agglomerated, as shown in Fig4.18a. From previous work, it is known that AgNO₃ can adsorb on the surface of TiO₂ particles in the suspension. Thus the Ag⁺ ions that are initially adsorbed on the surface of TiO₂ particles can be reduced by the photo generated electrons to silver metal atoms which tend to cluster into small nanoparticles of 3 nm (containing around 850 atoms per particle)



In water, normally holes take part in counter-oxidation reaction by oxidizing surface adsorbed water molecules into hydroxyl radical (Zhao et al. 2003; Chan et al. 2005; Hirakawa et al. 2005). Since the pH in our work is controlled by the addition of HCl or NaOH, account must be taken of the relatively low solubility products of AgCl and AgOH. At a low pH (< 4), AgCl and at high pH (> 9), AgOH, can be expected to be precipitated onto the TiO₂ surface which can be then assumed to be photochemically reduced to Ag under UV light. This can be described as follows



The oxidation of adsorbed water, Cl⁻ or OH⁻ can be expected to provide the hole scavenging reaction. The high BET surface area and the low degree of agglomeration at pH 4 and a relatively sharp decline in the BET surface area accompanied by an increase of agglomeration at pH 10 (or >9) are clearly related in some way to nucleation and growth of AgCl (at pH < 4) and AgOH (at pH > 9) precipitates followed by photo reduction of AgCl and AgOH.

In summary, we have deduced the conditions under which it is possible to produce a fine nanocomposite morphology of Ag - TiO₂ such that a small (3 nm) sized

Ag particle is anchored by photo deposition onto a larger (18 nm) sized TiO₂ particle, while retaining the surface area. Using these results we are currently designing the morphological architecture of the Ag - TiO₂ nanocomposite system for optimal applications in photocatalysis, chemical sensing and hydrogen production.

By combining results from X-ray diffraction, BET, EDX and TEM, It was found that a fine structured Ag-TiO₂ nanocomposite with an average TiO₂ and Ag particle size 18±6 nm and 3±1 nm respectively can be produced by photo deposition of Ag in a titania sol at pH values from 1-10. At a loading of 1.25 wt % Ag, all the Ag was photo harvested as metallic particle anchored on the surface of TiO₂, such that each TiO₂ particle is attached with one Ag particle. The N₂ adsorption-desorption isotherm showed highest BET surface area was obtained at pH 4, associated with optimal inhibition of particle agglomeration.

Results and Discussion

Bacterial Interaction with Ag-TiO₂ Nanocomposite

TiO₂ was synthesized using sol gel method and the photocatalyst Ag-TiO₂ was synthesized by photoreduction method with a primary particle size of 20 nm and surface area of 50 m²/g (as described in Chapter 4). During photoreduction method Ag ions were photoreduced to Ag nanoparticles and consequently deposited on the TiO₂ surface.

The goal of this work was to investigate the bacterial interaction with the Ag-TiO₂ nanoparticles. Therefore, thin sections of *E. coli* after nanoparticles exposure were analysed through bright field transmission electron microscope in order to assess the interaction of Ag-TiO₂ nanoparticles with bacteria. LB medium was used to culture bacteria until mid-exponential phase. Approximately 10⁹ colony forming units were exposed to 10 mL of the synthesised Ag-TiO₂ nanoparticles in water. After the nanoparticles exposure the bacteria were fixed, stained and sectioned for the preparation of transmission electron micrographs (TEM).

Prior to each experiment, all glassware and apparatus were autoclaved at 121 °C for 15 min to certify sterility. Liquid cultures of *E. coli* (ATCC 25922) were developed overnight aerobically in Luria-Bertani broth (Oxoid, Basingstoke, England) at 37°C on a rotatory platform (200 rpm). Solid medium was created by adding 1.2% agar (Oxoid, Basingstoke, England). Optical density (600 nm) was used to measure the bacterial density of the liquid cultures. Bacterial cells were collected by centrifugation at 4000/g for 15 min, this culture was washed two times in sterile phosphate-buffered saline (PBS) (pH 7.2), and resuspended in PBS or sterile

deionized water. The bacterial concentration was determined by a viable count method on Luria–Bertani (LB) agar plates after serial dilutions of the culture.

This research aimed to investigate *In vitro* photocatalytic bactericidal effect of Ag-TiO₂ nanocomposite using *E.coli* as a model organism. Highly dispersed, Ag-TiO₂ nanocomposite is used with an average particle size of less than 20nm. Bactericidal analysis was carried out in Luria Bertani medium on solid agar plates with various illumination time and different concentrations of Ag-TiO₂ nanocomposite. Transmission electron microscope (TEM) analysis of bacterial section was used to detect the effect of irradiation of Ag-TiO₂ nanocomposite on the ultra structure of the bacterial cell in order to reveal possible cellular damage. The mechanism underlying the action of photo excited Ag-TiO₂ nanocomposite on *E.coli* cell membrane is also evaluated. The results confirmed that *E. coli* cells after contact with Ag-TiO₂ nanocomposite was damaged showing membrane disorganization. This causes the enhanced level of membrane permeability leading to buildup of Ag-TiO₂ nanocomposite in the bacterial membrane and also cellular internalization of these nanoparticles.

This research work aimed to investigate the antibacterial activity of Ag containing visible light responsive TiO₂ and the potential of dosage/deposition significance on the bactericidal activity using *E. coli*. Moreover, the detailed mechanism of the antibacterial behaviour of the Ag-TiO₂ nanocomposite is also discussed with respect to the Transmission Electron Micrographs of the thin section of the *E. coli*.

As Ag deposition on TiO₂ surface can promote the transfer of electrons from the hole. Better charge separation results in less recombination and therefore, improving the photocatalytic activity. In addition, Ag-TiO₂ nanocomposite also

results in generation of high surface area and creates more OH⁻ groups that are crucial to the inhibition of bacterial growth. In addition, the implications and possible applications of this work will be discussed.

The Ag-TiO₂ was used as a photocatalyst with a primary particle size of 20 nm and surface area of 50 m²/g, and *E. coli* ATCC 25922 was taken as a model microorganism for all inactivation experiments. Stock suspensions were prepared by mixing 0.05 g of Ag-TiO₂ in 5 ml deionised water. The dispersion was vortex mixed for 1 min, and was subsequently diluted to 25 ml in order to produce a 0.2% stock suspension. The desired concentrations were prepared from the stock suspension using deionized H₂O.

UV-Vis spectroscopy (Perkin Elmer Lambda25 UV spectrophotometer) was used to investigate the absorption spectrum of the specimen. TEM (Transmission electron microscope) micrographs were taken on a JEOL 2000FX to evaluate the cell membrane disintegration.

5.1 Bacterial Culture Preparation:

E. coli (*E. coli* strain ATCC 25922) cultures were grown overnight aerobically in LB broth (Oxoid, Basingstoke, England) at 37°C on a rotatory platform at 200 rpm. Agar 1.2 % was added to solidify the liquid medium (Oxoid, Basingstoke, England). Optical density of 600 nm was used to calculate the bacterial density of the liquid cultures. Bacterial cells were collected by centrifugation at 4000/g for 15 min. The bacterial culture was washed twice in sterile phosphate-buffered saline (PBS) at pH 7.2, and resuspended in PBS or sterile deionized water. Subsequent to the serial dilution of the culture the viable colony counting method was used to determine the bacterial concentration on Luria–Bertani (LB) agar plates.

5.2 Measurement of photocatalytic antibacterial properties.

The Ag-TiO₂ was used as a photocatalyst which was synthesized by photoreduction method having primary particle size of 20 nm and surface area of 50 m²/g. In the photocatalytic experiments, Ag-TiO₂ suspension (1 mg/mL in deionized water) was prepared instantaneously prior to photocatalytic reaction and was kept in the dark. Washed bacteria (approximately 2×10⁵ cfu/mL) were resuspended in deionized water. Aliquots of 1-mL stock aqueous Ag-TiO₂ were added to 8 mL of sterilized deionized water and 1 mL of washed cells in a 100mL flask at room temperature. The Ag-TiO₂ bacterial suspension was positioned on a magnetic stirrer with constant stirring and was irradiated with a bulb from above to ensure homogeneity throughout the experiments. The suspension was sampled at various time gaps and diluted to ensure cells were well suspended. The slurry was spread on the nutrient agar prepared petri dishes and incubated for 18 h at 37 °C before counting the colonies and calculating the number of viable cells. The wavelength of the bulb was 265 nm. The light intensity was examined by a long-wave UV meter (peak sensitivity of 365 nm; Black-Ray, UVP, Inc., Upland, CA, USA) and the light intensity getting the surface of TiO₂ slurry was approximately 8 W/m².

5.3 Bacterial Viability Assay:

In this study, *E. coli* was used as a model organism. The loss of *E. coli* viability was observed by the colony forming unit count method. The slurry of Ag-TiO₂ and bacteria was illuminated by UV light with constant stirring. An *E. coli* suspension with no Ag-TiO₂ was illuminated as a control. Moreover, the reaction of the Ag-TiO₂-bacteria slurry in the dark was also observed. Samples were taken at 15 min intervals for an hour in six repeats. The viable count was carried out on agar

plates after serial dilutions of the sample in Phosphate buffer saline (PBS). All plates were incubated at 32°C for 24 hours. It is essential to retain a septic method while working with microorganisms to avoid contamination. All materials were sterilized.

5.4 Field-emission Gun Scanning Electron Microscope (FEGSEM) and Transmission Electron Microscopy (TEM)

For FEGSEM and TEM 1ml of the photocatalyst bacterial suspension was taken at various time intervals, washed thrice with PBS (Phosphate Buffer Saline) and centrifuged. The samples were then fixed with 2.5% glutaraldehyde for 30 min, washed twice with PBS buffer, and post-fixed with 1% osmium tetroxide for 30 min. After fixing, the *E. coli* cells were concentrated by centrifugation at 4000 rpm for 10 min, and again washed twice with PBS buffer. Consequently, the bacterial cells were steadily dehydrated with mounting the concentration of ethanol (50%, 70%, 80%, 90% and 100% for 5 min, correspondingly). When the cells were dried, their morphology was studied using a field emission gun scanning electron microscope (JEOL 6340F FEGSEM) and transmission electron microscope (TEM JEOL 2000FX).

5.5 Effect of Ag-TiO₂ Concentration

Experiments were carried out to explore the effect of Ag-TiO₂ concentration on the photocatalytic inactivation of *E. coli* as described in Fig. 5.1. The bacterial cell suspension was incubated on different concentration of Ag-TiO₂ nanocomposite and UV treatments. The data described in the figures are the average values of six experiments.

Fig. 5.1 shows a considerable dependence of the *E. coli* inactivation potential on the Ag-TiO₂ nanocomposite concentration. The tests performed without addition

of Ag-TiO₂ nanocomposite resulted in an insignificant inhibition of bacterial growth. On contrary, adding the Ag-TiO₂ nanocomposite with concentrations of 0.2, 0.4, 0.6, 0.8, 1g/L has a prominent antibacterial outcome (Fig 5.1), and increasing the concentration of Ag-TiO₂ resulted in enhanced inhibition of bacterial growth. A tremendous antibacterial effect attained in case of Ag-TiO₂ nanocomposite when the concentration of the nanocomposite was 0.8 g/L and the growth of *E. coli* was completely inhibited, which is comparable to what was observed in the LB agar plate (Thiel, J et al. 2007; Gunawan et al. 2009). Generally, the antimicrobial effect increased with increasing concentration of the Ag-TiO₂ nanocomposite, therefore, higher efficiencies of *E. coli* inactivation were achieved at higher Ag-TiO₂ concentrations as reported in ealier literature (Niño-Martínez, et al. 2008).

In general, there was an inverse relationship between antibacterial activity and concentration of Ag-TiO₂ nanocomposite. Nevertheless the extent of *E. coli* inactivation was not linearly relative to the Ag-TiO₂ concentration, as illustrated in Figure 5.1.

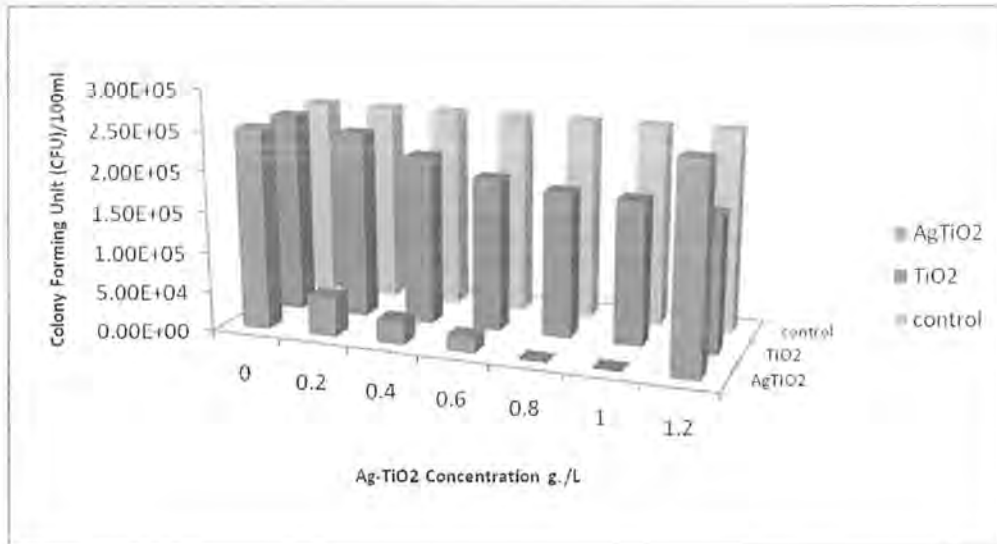


Figure 5.1 Bactericidal effect of various Ag-TiO₂ concentration on *E.coli* (2×10^5 CFU ml⁻¹)

The antibacterial activity enhances linearly with the Ag-TiO₂ concentration until a definite value around 0.1 g L⁻¹, reaching a plateau for higher values, which means the activity is not evidently improved if Ag-TiO₂ concentration increases (Figure 5.2).

This clearly showed that a higher Ag-TiO₂ concentration produces more reactive species accountable for *E. coli* inactivation, but not in a relative way. *E. coli* inactivation at a concentration of 1.0 g/L of Ag-TiO₂ is far more effective than that at 0.2 g/L Ag-TiO₂ concentration. On the other hand, increasing the concentration of Ag-TiO₂ from 1.0 to 1.2 g/L did not improve the inactivation capability of *E. coli* owing to the saturation effect. The saturating photo activity with rising Ag-TiO₂ concentration should be comprehend in terms of the competition between surface area and light scattering failure. Whereas the higher Ag-TiO₂ concentration offers more surface sites, it also decreases the light penetration depth into the suspension through

increasing light scattering, which reduces the efficiency of the photocatalytic inactivation of *E. coli* (Wang Y et al. 2008).

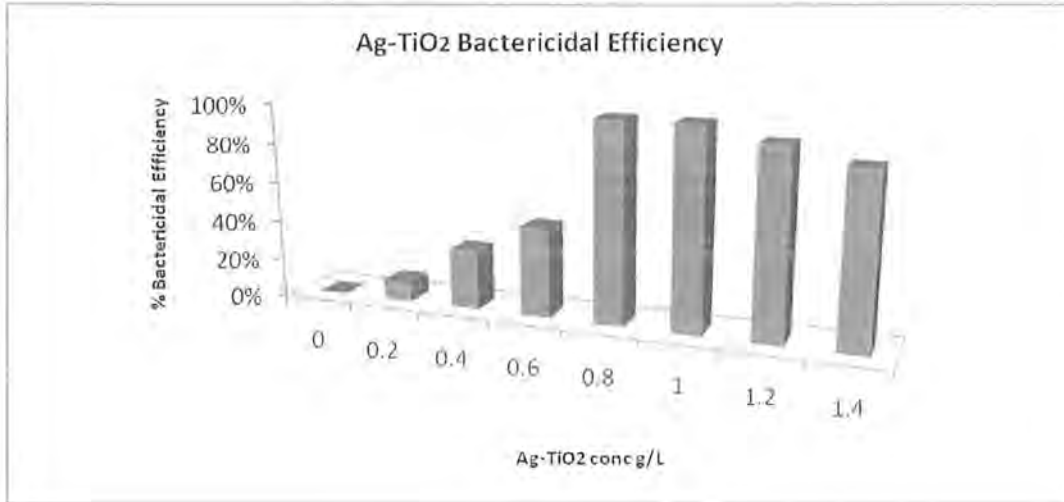


Fig 5.2 Ag-TiO₂ Bactericidal Efficiency (2×10^5 CFU ml⁻¹)

5.6 Effect of Light Intensity

Figure 5.3 represents experiments showing bactericidal effect of TiO₂ and Ag-TiO₂ in dark and light. In the dark experiment, an insignificant bacterial removal was shown by Ag-TiO₂ nanocomposite while TiO₂ did not demonstrate any antibacterial effect in dark. The effect of light intensity on the bactericidal effect of TiO₂ and Ag-TiO₂ with irradiation time illustrates that more rapid inactivation happened at higher light intensity, even though not in a proportional behaviour. These observations are in accordance with the results of previous studies (G. Rothenberger et al. 1985; Gunawan, C et al. 2009). The experiments were done at initial bacterial concentration of 2×10^5 CFU/ml, for up to 90 minutes. It was found that elimination efficiency of *E. coli* in the absence of each of Ag-TiO₂ or UV irradiation, with time was low (Figure 5.3), whereas in the presence of both of them, elimination efficiency was increased

and found to be 95% at an optimal conc. of 0.8 g/ L in 10 min as shown in Figure 5.3. It was concluded from these results that disinfection capability was much higher using both Ag-TiO₂ and UV light. In the mutual occurrence of TiO₂ and UV irradiation, hydroxyl radicals (OH⁻) are produced, which increased the efficiency of the method. In the absence of UV irradiation, Ag-TiO₂ particles might adsorb some of microorganisms, which cause low decrease in the amount of *E. coli* with time (H.N. Pham, et al. 1985; K.D. Kim et al. 2006; Matsunaga T et al. 1985). It did not show any significant result in dark as shown in Figure 5.3.

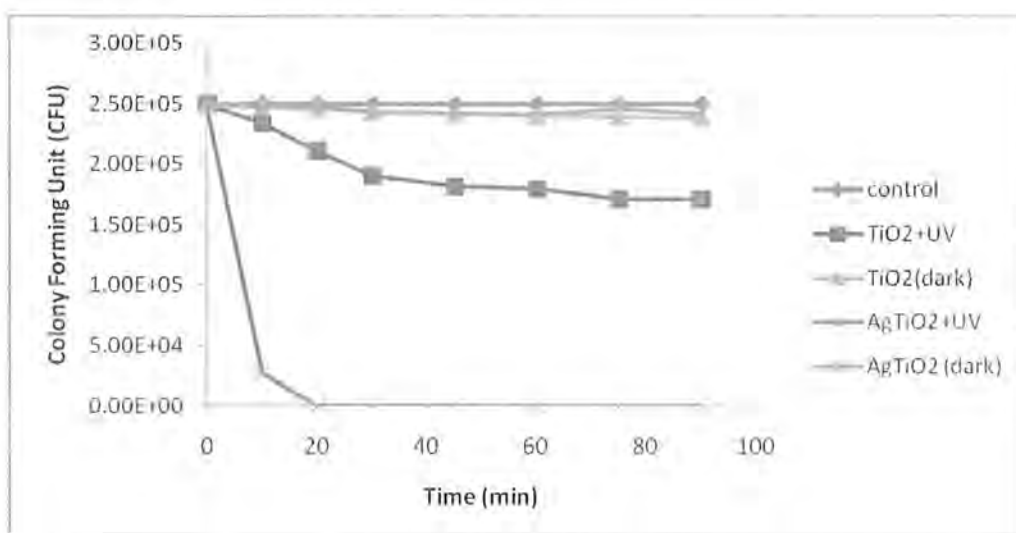


Figure 5.3 Bactericidal Effect of TiO₂ and Ag-TiO₂ in UV and Dark (2×10^5 CFU ml⁻¹) (Ag-TiO₂ 1.0 g/l)

In addition to the effect of photocatalyst concentrations, the effect of stirring speed in bactericidal efficiency was investigated. It was found that increasing the stirring speed from 300 to 380 rpm improved bactericidal activity, as photocatalytic reactions can occur only on the surface of photocatalyst, increasing collision between photocatalyst and target compound advances the oxidation (San *et al.* 2001). It is important to ensure that cells and Nanocomposite particles in the sample vessel are in

constant exposure with the UV light exposure. The antibacterial activity tremendously improves with the stirring of the cell particle mixture. It also helps to avoid light scattering by sediments or static aggregates of the nanoparticle or clumping of the microorganisms. Moreover, it enhances the nano particles and cell contact frequency.

5.7 Scanning Electron Microscopy (SEM)

Scanning electron microscope (SEM) analysis of bacterial section was used to detect the effect of irradiation and concentration of Ag-TiO₂ nanocomposite on the ultra structure of the bacterial cell in order to reveal possible cellular damage. Figure 5.4a exhibited the SEM images of untreated *E. coli* cell while Figure 5.4b showed the cells treated with 1gr/L of Ag-TiO₂ nanocomposite and irradiated with UV light for 20 min. Figure 5.4b showed morphological changes with considerable damage and disorganization in cell morphology. The cell membrane in all *E. coli* cells is extensively damaged and, most probably, the intracellular content has leaked out. Figure 5.4b also showed Ag-TiO₂ nanoparticles inside and outside the cell surrounded by lipo polysaccharides released by the bacteria. Consequently, the internal structure was lysed as a result of the acute damage of the structure of the cell wall and the inner contents of cell as shown in figure Figure 5.4b

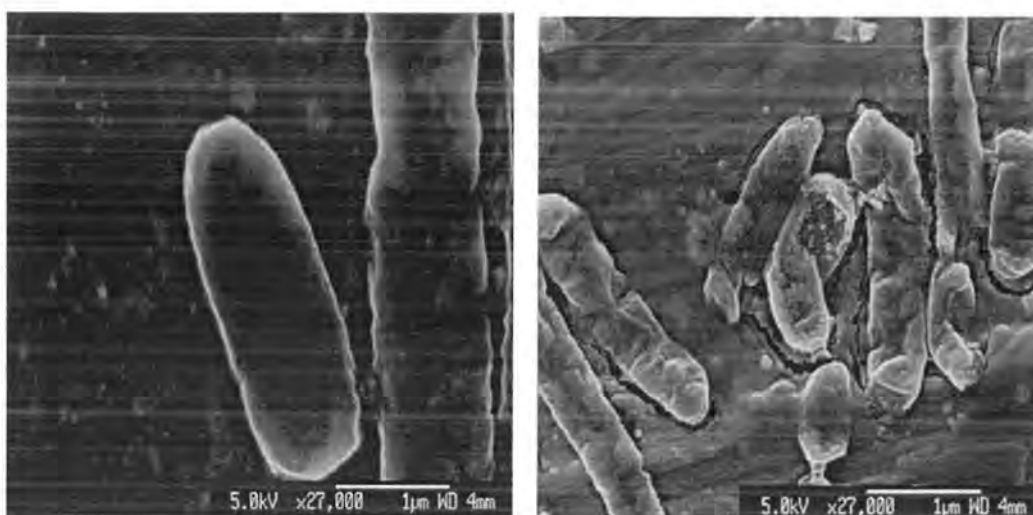


Figure 5.4 (a) Untreated Bacterial cells (b) Treated bacterial cells showing damage of the cell membrane

The survival ratio of bacterial population began to decrease with the onset of irradiation. A previous study found that the photocatalyst was unable to attack cell wall as it was protected by the outer peptidoglycan layer in the earlier stage of reaction (Saito *et al.* 1992). Instead, the plasma membrane was firstly attacked by reactive oxygen species (also known as superoxide radicals) which were produced from water molecules around the photocatalyst and were able to enter the external layer of bacteria. These reactive species oxidized the membrane and broke the main permeability barrier of bacteria. The gradual leakage of intracellular materials, including protein, ribo nucleic acid (RNA) and minerals were the main cause of the loss of cell viability at the early stage of photocatalytic oxidation. Cell wall destruction was believed to be a secondary phenomenon after the loss of cell viability.

5.8 Transmission Electron Microscopy of Bacterial-Nanoparticle Interactions

E. coli were mixed with Ag-TiO₂ nanoparticles, for 30 minutes, at which time the majority of the bacteria were viable, and imaged by bright field TEM. The bacteria were embedded in an epoxy resin, which was sectioned at a thickness of approximately 80 nm. This was consistent with the interference colour of transmitted light through the resin fragments. In general, the preparation protocol gave lucid staining of the cell envelope with least staining artefacts. The bacteria were 0.4-0.7 μm wide and 2.5-8.5 μm long (or longer where a bacterium was about to undergo cytokinesis). There are oblong or spherical sections of *E. coli* depending on longitudinal or transverse sections of the bacterium. The experiments were repeated in triplicates which produced the same micrographs of bacterial cells. Distinctive transmission electron micrographs for *E. coli*, without exposure to nanoparticles, are shown in Figure 5.5.



Figure 5.5 Transmission electron micrographs of *E. coli* sections prepared from specimens (without Ag-TiO₂ nanoparticles treatment). The specimens showed some minor cell-cell variation as is typical of TEM.

When *E. coli* was exposed to the Ag-TiO₂ nanocomposite, the nanoparticles were associated with the cell surface as revealed in the micrograph (Figure 5.6). Nevertheless, the bacteria had been successively regime entered and resuspended throughout the procedure, removing most of the unbound nanoparticles in the supernatants.

The Nanocomposite typically appeared on the extra-cellular surface of the cell envelope and associated with material surrounding the cell surface, Figure 5.6. In addition, the nanoparticles were within the circumferential cell envelope appearing as if they were within the cytosol (Figure 5.7). The bacterial sections with nanoparticles within the cell envelope were typically cut along the longitudinal axis of the bacterium, however with exceptions as shown in Figure 5.7.

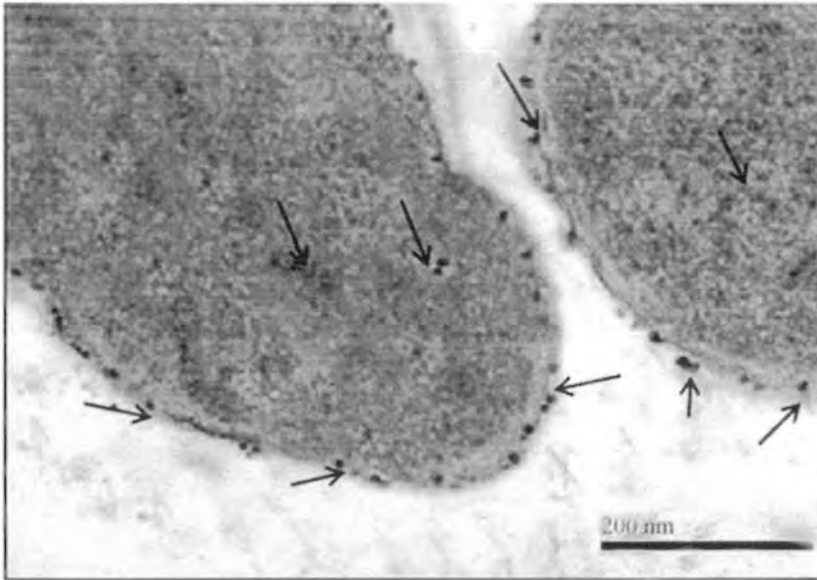


Figure 5.6 TEM of *E. coli* sections post treatment with Ag-TiO₂ nanoparticles
(Transverse sections of the bacteria are shown)

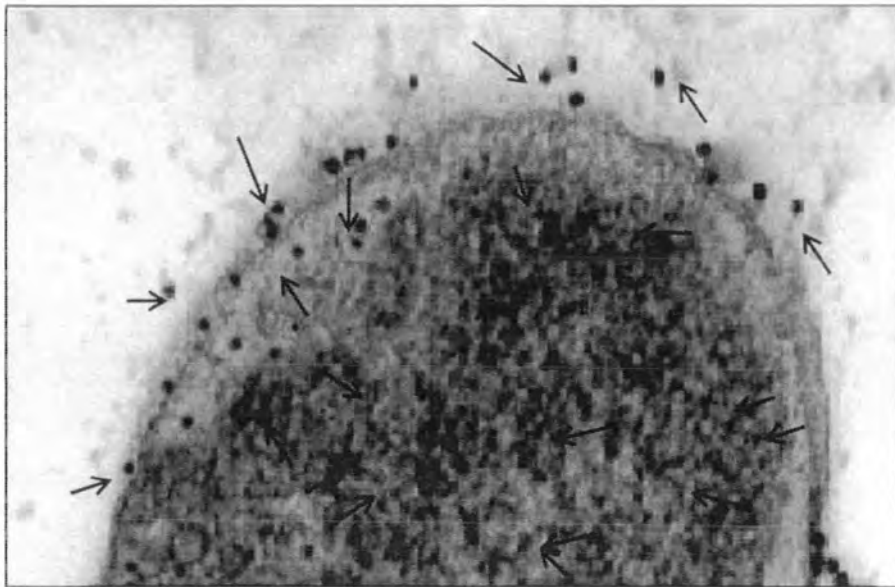


Figure 5.7 TEM of *E. coli* sections post treatment with Ag-TiO₂ nanoparticles
(longitudinal sections of the bacteria are shown)

The micrographs clearly indicate the presence of nanocomposite on the surface as well as inside the bacterial cells indicating the damage of the cell wall due to the Ag-TiO₂ nanocomposite. However, overall there was a quantitative difference between the numbers of nanoparticles that were associated with each bacterial section. From a sample of 200 bacteria an average of 16 ± 8 Ag-TiO₂ nanoparticles were adhered to each bacterial section and the bacterial cells after the exposure of the Ag-TiO₂ nanocomposite had very discrete morphology.

The nanoparticles had a negative surface charge and therefore an effective negative charge in water (pH 7) (Bohme et al. 2007). Thus, the primary interaction of the Ag-TiO₂ nanocomposite the bacterium is possibly an electrostatic attraction between the nanoparticle surfaces and positively charged outer membrane proteins on the *E. coli* surface. Therefore, the TEM images show the interactions and change in the outer membrane of the *E. coli* bacterium. The lipopolysaccharides on the surface of the bacteria also carry a negative charge from phosphate residues on the inner and outer core polysaccharide chains (Schletter et al. 1995). Hence, nanoparticles binding by electrostatic attraction could occur at sites where the LPS molecules are interspaced by protein. A variety of surface proteins are present on *E. coli* and the nanoparticles interaction will depend upon the specific charge and topology of each molecule. Smaller nanoparticles bind with the bacteria more favourably and larger nanoparticles may not fit into the domain of the protein molecules (Bohme et al. 2007). In general the larger proteins may favour interaction, having a greater contact area and number of charges. The domain of some surface proteins would accommodate the nanoparticles adequately, assuming that the contact surface is smaller than the radius of the sphere (Lou et al. 2010).

The surface of the nanoparticles is evidently vital for the bacterial interaction with the Nanocomposite and the many possible orientations of nanoparticles surface increases the possible electrostatic combinations that are available to corresponding attachment sites at the cell surface. The association of bacteria and nanoparticles is dependent on the diameter of the nanoparticles as well. The difference in the number of nanoparticles that bound to the cells indicates that *E. coli* has more possible binding sites.

Some nanoparticles did not attach directly on the cell surface and appeared proximal to the cell envelope. Within each specimen preparation there were bacterial sections that contained nanoparticles within the circumferential cell envelope, and towards the centre of the cell, as in Figure 5.7.

5.9 Mechanism of Antibacterial Activity:

The proposed mechanism of *E. coli* disinfection by Ag-TiO₂ nanocomposite is by means of photo-oxidation of water (H₂O) and dissolved oxygen (O₂), which most likely results in the production of reactive oxygen species (ROS), for instance hydroxyl radicals (OH[•]), superoxide anion (O₂^{•-}) and hydrogen peroxide (H₂O₂). These reactive oxygen species are formed by the reactions on the conduction and valence band. The reactions relating conduction band electron and valence band hole are in table 5.1 as follows:

Table 5.1 The reactions relating conduction band electron and valence band hole

Formation of Reactive Species	
Conduction Band Electron Reactions	Valence Band Hole Reactions
$\text{TiO}_2 (e^-) + \text{O}_2 \rightarrow \text{TiO}_2 + \cdot\text{O}_2^-$	$\text{TiO}_2 (h^+) + \text{H}_2\text{O}_{\text{ads}} \rightarrow \text{TiO}_2 + \cdot\text{OH} + \text{H}^+$
$\text{TiO}_2 (e^-) + \cdot\text{O}_2^- + 2\text{H}^+ \rightarrow \text{TiO}_2 + \text{H}_2\text{O}_2$	$\text{TiO}_2 (h^+) + 2\text{H}_2\text{O}_{\text{ads}} \rightarrow \text{TiO}_2 + \text{H}_2\text{O}_2 + 2\text{H}^+$
$\text{TiO}_2 (e^-) + \text{H}_2\text{O}_2 \rightarrow \text{TiO}_2 + \cdot\text{OH} + \text{OH}^-$	$\text{TiO}_2 (h^+) + \text{OH}^- \rightarrow \text{TiO}_2 + \cdot\text{OH}_{\text{ads}}$

The reactive oxygen species can act together with the components of the cell wall including amino acids (e.g. l-alanine, d-glutamine) and peptidoglycans (beta-1,4-N acetylglucosamine and beta-1,4-N acetylmuramic acid) causing development of malondialdehyde (MDA) and lipid peroxidation which can bind to DNA and cellular protein and inactivate them resulting in cell lysis.

The process of *E. coli* photo killing on Ag-TiO₂ nanocomposite can be schematically illustrated as in Figure 5.8 (a, b, c).

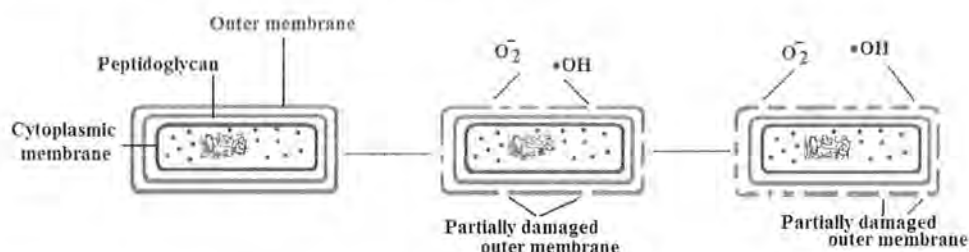


Figure 5.8 (a, b, c) Proposed mechanism of Ag-TiO₂ bactericidal activity

In the preliminary reaction of the *E. coli* photo killing, the outer membrane is partially decomposed by the reactive species which were produced by the Ag-TiO₂ photocatalysis (Figure. 5.8). Therefore the cells are viable with a moderate damage. The partial decomposition of the membrane, however, modifies the permeability of the cell membrane, thus allowing the reactive species to penetrate into the cytoplasm

membrane more effectively (Thiel et al. 2007). Hence, the cytoplasmic membrane is attacked by reactive species, causing the peroxidation of membrane lipid (Figure. 5.8c). The lipid peroxidation of the membrane is specified by the formation of Malondialdehyde (MDA), as observed by Jacob et al. during treatment of *E. coli* cells with TiO₂ and UV light. Lipid peroxidation causes improper functioning of the cytoplasmic membrane leading to the cell death (Sondi et al. 2004). Various researchers also found that lack of proper functioning of cytoplasmic membrane is the origin of the killing effect by Ag-TiO₂ photocatalysis (S X Liu et al. 2004; P.K. Stoimenov et al. 2002). Therefore, the partial decomposition of the outer membrane in *E. coli* cells by the preliminary Ag-TiO₂ nanocomposite reaction eventually results in cell death, describing the photo killing activity of Ag-TiO₂ nanocomposite.

The formation of the reactive oxygen species (ROS) is enhanced by the decreased band gap TiO₂-Ag Nanocomposite under visible light conditions. It is noteworthy that pure TiO₂ (3.21 eV) confines its bacterial elimination activity and can only be used with light in the UV region owing to TiO₂'s large band gap. Since few decades the metal doping has been known to be the main successful method to modify TiO₂'s inherent band structure to enhance its visible light activity. To decrease the band gap energy of TiO₂, a range of metal elements (Au, Ag, Cu, Pd, and Pt) have been used as dopants (M S Lee et al. 2005). The main advantage of Ag doping with TiO₂ is that it decreases the band gap of TiO₂ by inhibiting the recombination of the electrons and holes and promotes the formation of reactive oxygen species (ROS) (Figure. 5.8). The generation of the ROS was commencing from conduction band electrons or valence band holes supplied by TiO₂ through excitation of the electrons leading to the generation of the TiO₂ cationic species. As described earlier, this generally does not take place with TiO₂ as the band gap of TiO₂ is usually satisfied in

the UV range. However, during the colloidal formation of Ag-TiO₂, the Ag⁺ ions cannot get into the lattice of the TiO₂. As a consequence, Schottky barriers are formed at the Ag-TiO₂ contact region which results in charge separation facilitating the electron transfer from TiO₂ to Ag in the presence of UV light. To this end, the Ag-TiO₂ antibacterial activity was significantly improved.

This study suggested that Ag-TiO₂ nanocomposite exhibits satisfactory antibacterial property, the growth inhibition rates against *E. coli* was 99.99% as the concentration of Ag-TiO₂ was 1g/L. The results also confirmed specific regions of the *E. coli* surface accommodate the interaction with nanoparticles, possibly through an attachment of the nanoparticles to the extracellular domains of integral outer membrane proteins and *E. coli* cells after contact with Ag-TiO₂ were damaged showing a membrane disorganization which caused the increase of membrane permeability leading to accumulation of Ag-TiO₂ nanoparticles in the bacterial membrane and also cellular internalization of these nanoparticles. Ag nanoparticles could not only inactivate *E. coli* cells directly but enhance the generation of reactive oxygen species of TiO₂ by preventing electron-hole pair recombination. However, the particles, if present at high enough concentrations, may also enhance electron-hole pair recombination thus it is likely that an optimum loading exists where the bactericidal effect of such photo-catalysts is maximized.

Thus Ag-TiO₂ was proven to have antibacterial capabilities that render them potentially useful as antibacterial agents for variety of applications.

CONCLUSION

- TiO_2 nanoparticles were synthesized and characterized by different experimental techniques. The experimental results projected that TiO_2 Nanoparticles are secondary particles composed of primary particles.
- The addition of alcohol exhibited to aid aggregation and packing of the primary particles which result in a rapid size enlargement at a high temperature.
- A method of photo deposition has been demonstrated for synthesis of Ag- TiO_2 nanocomposite.
- The influence of pH on the preparation of dispersed Ag- TiO_2 nanocomposite was investigated.
- By combining results from X-ray diffraction, BET, EDX and TEM, It was found that a fine structured Ag- TiO_2 nanocomposite with an average TiO_2 and Ag particle size 18 ± 6 nm and 3 ± 1 nm respectively can be produced by photo deposition of Ag in a titania sol at pH values from 1-10.
- At a loading of 1.25 wt % Ag, all the Ag was photo harvested as metallic particle anchored on the surface of TiO_2 , such that each TiO_2 particle is attached with one Ag particle. The N_2 adsorption-desorption isotherm showed highest BET surface area was obtained at pH 4, associated with optimal inhibition of particle agglomeration.
- The effect of Ag- TiO_2 nanocomposite and the interaction of nanoparticles with bacterial cells were studied by using *E. coli* as a model organism. Also, the possible cellular disorientation of the bacterial cell was investigated.

- The results inveterate specific regions of the *E. coli* surface lodge the contact with nanoparticles, probably through an attachment of the nanoparticles to the extracellular realm of essential outer membrane proteins.
- The *E. coli* cells after contact with Ag-TiO₂ were damaged presenting a membrane disorganization which causes the enhancement of membrane permeability leading to accumulation of Ag-TiO₂ nanoparticles in the bacterial membrane and also cellular internalization of these nanoparticles.
- Ag nanoparticles could not only inactivate *E. coli* cells directly but augment the generation of reactive oxygen species of TiO₂ by preventing electron–hole pair recombination. However, the particles, if present at high enough concentrations, may also enhance electron–hole pair recombination thus it is likely that an optimum loading exists where the bactericidal effect of such photo- catalysts is maximized.
- It is proposed that the oxidative power of nanocomposite and the electrostatic attraction are the major rationale for high antibacterial activity.
- Thus Ag-TiO₂ was confirmed to have antibacterial capabilities that render them prospectively useful as an antibacterial agent for various applications

FUTURE RECOMMENDATIONS

- The future work should be extended to better understand the mechanism of inactivation using the Ag-TiO₂ nanocomposite.
- Continued study is needed for the exploration of the inactivation of various microbial strains and also to develop the mechanism towards the inactivation method.
- As this study explores the antimicrobial activity of the Ag-TiO₂ nanocomposite against Gram negative bacterium *E. coli* as a model bacterium, many other bacteria could also be used to evaluate the antibacterial activity of the nanocomposite further.
- Future work can be extended to study the effects of the Ag-TiO₂ nanocomposite on a range of bacterial species and also on various microorganisms including viruses, fungi etc.

List of Publications

Bano I, Kumar RV, Hameed A; Influence of pH on the preparation of dispersed Ag-TiO₂ nanocomposite; IONICS 18(3):307-313 Mar 2012

Bano Ishrat, Hameed Abdul, Kumar RV “*In Vitro* Bactericidal and TEM Study of the Interaction of Ag Modified Titania with Coliform Bacteria” Int J Env Health Research DOI: 10.1080/09603123.2012.743115.

References

- A. Barringer, Bowen HK. (1985) High-Purity, Monodisperse TiO₂ Powders by Hydrolysis of Titanium Tetraethoxide. 1. Synthesis and Physical Properties-Longmuir 1, 414-420.
- A. Egerton and J. A. Mattinson, (2008) The influence of platinum on UV and 'visible' photocatalysis by rutile and Degussa P25. Journal of Photochemistry and Photobiology A-Chemistry, vol. 194, pp. 283-289
- A. Tomalia, H. Baker, J. Dewald, M. Hall, G. Kallos, S. Martin, J. Roeck, J. Ryder and P. Smith (1985). A New Class of Polymers: Starburst-Dendritic Macromolecules. Polymer Journal 17: 117. doi:10.1295/polymj.17.117
- A. Dawson, P V Kamat (2001), Semiconductor-metal nanocomposites. Photoinduced fusion and photocatalysis of gold-capped TiO₂ (TiO₂/Gold) Nanoparticles. J Phys Chem B (105) 960-966
- Acher, A., Fischer, E., Turnheim, R., Manor, Y. (1997). Ecologically friendly wastewater disinfection techniques. Water Research 31:1398-1404.
- Acra, A., Raffoul, Z., Karahagopian, Y. (1984). Solar disinfection of drinking water and oral rehydration solutions: guidelines for household application in developing countries. Amman UNICEF 1-46.
- Ahmadi, Z., M. Ashjari, et al. (2009). Synthesis and Morphological Study of Nanoparticles Ag/ TiO₂ Ceramic and Bactericidal Investigation of Polypropylene-Ag/ TiO₂ Composite. Journal of Inorganic and Organometallic Polymers and Materials 19(3):322-327
- Ahmed, W., Neller, R., Katouli, M. (2005). Host Species-Specific Metabolic Fingerprint Database for Enterococci and Escherichia coli and Its Application to Identify Sources of Fecal Contamination in Surface Waters. Appl. Environ. Microbiol. 71:4461-4468
- Aitken, R. J., Creely, K. S., Tran, C. L. (2004). Nanoparticles: an occupational hygiene review. Sudbury, Suffolk, Grande-Bretagne. HSE 100p.

- Akhavan, O. (2009) Lasting antibacterial activities of Ag - TiO₂ /Ag/a - TiO₂ nanocomposite thin film photocatalysts under solar light irradiation. *Journal of Colloid and Interface Science*, 336 (1), 117 – 24.
- Akhtar, M. K. Pratsinis, S.E. Mastrangelo, S.V. R. (1994). Vapor phase synthesis of Al doped titania powders. *J. Mater. Res.* 9:1241-1249.
- Alivisatos, (1996) Perspectives on the physical chemistry of semiconductor nanocrystals. *J. Phys. Chem.*, vol. 100(31), pp. 13226–13239,
- Alt, V., Bechert, T., Steinrücke, P., Wagener, M., Seidel, P., Dingeldein, E., Domann, E., Schnettler, R. (2004). An *In vitro* assessment of the antibacterial properties and cytotoxicity of nanoparticulate silver bone cement. *Biomaterials* 25:4383-4391
- Amtout, A.; Leonelli, R. (1995) Phys. Rev. B. Optical properties of rutile near its fundamental band gap *Physical Review B (Condensed Matter)*, Volume 51, Issue 11, March 15, 1995, pp.6842-6851
- Ani, J. K., Savithri, S., Surender, G. D. (2005). Characteristics of Titania Nanoparticles Synthesized Through Low Temperature Aerosol Process. *Aerosol and Air Quality Research* 5: 1-13.
- Armelao, L., Bertagnolli, H., Bleiner, D., Groenewolt, M., Gross, S., Krishnan, V., Sada, C., Schubert, U., Tondello, E. and Zattin, A. (2007), Highly Dispersed Mixed Zirconia and Hafnia Nanoparticles in a Silica Matrix: First Example of a ZrO₂-HfO₂-SiO₂ Ternary Oxide System. *Adv. Funct. Mater.* 17: 1671–1681. doi: 10.1002/adfm.200600458
- Asahi, Y. Taga, W. Mannstadt, and A. J. Freeman, (2000) Electronic and optical properties of anatase TiO₂. *Physical Review B*, vol. 61, no. 11, pp. 7459–7465
- Barbe, J. Bartlett, L. G. Kong, K. Finnie, H. Q. Lin, M. Larkin, S. Calleja, A. Bush, and G. Calleja (2004) Silica particles: A novel drug-delivery system". *Advanced Materials*, 16(21), p. 1959-1966
- Barboux-Doeuff, S.; Sanchez, C. ((1994),) *Mat. Res. Bull.* 29, 1
- Behar, D., Rabani, (2006), *J. J. Phys. Chem. B* 110, 8750
- Berger, M. (2006). Nanotechnology Risks – The Real Issues. *nanoRisk* 1(1): 1-8

- Blake, D. M., Maness, P. C., Huang, Z., Wolfrum, E. J., Huang, J. (1999). Application of the Photocatalytic Chemistry of Titanium Dioxide to Disinfection and the Killing of Cancer Cells. *Separation and Purification Methods* 28:1-57.
- Böhme, U. and U. Scheler, (2007). Effective charge of bovine serum albumin determined by electrophoresis NMR. *Chemical Physics Letters*, 435(4-6): p. 342-345
- Bramley, M. J. Hounslow, and R. L. Ryall, (1996). *J. Collid. Inter. Sci.* 183, 155
- Brauer, (2003) In vivo monitoring of apoptosis. *Prog. Neuro-Psychopharmacol. Biol. Psychiatr.*, vol. 27(2), p. 323,
- Brinker, C. J., Wallace, S., Raman, N. K., Sehgal, R., Samuel, J. Contakes, S. M. (2006), Book Chapter "Sol-Gel Processing of Amorphous Nanoporous Silicas: Thin Films and Bulk" Part 3 *Access in Nanoporous Materials*, 123-139
- Brinker, C. J.; Scherer, G. W. (1990). *The Physics and Chemistry of Sol-Gel Science*; Academic Press: New York,
- Brook L A, P. Evans, H A Foster, M E Pemble, A Steele, D W Sheel, H M Yates (2007) Highly bioactive silver and silver/titania composite films grown by chemical vapour deposition. *J. Photochem. Photobiol, A Chem.* 187:53–63
- Brown D. M, M.R. Wilson, W. MacNee, V. Stone, K. Donaldson (2001) Dependent Proinflammatory Effects of Ultrafine Polystyrene Particles: A Role for Surface Area and Oxidative Stress in the Enhanced Activity of Ultrafines. *Toxicol. Appl. Pharmacol.* 175:191-199.
- Bura C, Lou Y, Chen X (2003) *Nano Lett* 3:1049
- Byun, K.T., Seo, K.W., Shim, I.W., Kwak, H.Y. (2008). Syntheses of ZnO and ZnO-coated TiO₂ nanoparticles in various alcohol solutions at multi bubble sono luminescence (MBSL) condition. *Chem. Engg. J.* 135:168–173.)
- C. Chan, et al. (1998) Quantum dot bioconjugates for ultrasensitive non isotopic detection. *Science*, vol. 281(5385), pp. 2016–2018
- C. Hague and M. J. Mayo, (1993) *Nanostructured Materials* 3, 61

- C.D. Kobayashi, M. A.; Liz-Marzán, L. M.,(2001) Sol-Gel Processing of Silica-Coated Gold Nanoparticles. *Langmuir*, 17(20), p. 6375 – 6379
- Carmona, M. A. Villegas, and J. M. Fernandez Navarro (2006) Sol-gel coatings in the ZrO₂-SiO₂ system for protection of historical works of glass". *Thin Solid Films*, 515(4), p. 1320-1326
- Carp, O., Huisman, C.L., Reller, A. (2004). Photoinduced reactivity of titanium dioxide. *Progress in Solid State Chemistry*, 32, 33-177.
- Chan et al. (2007) Chemistry and Properties of Nanocrystals of Different Shapes. *Chem. Rev*, 105, 1025-1102
- Chan S C, M A Barteau (2005) Preparation of Highly Uniform Ag/TiO₂ and Au/TiO₂ Supported Nanoparticle Catalysts by Photodeposition. *J Langmuir* 21(12): 5588-5595
- Chen, D.-H. and X.-R. He (2004).Synthesis of nickel ferrite nanoparticles by sol-gel method. *Materials Research Bulletin* 36(7-8): 1369-1377.
- Chen, W., Jun, L., Giuseppe, M., Gao-Mai, Y., Feng-Xing, Z., Leonardo, P., Giuseppe, V. (2007). *App. Cat. B: Environmental* 76:218–226.
- Cheng, H., Ma, J., Zhao, Z., Qi, L. (1995). Hydrothermal Preparation of Uniform Nanosize Rutile and Anatase Particles. *Chem. Mater.* 7:663-671.
- Cheng, Q., Li, C., Pavlinek, V., Saha, P., Wang, H. (2006). Surface-modified antibacterial TiO₂/Ag⁺ nanoparticles: Preparation and properties. *App. Surface Sci.* 252:4154-4160
- Choi, W.; Termin, A.; Hoffmann, M. R. (1994) *J. Phys. Chem. B*, 98. (75)
- Choy, K. L. (2003), *Prog. Mater. Sci.* 48
- Chun Hu, Yongqing Lan, Jiuhui Qu, Xuexiang Hu, and Aimin Wang (2006) Ag/AgBr/TiO₂ Visible Light Photocatalyst for Destruction of Azodyes and Bacteria. *J. Phys. Chem. B* 110: 4066 –4072
- Chung, C.J., Lin, H.I., He, J.L. (2007). Antimicrobial efficacy of photocatalytic TiO₂ coatings prepared by arc ion plating. *Surface and Coatings Technology* 202:1302–1307.
- Clemens Burda, Yongbing Lou, Xiaobo Chen, Anna C. S. Samia, John Stout, James L. Gole, (2003), Enhanced Nitrogen Doping in TiO₂ Nanoparticles. *Nano Lett.* 3(8), 1049

- Corradi A. B., Bondioli F., Focher, B. Ferrari, A. M., Grippo C., Mariani E., Villa, C.(2005). *J. Am. Ceram. Soc.*, 88
- Cozzoli P. D., Comparelli R., Fanizza. E., Curri M. L., Agostiano A., (2003) *Mat. Sci. Engg. C*, 23, 707
- Cristina Buzea, Ivan Pacheco, and Kevin Robbie (2007). *Nanomaterials and Nanoparticles: Sources and Toxicity. Biointerphases* 2(4)
- Crystallography Software Database, XRD Department, University of Cambridge, United Kingdom.
- D. Schierbaum, U. K. Kirner, J. F. Geiger, and W. Gopel, (1991) "Schottky-barrier and conductivity gas sensors based upon Pd/SnO₂ and Pt/TiO₂," *Sensors and Actuators B-Chemical*, vol. 4, pp. 87-94,
- D. Vorkapic and T. Matsoukas, (1998) *J. Am. Ceram. Soc.* 81, 2815.
- Davis C.P. and Marks J.W. (2001) *Escherichia coli O157:H7 infection.*
- Dhananjeyan, M.R., Kandavelu, V., Renganathan, R. (2000). A study on the photocatalytic reactions of TiO₂ with certain pyrimidine bases: effects of dopants (Fe³⁺) and calcination. *J. Mol. Catal. A: Chem.* 151:217-223.
- Diebold U., (2003), *The surface Science of Titanium dioxide. Surface Science Reports*, 48, 53
- Dislich, (1983) *Glassy and Crystalline Systems from Gels - Chemical Basis and Technical Application. Journal of Non-Crystalline Solids*, 57(3), p. 371-388
- Do, Y. R.; Lee, K.; Dwight, K.; Wold, W. J. *Sol. State Chem.* (1994), 108.(78)
- Dong B., He B., Huang J., Gao G., Yang Z., Li H. (2008). High dispersion and electrocatalytic activity of Pd/titanium dioxide nanotubes catalysts for
- Doong R., Chang S., Hung Y., Kao. I. (2007). Preparation of highly ordered titanium dioxide porous films: Characterization and photocatalytic activity. *Separation and Purification Technology* 58:192–199.
- E. A. Barringer and H. K. Bowen (1985) *Langmuir*, 1, 420.
- Edington J. W., Chapter 1. (1974) *The operation and calibration of the electron microscope. In Practical Electron Microscopy in Material Science; Education: Hong Kong.*

- Emilio, C. A.; Litter, M. I.; Kunst, M.; Bouchard, M.; Colbeau-Justin, C. (2006) *Langmuir*, 22
- Eric Drexler (1991). *Nanosystems: Molecular Machinery, Manufacturing, and Computation*. MIT PhD thesis
- Ershad-Langroudi, A.; Mai, C.; Vigier, G.; Vassoile, R. J. (1997) *Appl. Polym. Sci.* 65
- European Commission (EC). (2004). *Nanotechnology: Innovation for tomorrow's world* EUR 21151EN [Online] Available: www.cordis.lu/nanotechnology)
- F. Xin, L. Q. Jing, Z. Y. Ren, B. Q. Wang, and H. G. Fu, (2005) Effects of simultaneously doped and deposited Ag on the photocatalytic activity and surface states of TiO₂. *Journal of Physical Chemistry B*, vol. 109, pp. 2805-2809
- Frank, S. N.; Bard, A. (1977) *J. J. Am. Chem. Soc.* 99.
- Friedmann, H. Hansing, and D. Bahnemann, (2007) Primary processes during the photodeposition of Ag clusters on TiO₂ nanoparticles. *Zeitschrift für Physikalische Chemie*, vol. 221, pp. 329-348
- Fu, G.F., Vary, P.S. et al. (2005) Anatase TiO₂ nanocomposites for antimicrobial coatings. *Journal of Physical Chemistry B*, 109 (18), 8889 – 98.
- Fujishima, A. and Honda, K. (1972) Electrochemical Photolysis of Water at a Semiconductor Electrode. *Nature* 238:37-38
- Fujishima, T N Rao, D A Tryk, (2000) Titanium dioxide photocatalysis, *J. Photochem. Photobiol. C: Photochem. Rev.* 1 .1–21
- G. Highfield and P. Pichat, (1989) Photoacoustic study of the influence of platinum loading and bulk doping with chromium(III) ions on the reversible photochromic effect in titanium-dioxide - Correlation with photocatalytic properties. *New Journal of Chemistry*, vol. 13, pp. 61-66
- G. Rothenberger, J Moser, M Gratzel, N Serpone, D K Sharma (1985) Charge carrier trapping and recombination dynamics in small semiconductor particles, *J Am Chem Soc* 107 , 8054–8059

- Garvie, R.C. (1978). Stabilization of the Tetragonal Structure in Zirconia Microcrystals. *J. Phys. Chem.* 82:218-224.
- Gervais, C., Smith, M. E., Pottier, A., Jolivet, J. P., Babonneau, F. 2001. Solid-State $^{47,49}\text{Ti}$ NMR Determination of the Phase Distribution of Titania Nanoparticles. *Chem. Mater.* 13:462-467
- Glassford, K. M.; Chelikowsky, J. R. *Phys. Rev. B* 1992, 45.
- Gou Y., Yang S., Zhou X., Lin C., and Wang Y. *Journal of Nano-materials.* (2011) 4-5.
- Grätzel, M. (2001) *Nature*, review article Photoelectrochemical cells.
- Grzmil, B., Kic, B., Rabe, M. (2004). Inhibition of the Anatase-Rutile Phase Transformation with Addition of K_2O , P_2O_5 and Li_2O . *Chem. Pap.* 58:410-414.
- Guizard, A. C. Julbe, and A. Ayrat (1999) Design of nanosized structures in sol-gel derived porous solids. Applications in catalyst and inorganic membrane preparation. *Journal of Materials Chemistry*, 9(1), p. 55-65
- Guizard, C. Mouchet, R. Vacassy, A. Julbe, and A. Larbot, (1994) Sol-gel processing of inorganic membranes. *Journal of Sol-Gel Science and Technology*, 2(1 - 3), p. 483-487
- Gunawan C, Teoh W Y, Marquis C P, Lifa J, Amal R, (2009) Reversible antimicrobial photo switching in nanosilver. *Small* 341–344
- Gwinn, M. R.; Vallyathan, V., *Environmental Health Perspectives*, (2006), 114, 1818-1825
- H Gerischer, A Heller, (1991) The role of oxygen in photooxidation of organic molecules on semiconductor particles. *J Phys Chem* vol 95 ,5261–5267
- H M Sung, J R Choi, H J Hah, S M Koo, Y C Bae, (2004) Comparison of Ag deposition effects on the photocatalytic activity of nanoparticulate TiO_2 under visible and UV light irradiation, *J Photochem. Photobiol A Chem.* 163. 37–44
- H N Pham, T McDowell, E Wikins, (1995) Photocatalytically-mediated disinfection of water using TiO_2 as a catalyst and spore-forming *Bacillus pumilus* as a model, *J Environ Sci Health Part A* 30 ,627–636
- H. Gerischer, (1995) Photocatalysis in aqueous-solution with small TiO_2 particles and the dependence of the quantum yield on particle-size and light-intensity. *Electrochimica Acta*, vol. 40, pp. 1277-1281.

- H. Liu, J. Yang, L. Wang, X. J. Yang, L. D. Lu, and X. Wang, (2000) An improvement on sol-gel method for preparing ultrafine and crystallized titania powder. *Materials Science and Engineering a-Structural Materials Properties Microstructure and Processing*, 289(1-2), p. 241-245
- H. Schmidt, (1989) Preparation, Application and Potential of Ormocers. in *Proceedings of The Winter School On Glasses and Ceramics from Gels, Sol-Gel Science and Technology*, Sao Carlos (SP), Brazil
- H. Shimakawa, F. Sakamoto and Y. Tsuchida, (1993) *Ceram. Powder Sci.*, 4, 115.
- H. Tang, et. al. (1994) *Appl. Phys.* 75, 2042.
- Hagfeldt, M. Grätzel, (2000) *Acc. Chem. Res.*, 33, 269-277
- Hah, S. M. Koo, and Y. C. Bae, (2004) Comparison of Ag deposition effects on the photocatalytic activity of nanoparticulate TiO₂ under visible and UV light irradiation. *Journal of Photochemistry and Photobiology A-Chemistry*, vol. 163, pp. 37-44.
- Hamal, D. B.; Klabunde, K. J.(2007) *J. Colloid Interface Sci.*, 311, 514
- Hirakawa T, P V Kamat (2005) Charge Separation and Catalytic Activity of Ag-TiO₂ Core-Shell Composite Clusters under UV-Irradiation. *J. Am. Chem. Soc* 127(11): 3928-3934
- Hirsch, et al., (2006) Metal nanoshells. *Ann. Biomed. Eng.*, vol. 34(1), p. 15
- Hoertz P G, Thompson D W, Friedman L A, Meyer G J (2002) Ligand Localized Electron Trapping at Sensitized Semiconductor Interfaces. *J. Am. Chem. Soc.* 124: 9690-9691
- Hoffmann M R, S T Martin, W Choi, D W Bahnemann, (1995) Environmental applications of semiconductor photocatalysis, *Chem Rev* 95 , 69–96.
- Hosaka, N.; Sekiya, T.; Aatoko, C.; Kurita, S.(1997) *J. Phys. Soc. Japan*, 66
- Hosaka, N.; Sekiya, T.; Fujisawa, M.; Satokob, C.; Kurita, S. (1996) *J. Electron Spectrosc. Relat. Phenom.*, 78
- <http://en.wikipedia.org/wiki/Sol-gel>
- <http://staff.aist.go.jp/nomurak/>
- <http://www.bmsc.washington.edu/people/merritt/bc530/bragg>

- <http://www.nanoword.net/library/defgen/generate.php?termid=109>.
- <http://www.pilkingtonselfcleaningglass.co.uk/trade/>; 28-May-2010
- Hu, Y., Tsai, H. L., Huang, C.L. (2003). Phase transformation of precipitated TiO₂ nanoparticles. *Materials Science and Engineering A* 344:209-214.
- hydrazine oxidation. *J. of Power Sources* 175:266–271.
- Ihara T, Miyoshi M, et al. (2003) Visible-light-active titanium oxide photocatalyst realized by an oxygen-deficient structure and by nitrogen doping. *Applied Catalysis B: Environmental* 42(4): 403-409
- Isley, S. L., and Penn, R. L. (2006). Relative Brookite and Anatase Content in Sol-Gel-Synthesized Titanium Dioxide Nanoparticles. *J. Phys. Chem B* 110:15134-15139)
- J M Herrmann, H Tahiri, Y Ait-Ichou, G Lassaletta, A R Gonzalez-Elipe, and A Fernandez, (1997) Characterization and photocatalytic activity in aqueous medium of TiO₂ and Ag-TiO₂ coatings on quartz. *Applied Catalysis B*, vol. 13, no. 3-4, pp. 219–228
- J. G. Yu and X. J. Zhao, (2000) Ag-doped TiO₂ composite thin films prepared by sol-gel and its photocatalytic activity. *Rare Metal Materials and Engineering*, vol. 29, pp. 390-393.
- J. G. Yu, J. F. Xiong, B. Cheng, and S. W. Liu, (2005) Fabrication and characterization of Ag-TiO₂ multiphase nanocomposite thin films with enhanced photocatalytic activity. *Applied Catalysis B-Environmental*, vol. 60, pp. 211-221,
- J. H. Schattka, D. G. Shchukin, J. G. Jia, M. Antonietti, R. A. Carusa, *Chem. Mater.* (2002), 14, 5103-5108.
- J. K. Burdett et al., T. Hughbanks, G. J. Miller, J. W. Richardson Jr., and J. V. Smith,(1987) Structural-electronic relationships in inorganic solids: powder neutron diffraction studies of the rutile and anatase polymorphs of titanium dioxide at 15 and 295 K. *Journal of the American Chemical Society*, vol. 109, no. 12, pp. 3639–3646
- J. Livage and J. Lemerle, (1982) Transition metal oxide gels and colloids. *Annual Review. Materials Science*, 12 , 103
- J. Livage, M. Henry, and C. Sanchez, (1989) Sol-gel Chemistry of Transition Metal Oxides. *Prog. Solid State Chem.*, 18(4), p. 259-341

- J. S. Lee and W. Y. Choi, (2004) Effect of platinum deposits on TiO₂ on the anoxic photocatalytic degradation pathways of alkylamines in water: Dealkylation and N-alkylation. *Environmental Science & Technology*, vol. 38, pp. 4026-4033.
- J. S. Olsen, L. Gerward, and J. Z. Jiang, (1999) On the rutile/[alpha]- PbO₂-type phase boundary of TiO₂. *Journal of Physics and Chemistry of Solids*, vol. 60, no. 2, pp. 229–233
- J. X. He, P. J. Yang, H. Sato, Y. Umemura, and A. Yamagishi, (2004) Effects of Ag-photodeposition on photocurrent of an ITO electrode modified by a hybrid film of TiO₂ nanosheets. *Journal of Electroanalytical Chemistry*, vol. 566, pp. 227-233
- J. Y. Wen and G. L. Wilkes, (1996) Organic/inorganic hybrid network materials by the solgel approach. *Chemistry of Materials*, 8(8), p. 1667-1681
- Jeon, H.-J., S.-C. Yi, et al. (2003). Preparation and antibacterial effects of Ag-SiO₂ thin films by sol-gel method. *Biomaterials* 24(27): 4921-4928.
- Jones, A. C.; Chalker, P. R. *J. Phys. D: Appl. Phys.* (2003), 36, R80
- K D Kim, D N Han, J B Lee, H T Kim, (2006) Formation and characterization of Ag-deposited TiO₂ nanoparticles by chemical reduction method, *Scr. Mater.* 54 : 143–146
- Kahn, Jennifer (2006). "Nano's big future ". *National Geographic* vol 209, no.6 (June 2006): 98–119.
- Kahn, Jennifer (2006). "Nanotechnology". *National Geographic* 2006: 98–119
- Kamat P V and N M Dimitrijevic, *Solar Energy*, 44,83 (1990)
- Karout, P. Buisson, A. Perrard, and A. Pierre. (2005) Shaping and Mechanical Reinforcement of Silica Aerogel Biocatalysts with Ceramic Fiber Felts. *Journal of Sol-Gel Science and Technology*, 36(2), p. 163-171
- Kato S, Hirano Y, Iwata M, Sano T, Takeuchi K, Matsuzawa S (2005) Photocatalytic degradation of gaseous sulfur compounds by silver-deposited titanium dioxide. *Appl. Catal. B-Environ* 57:109-115
- Kato, N.; Higuchi, K.; Tanaka, H.; Nakajima, J.; Sano, T.; Toyoda, T. *Sol.*
- Kavan, L.; Gratzel, M.; Gilbert, S. E.; Klemenz, C.; Scheel, H. (1996) *J. J. Am. Chem.Soc.*, 118

- Kawashita, M., Tsuneyama, S., Miyaji, F. (2000). Antibacterial silver containing silica glass prepared by sol-gel method, *Biomaterials* 21:393-398
- Keller V, G. Bernhardt, F. Garin, (2003) *J Langmuir* 21(12): 5588-5595). 215
- Keshmiri, M., Mohseni, M., Troczynski, T. (2004). Development of novel TiO₂ sol-gel derived composite and its photocatalytic activities for trichloroethylene oxidation. *App. Cat. B: Environmental* 53:209-219.
- Khan SUM, Al-Shahry M, Ingler W B (2002) Efficient Photochemical Water Splitting by a Chemically Modified n-TiO₂. *Science* 297:2243-2245
- Ki, D., Liu, H., Peng, T., Liu, X., Dai, K. (2008). Preparation and photocatalytic activity of WO₃/TiO₂ nanocomposite particles. *Mat. Let.* 62:447-450.
- Kim, Kim, T. K., Lee, M. N., Lee, S. H., Park, Y. C., Jung C. K., Boo, J. H. (2005). Development of surface coating technology of TiO₂ powder and improvement of photocatalytic activity by surface modification. *Thin Solid Films* 475:171-177.
- Klabunde, K., Ed.(2001) *Nanoscale Materials in Chemistry*, Wiley Interscience: New York, ; p 23
- Koelsch, M.; Cassaignon, S.; Thanh Minh, C. T.; Guillemoles, J.-F.; Jolivet, (2004) *J.-P. Thin Solid Films*, 451
- Kroto, H.W. et al. (1985). "C₆₀: Buckminsterfullerene". *Nature* 318: 162–163. doi:10.1038/318162a0
- Kuhn KP, Chaberny IF, Massholder K, et al. (2003) Disinfection of surfaces by photocatalytic oxidation with titanium dioxide and UVA light. *Chemosphere* 53:71–7
- Kumar R V, Raza G (2009) Photocatalytic disinfection of water with Ag-TiO₂ nanocrystalline composite. *Ionics* 15(5): 579-587
- Kuo, Y.-L.; Chen, H.-W.; Ku, Y. (2007), *Thin Solid Films* ,515, 3461
- L A Brook, P Evans, H A Foster, M E Pemble, A Steele, D W Sheel, H M Yates, (2007) Highly bioactive silver and silver/titania composite films grown by chemical vapour deposition, *J Photochem Photobiol, A Chem.* 187 ,53–63

- L. L. Hench and J. K. West (1990), *The Sol-Gel Process*, Chemical Reviews, 90(1), p. 33-72
- L. Linsebigler, G. Q. Lu, and J. T. Yates (1995) Photocatalysis on TiO₂ surfaces - Principles, mechanisms, and selected results. Chemical Reviews, vol. 95, pp. 735-758.
- L. Stroyuk, V. V. Shvalagin, and S. Y. Kuchmii (2005) Photochemical synthesis and optical properties of binary and ternary metal-semiconductor composites based on zinc oxide nanoparticles. *J. Photochem. Photobiol., A: Chem.*, vol. 173(2), pp. 185–194
- L. X. Chen, T. Rajh, Z. Y. Wang, M. C. Thurnauer, *J. Phys. Chem. B* (1997), 101, 10688-10697
- Li W, C Ni, H Lin, C P Huang, Ismat Shah S (2004) Size dependence of thermal stability of TiO₂ nanoparticles. *J App Phys* 96(11) 6663-6668
- Li XZ, Li FB, Yang CL, Ge WK (2001) Photocatalytic activity of WO_x-TiO₂ under visible light irradiation. *J Photochem Photobiol A* 141(2-3): 209-217
- Li, C.H., Hsieh, Y.H., Chiu, W.T., Liu, C.C., Kao, C.L. (2007). Study on preparation and photocatalytic performance of Ag/TiO₂ and Pt/TiO₂ photocatalysts. *Separation and Purification Technology* 58:148–151.
- Li, Y.; Hwang, D.-S.; Lee, N. H.; Kim, S.-J. (2005), *Chem. Phys. Lett.* 404
- Lifshin, E. (1999). *X-ray Characterization of Materials*. Wiley-VCH, Germany)
- Lin Y., Li D., Hu J., and Xiao G. *J. Phys. Chem. C*, 4 (2011) 20-25
- Liqiang, J.; Yichun, Q.; Baiqi, W.; Shudan, L.; Baojiang, J.; Libin, Y.; Wei, F.; Honggang, F.; Jiazhong, S. (2006) *Solar Energy Materials & Solar Cells* 90, 1773
- Litter, M.I. and Navio, A. (1996) Photocatalytic properties of iron-doped titania semiconductors. *J. Photochem. Photobiol. A: Chem.* 98:171-181.
- Liu, Y., Wang, X.L. et al. (2008) Excellent antimicrobial properties of mesoporous anatase TiO₂ and Ag/TiO₂ composite films. *Microporous and Mesoporous Materials*, 114 (1 – 3), 431 – 9.

- Liu G, Zhao J, Hidka H, et al. (2000) ESR spin-trapping detection of radical intermediates in the TiO₂-assisted photooxidation of sulforhodamine B under visible irradiation. *J Photochem Photobiol A:Chem* 133: 83-88
- Lou, H., Chen, M., Beis, K., Low, A., Bayley, H., Booth, I. R., Naismith, J., H., (2010) Molecular Insights Into Clinically Isolated OmpC Mutants and Their Role in Multi-Drug Resistance
- Luo, H., Wang, C., Yan, Y. (2004) Synthesis of Mesoporous Titania with Controlled Crystalline Framework. *Chem. Mater.* 15:3841-3846
- Luo, S. F. Yang, Z. C. Wang, et al. (2005) Structural phase transitions in brookite-type TiO₂ under high pressure. *Solid State Communications*, vol. 133, no. 1, pp. 49–53
- M C Ramos-Sánchez, F J Rey, M L Rodríguez, F J Martín-Gil, J Martín-Gil, (1988) DTG and DTA studies on typical sugars. *Thermochim Acta*, 134: 55-60.. Elsevier Science Publishers B.V., Amsterdam
- M S Lee, S S Hong, M Mohseni, (2005) Synthesis of photocatalytic nanosized TiO₂-Ag particles with sol-gel method using reduction agent, *J Mol Catal, A Chem* 242 135–140
- M. Crisan, M. Gartner, L. Predoana, R. Scurtu, M. Zaharescu, and R. Gavrilă, (2004) Sol- Gel SiO₂-ZrO₂ Coatings for Optical Applications. *Journal of Sol-Gel Science and Technology*, 32(1 - 3), p. 167-172
- M. Howard, (1999), Brookite, Rutile Paramorphs after Brookite, and Rutile Twins from Magnet Cove, Arkansas. *Rocks and Minerals*. Heldref Publications.
- M. Koo, I. Rubinstein, and H. Onyuksel, (2005) Role of nanotechnology in targeted drug delivery and imaging: a concise review. *Nanomed. Nanotechnol., Biol. Med.*, vol. 1(3), p. 193.
- M. R. Hoffmann, S. T. Martin, W. Y. Choi, and D. W. Bahnemann, (1995) Environmental applications of semiconductor photocatalysis. *Chemical Reviews*, vol. 95, pp. 69-96,
- M. Ratner, D. Ratner (2003) *Nanotechnology: A Gentle Introduction to the Next Big Idea*, Person Education, Inc.,

- M. S. W. Vong, N. Bazin, and P. A. Sermon, (1997) "Chemical modification of silica gels", *Journal of Sol-Gel Science and Technology*, 8(1-3), p. 499-505
- M. Serwaczak, M. W. Ubbenhorst, and S. Kucharski (2006) Optical and dielectric characteristics of photochromic hybrid sol-gel materials. *Journal of Sol-Gel Science and Technology*, 40(1), p. 39-44
- M. Winterer, (2002) *Nanocrystalline Ceramics, Synthesis and Structure*, Springer, Heidelberg, Springer Series in Materials Science, Volume 53
- Madigan M.T. and Martinko J. *Brock microbiology of Microorganisms*. 11th edition (2006) Pearson Education
- Martyanov, I. N. and Klambunde, K. J. (2004). Comparative study of TiO₂ particles in powder form and as a thin nanostructured film on quartz. *J. Cat.* 225:408- 416
- Matijevic, E. (1985). Production of Monodispersed Colloidal Particles. *Ann. Rev. Mater.Sci.* 15:483-516.
- Matsunaga T, Tomoda R, Nakajima T, Wake H. (1974) Photo electrochemical sterilization of microbial cells by semiconductor powders. *FEMS Microbiol Lett* (1985); 29: 211-214 McMillan Press Ltd. London.
- Mi, L., Xu, P., Shen, H., Wang P. (2008). Recovery of visible-light photocatalytic efficiency of N-doped TiO₂ nanoparticulate films. *J. Photochem. Photobiol. A: Chemistry* 193:222–227.
- Millis, A.; Hunte, S. L. J. *Photochem. Photobiol. A*, (1997), An overview of of semiconductor photocatalysis 108, 1-35
- Muller-Goymann, C. C. (2004) Physicochemical characterization of colloidal drug delivery systems such as reverse micelles, vesicles, liquid crystals and nanoparticles for topical administration. *Eur. J. Pharm. Biopharm.* 58:343-356.
- N. Kato, K. Higuchi, Y. Takeda, A. Takeichi, T. Motohiro, T. Sano and T. Toyoda. (2006) Long-term stability of the DSC module under outdoor working condition. *Proceedings of Renewable Energy*, Makuhari, Japan
- N. Morimoto, et al. (2004) Nano-scale surface modification of segmented polyurethane with a phospholipid polymer. *Biomaterials*, vol. 25(23), p. 5353.

- N. R. Rao, A. Mueller, A. K. Cheetham (2004) *The Chemistry of Nanomaterials: Synthesis, Properties and Applications*, Vol.1, Wiley-VCH, Weinheim
- N. Taniguchi (1974). On the Basic Concept of 'Nano-Technology'. Proc. Intl. Conf. Prod. London, Part II British Society of Precision Engineering
- Nagaveni, K., Sivalingam, G., Hegde, M.S. and Madras, G.,(2004) Solar Photocatalytic Degradation of Dyes: High Activity of Combustion Synthesized Nano TiO₂. *Appl. Catal. B Env.*, 48, 83-93
- Nakamura Ryuhei, Tomoaki Tanaka, and Yoshihiro Nakato (2005) Oxygen Photoevolution on a Tantalum Oxynitride Photocatalyst under Visible-Light Irradiation: How Does Water Photooxidation Proceed on a Metal–Oxynitride Surface *J Phys Chem B* 109 (18): 8920-8927
- Nanotechnology-size matters building a successful nanotechnology company," E.I.U.a.t.I.o. *Nanotechnology*, (2002) 252:4154-4160
- Nanoword Net, Encyclopedia Nanotech.
- National Nanotechnology Initiative (NNI): <http://www.nano.gov/html/facts/faqs.html>. Browsed February 12, 2008.
- Nicholls, D. (1974) *Complexes and First-Row Transition Elements*; MacMillan Education: Hong Kong.
- Nie, X. L., S. P. Zhuo, et al. (2009). Doping of TiO₂ Polymorphs for Altered Optical and Photocatalytic Properties. *International Journal of Photoenergy*. (2) 115-121
- Niño-Martínez, N Martínez-Castañón, G A Aragón-Piña, A Martínez-Gutierrez, F Martínez-Mendoza, J R Ruiz, (2008) Characterization of silver nanoparticles synthesized on titanium dioxide fine particles. *Nanotechnology* ,19, 065711 of coliform bacteria and viruses in secondary waste water effluent, *Water Res.*
- Ohno T, M Akiyoshi, et al. (2004) Preparation of S-doped TiO₂ photocatalysts and their photocatalytic activities under visible light. *Appl Catal A: Gen* 265(1): 115-121
- Ohtani, M. Kakimoto, S. Nishimoto, and T. Kagiya (1993) Photocatalytic reaction of neat alcohols by metal-loaded titanium(IV) oxide particles.

Journal of Photochemistry and Photobiology A-Chemistry, vol. 70, pp. 265-272

- Oliveira, M. M., Schnitzler, D.C., Zabin, A. J. G. (2003). (Ti,Sn)O₂ Mixed Oxides Nanoparticles Obtained by the Sol-Gel Route. Chem. Mater. 15:1903-1909.
- Ollis, E. Pelizzetti, and N. Serpone, (1991) Photocatalyzed destruction of water contaminants. Environmental Science & Technology, vol. 25, pp. 1522-1529
- Yang, J. and Ferreira, J.M.F. (1998). Inhibitory effect of the Al₂O₃-SiO₂ mixed additives on the anatase-rutile phase transformation. Mater. Lett. 36:320-324
- P. Etienne, J. Denape, J. Y. Paris, J. Phalippou, and R. Sempere, (1996) Tribological properties of ormosil coatings. Journal of Sol-Gel Science and Technology, 6, p. 287-297
- P. Pichat,(1987) Surface-properties, activity and selectivity of bifunctional powder photocatalysts. New Journal of Chemistry, vol. 11, pp. 135-140,
- P.M. Ajayan, L.S. Schadler, P.V. Braun (2003). Nanocomposite science and technology. Wiley. ISBN 3527303596
- Palomares, R. Vilar, A. Green, J. R. Durrant, Adv. Funct. Mater. (2004), 14, 111-115
- Perrin, F. X.; Nguyen, V.; Vernet, J. L. J. Sol-Gel Sci. Technol. (2003), 28, 205
- Pettibone John M, Cwiertny David M, Michelle Scherer, Vicki H (2008) Grassian Adsorption of Organic Acids on TiO₂ Nanoparticles: Effects of pH, Nanoparticle Size, and Nanoparticle Aggregation. J Langmuir, 24(13): 6659-6667
- Pierre, (1998) "Introduction to Sol-gel Processing", Kluwer Academic Publishers, 1-4.
- Pope, E. J. A. and J. D. Mackenzie (1988). Nd-doped silica glass I: Structural evolution in the sol-gel state. Journal of Non-Crystalline Solids 106(1-3): 236-241.

- R. J. Watts, S. Kong, M. P. Orr, G. C. Miller, B. E. Henry (1995) Photocatalytic inactivation of coliform bacteria and viruses in secondary wastewater effluent *Water Research*, 29 (1) pp. 95–100
- R. Bakalova, et al. Quantum dots as photosensitizers *Nat. Biotech.*, vol. 22(11), p. 1360,
- R. Bamwenda, S. Tsubota, T. Nakamura, and M. Haruta, (1995) Photoassisted hydrogen-production from a water-ethanol solution - A comparison of activities of Au-TiO₂ and Pt-TiO₂. *Journal of Photochemistry and Photobiology A-Chemistry*, vol. 89, pp. 177-189.
- R. Buonsanti, V. Grillo, E. Carlino, et al. (2008) Nonhydrolytic synthesis of high-quality anisotropically shaped brookite TiO₂ nanocrystals. *Journal of the American Chemical Society*, vol. 130, no. 33, pp. 11223–11233.
- R. J. P. Corriu, D. Leclercq, P. Lefevre, P. H. Mutin, and A. Vioux, (1992) "Preparation of Monolithic Metal-Oxide Gels by a Non-Hydrolytic Sol-Gel Process" *Journal of Materials Chemistry*, 2(6), p. 673-674.
- R. Li, X. H. Wang, M. Y. Yan and L. T. Li, *Mater. Chem. Phys.*, 78, (2002) 184.
- R. Uhlmann and G. Teowee, (1998) Sol-gel science and technology: Current state and future prospects. *Journal of Sol-Gel Science and Technology*, 13(1-3), p. 153-162
- Ranjit, K.T., Cohen, H., Willer, L., Bossmann, S., Braun, A.M. (1999). Lanthanide oxidedoped titanium dioxide: Effective photocatalysts for the degradation of organic pollutants. *J. Mater. Sci.* 34:5273-5280.
- Rao, C. N. R.; Cheetham, A. K., (2006) *Nanomaterials Handbook*, CRC Press LLC, Boca Raton
- Rao, C. N. R.; Mueller, A.; Cheetham, A. K. (2004) *Nanomaterials – An Introduction*, 1, 1-11.
- Rengaraj, S., Venkataraj, S., Jei-Won, Y., Younghun, K., Li, X.Z., Pang, G.K.H. (2007). Preparation, characterization and application of Nd-TiO₂ photocatalyst for the reduction of Cr(VI) under UV light illumination. *App. Cat. B: Environmental* 77:157–165.

- Reyes-Coronado, G. Rodríguez-Gattorno, M.E. Espinosa- Pesqueira, C. Cab, R. de Coss, and G. Oskam, (2008) Phase-pure TiO₂ nanoparticles: anatase, brookite and rutile. *Nanotechnology*, vol. 19, no. 14, Article ID 145605.
- Riboh J. C, A. J. Haes, A. D. McFarland, C. R. Yonzon, and R. P. Van Duyne (2003) A Nanoscale Optical Biosensor:Real-Time Immunoassay in Physiological Buffer Enabled by Improved Nanoparticle Adhesion. *J Phys. Chem. B*, 107(8): 1772-1780
- Rincon, A. G. and Pulgarin, C. (2004). Bactericidal action of illuminated TiO₂ on pure Escherichia coli and natural bacterial consortia: post-irradiation events in the dark and assessment of the effective disinfection time. *App. Cat. B:Environmental* 49:99-112
- Rodgers, P. (2006). "Nanoelectronics: Single file". *Nature Nanotechnology* doi:10.1038/nnano.2006.5
- Roduner E. (2006) Size matters: why nanomaterials are different. *Chem. Soc. Rev.*, 35, pp. 583-592.
- Rupa A V, D Manikandan, et al. (2007) Effect of deposition of Ag on TiO₂ nanoparticles on the photodegradation of Reactive Yellow-17. *Journal of Hazardous Materials* 147(3): 906-913
- S. Hore, E. Palomares, H. Smit, N. J. Bakker, P. Comte, P. Liska, K. R. Thampi, J. M. Karoon, A. Hinsh, J. R. Durrant, (2005) *J. Mater. Chem.*, 15, 412-418
- S. L. Goodman, P. A. Sims and R. M. Albrecht, (1996) Three-dimensional extracellular matrix textured biomaterials. *Biomaterials*. vol. 17(21), p. 2087
- S. Mo, W. Ching, *Phys. Rev. B* 51, 19, 13023 (1995)
- S. Qourzal, A. Assabbane and Y. Ait-Ichou (2004), *J. Photochem. Photobiol. A: Chem.*, 163, 317.
- S.-D.Mo and W. Y. Ching (2004) Electronic and optical properties of three phases of titanium dioxide: rutile, anatase, and brookite. *Physical Review B*, vol. 51, no. 19, pp. 13023– 13032.
- S'okmen M, F Candan, Z S'umer (2001) *J. Photochem. Photobiol. A* 143 241
- Saito *et al.* 1992

- Salmi, M., Tkachenko, N., Vehmanen, V., Lamminmaki, R. J., Karvinen, S., Lemmetyinen, H. 2004. The effect of calcination on photocatalytic activity of TiO_2 particles: femtosecond study. *J. Photochem. Photobiol. A: Chemistry* 163:395-401.
- Sanchez, C.; Livage, J.; Henry, M.; Babonneau, F. (1998) *J. Non-Cryst. Solids* 100. (165)
- Sanchez, C.; Ribot, F. (1994), *New J. Chem.* 18.
- Sanchez, C.; Ribot, F.; Lebeau, B. (1999) *J. Mater. Chem.*, 9.
- Sanderson R T *Science* (1951)
- Sasaki, Y. and Kato, H. (2004). Nanostructure analysis for applied research on zeolites. *Zeolites* 21:11-17.
- Sawai, J., Shoji, S., Igarashi, H., Hashimoto, A., Kokugan, T., Shimizu, M. and Kojima, H., (1998). Hydrogen Peroxide as an Antibacterial Factor in Ag- TiO_2 Powder Slurry. *Journal of Fermentation and Bioengineering*, Vol. 86, No. 5, pp. 521 – 522.
- Schletter, J., et al. (1995) Molecular mechanisms of endotoxin activity. *Archives of Microbiology*. 164(6): p. 383-389.
- Schmid G (ed.) (1994) *Clusters and Colloids. From Theory to Applications* (VCH, Weinheim, ISBN 3-527-29043-5, 555 Seiten, Preis: DM 248)
- Schubert, H.; Husing, N.; Lorenz, N. (1995), *Chem. Mater.* 7. (168)
- Schwietert, Yaghoubi et al. (2001)
- Sclafani, M. N. Mozzanega, and P. Pichat, (1991) Effect of silver deposits on the photocatalytic activity of titanium-dioxide samples for the dehydrogenation or oxidation of 2-propanol. *Journal of Photochemistry and Photobiology A-Chemistry*, vol. 59, pp. 181-189
- Seery, M.K, George R, Floris P (2007) Silver doped titanium dioxide nanomaterials for enhanced visible light photocatalysis, 258-263. In *Journal of Photochemistry and Photobiology A Chemistry* 189 (2-3).
- Serpone N, Pelizzetti Ezio (1989) *Photocatalysis: Fundamentals and Applications*, Wiley, New York, USA
- Seven, O., Dindar, B., Aydemir, S., Metin, D., Ozinel, M. A., Icli, S. (2004) Solar photocatalytic disinfection of a group of bacteria and fungi aqueous

suspensions with TiO₂, ZnO and Sahara desert dust. *J. Photochem. Photobiol. A: Chemistry* 165:103-107

- Smith, Ruan g, Rhyner m , (2006), engineering luminescent quantum dots for in vivo molecular and cellular imaging. *Ann. Biomed. Eng.*, vol. 34(1), p.3,
- Sondi, I., Salopek-Sondi, B. (2004). Silver nanoparticles as antimicrobial agent: a case study on *E. coli* as a model for Gram-negative bacteria. *Journal of Colloid and Interface Science*, 275: 177-182.
- Stoimenov P K, R L Klinger, G L Marchin, K J Klabunde, (2002) Metal oxide nanoparticles as bactericidal agents, *Langmuir* 18, 6679–6686
- Su, W., Fu, X., Wei, K., Zhang, H., Lin, H., Wang, X., Li, D. (2001). Spectrum studies on titania photocatalysts. *Guang Pu Xue Yu Guang Pu Fen Xi* 21:32-34.
- Su, W., Fu, X., Wei, K., Zhang, H., Lin, H., Wang, X., Li, D. (2001). Spectrum studies on titania photocatalysts. *Guang Pu Xue Yu Guang Pu Fen Xi* 21:32-34.2001
- Subramanian, E. E. Wolf, and P. V. Kamatb (2004) Catalysis with TiO₂/gold nanocomposites. Effect of metal particle size on the Fermi level equilibration. *Journal of the American Chemical Society*, vol. 126, pp. 4943-4950
- Sugimoto T and X Zhou (2002) Synthesis of Uniform Anatase TiO₂ Nanoparticles by the Gel-Sol Method: 2. Adsorption of OH⁻ Ions to Ti (OH)₄ Gel and TiO₂ Particles. *J. Colloid. Interface Sci.* 252(2): 347-353
- Sugimoto, T., Xingping, Z. Atsushi, M., (2003). Synthesis of uniform anatase TiO₂ nanoparticles by gel-sol method 4. Shape control. *J. of Colloid and Interface Sci.* 259:53–61.
- Sunada, K., Kikuchi, Y., Hashimoto, K., Fujishima, A., (1998). Bactericidal and detoxification effects of TiO₂ film photocatalysts. *Environ. Sci. Technol.* 32, 726–728.
- Suppan, P. *Chemistry and Light*; Royal Society of Chemistry: Cambridge, 1994.
- Sweatlock, L. A., Maier, S. A., Atwater, H. A. (2005). Highly confined electromagnetic fields in arrays of strongly coupled Ag nanoparticles. *Phys. Rev. B* 71:1-7.

- T. Hirakawa and P. V. Kamat, (2005) Charge separation and catalytic activity of Ag@TiO₂ core-shell composite clusters under UV-irradiation, *Journal of the American Chemical Society*, vol. 127, pp. 3928-3934,
- T. Hirakawa and P. V. Kamat, (2004). Photoinduced electron storage and surface plasmon modulation in Ag@TiO₂ clusters. *Langmuir*, vol. 20, pp. 5645-5647,
- T. Paunesku, T. Rajh, G. Wiederrecht, J. Maser, S. Vogt, N. Stojicevic, M. Protic, B. Lai, J. Oryhon, M. Thurnauer, and G. Woloschak, (2003) *Nature Materials* . Biology of TiO₂-Oligonucleotide Nanocomposites .2, 343-346
- Tachikawa, T.; Fujitsuka, M.; Majima, T. *J. Phys. Chem. C* (2007), 111, 5259
- Testino, A., Bellobono, I. R., Buscaglia, V., Canevali, C., Arienzo, M. D., Polizzi, S., Scotti, S., Morazzoni, F. (2007). Optimizing the Photocatalytic Properties of Hydrothermal TiO₂ by the Control of Phase Composition and Particle Morphology. A Systematic Approach. *J. Am. Chem. Soc.* 129:3564-3575.
- Thapa, et al. (2003) Nano-structured polymers enhance bladder smooth muscle cell function. *Biomaterials*, vol. 24(17), p. 2915
- Thiel J, Pakstis L, Buzby S, Raffi M, Ni C, Pochan D J, Shah S I, (2007) Antibacterial properties of silver-doped titania. *Small*, 3, 799–803
- Thomas, K., and Sayre, P. (2005). Research Strategies for Safety Evaluation of Nanomaterials, Part I: Evaluating the Human Health Implications of Exposure to Nanoscale Materials. *Toxicol. Sci.* 2:316-321.
- Tillotson, T. M., A. E. Gash, et al. (2001). Nanostructured energetic materials using sol-gel methodologies. *Journal of Non-Crystalline Solids* 285(1-3): 338-345.
- Tomanek, Carbon Nano Tubes—A time line. (2001) Sept 7, 2001
- Toshima N (2000) Core/shell-structured bimetallic nanocluster catalysts for visible-light-induced electron transfer. *Pure Appl. Chem.* 72(1-2): 317-325
Transformation with Addition of K₂O, P₂O₅ and Li₂O. *Chem. Pap.* 58:410
- Trapalis C. C., P. Keivanidis, G. Kordas, M. Zaharescu, M. Crisan, A. Szatvanyi and M.Gartner, (2003). TiO₂ (Fe³⁺) nanostructured thin films with antibacterial properties. *Thin Solid Films*. Vol. 433, No. 1-2, pp. 186-190).

- V Rupa, D Manikandan, D Divakar, T Sivakumar, (2007) Effect of deposition of Ag on TiO₂ nanoparticles on the photodegradation of reactive yellow-17, J. Hazard. Mater. 147 , 906–913
- Velikovska, P., and Mikulasek, P. (2007). The influence of Cl⁻, SO₄²⁻ and PO₄³⁻ ions on the potential and microfiltration of titanium dioxide dispersions. Separation and Purification Technology 58;295–298.
- Walker, S. A.; Christensen, P. A.; Shaw, K. E.; Walker, G. M. (1995) J. Electroanal. Chem. , 393
- Wang Y M, Du G J, Liu H, Liu D, Qin S B, Wang N, Hu C G, Tao, X T, Jiao J, Wang J Y, Wang Z L (2008) Nanostructured sheets of Ti-O nanobelts for gas sensing and antibacterial applications. Adv. Funct. Mater. 18, 1131–1137
- Wang, C. Y., Bahnemann, D.W., Dohrmann, J.K. (2000). A novel preparation of iron doped TiO₂ nanoparticles with enhanced photocatalytic activity. Chem. Commun. 1539-1540.
- Wang, J. (1999). Sol-gel materials for electrochemical biosensors. Analytica Chimica Acta 399(1-2): 21-27.
- Wang, W.-N.; Lenggoro, I. W.; Terashi, Y.; Kim, T. O.; Okuyama, K. Mat. (2005) Sci.Eng. B, 123.26
- Wang, X.C., Yu, J.C. et al. (2005) A mesoporous Pt/TiO₂ nanoarchitecture with catalytic and Photocatalytic functions. Chemistry , 11 (10), 2997 – 3004
- Wang, Y.; Huang, Y.; Ho, W.; Zhang, L.; Zou, Z.; Lee, S. J. (2009) Hazard. Mater. 169, 77
- Waterman, Pamela J. "The Life of Composite Materials". Desktop Engineering Magazine April (2007). <http://66.195.41.10/Articles/Feature/The-Life-of-Composite-Materials-200704101800.html>.
- Wikipedia, There's Plenty of Room at the Bottom, <http://en.wikipedia.org/wiki/Plenty_of_Room_at_the_Bottom
- Wilks, S.A., Michels, H.T., Keevil, C.W. (2005). The survival of Escherichia coli O157 on a range of metal surfaces. Int. J. Food Microbiol. 105, 445–454.
- Wisitsoraat, A.; Tuantranont, A.; Comini, E.; Sberveglieri, G.; Wlodarski, W. (2009) Thin Solid Films, 517, 2775

- Wood, M. Giersig, and P. Mulvaney, (2001). Fermi level equilibration in quantum dot-metal nanojunctions. *Journal of Physical Chemistry B*, vol. 105, pp. 8810-8815.
- Wu, X.; Jiang, Q. Z.; Ma, Z. F.; Fu, M.; Shangguan, W. F.(2005) *Sol. State Comm.*, 136
- Xiaobo Chen et al. (2004) A Simple Parallel Photochemical Reactor for Photodecomposition Studies. *J. Chem. Educ*
- Xiaobo Chen, Yongbing Lou, Anna C. S. Samia, Clemens Burda (2005) Investigation of the Crystallization Process in 2 nm CdSe Quantum Dots. *J. Am. Chem. Soc.*, 127(12), 4372-4375
- Xiaobo Chen, Yongbing Lou, Smita Dayal, Xiaofeng Qiu, Robert Krolicki, Clemens Burda (2005) Doped Semiconductor Nanomaterials. *J. Nanoscience and Nanotechnology*
- Xiaobo Chen; Weishen Yang, Jie Liu, Liwu Lin. (2004) Characterization of the formation of NaA zeolite membrane under microwave radiation. *J. Mater. Sci.*, 39(2), 671
- Y. Hu, (2000) Preparation of Lead Zirconate Titanate Ceramic Fibers by Sol-Gel Method, *Journal of Sol-Gel Science and Technology*, 18(3), p. 235-247,
- Y. Lirong and Y. Guoxing (1988) TiO₂-SiO₂ monolithic glass formation from sol-gel. *Journal of Non-Crystalline Solids*, 100(1-3), p. 309-315.
- Y. Zhang, et al. (2005) Synthesis of nano/micro zinc oxide rods and arrays by thermal evaporation approach on cylindrical shape substrate. *J. Phys. Chem. B*, vol. 109(27), pp.13091–13093,
- Y. Zhang, Y. Z. Huang, Y. Wang, X. B. Ji, S. J. Shih, and B. D. Jia, (2009) Study of nano-Ag particles doped TiO₂ prepared by photocatalysis. *Journal of Nanoscience and Nanotechnology*, vol. 9, pp. 3904-3908.
- Yamashita, H., Harada, M., Misaka, J., Takeuchi, M., Ichihashi, Y., Goto, F., Ishida, M., Sasaki, T., Anpo, M. (2001) Application of ion beam techniques for preparation of metal ion-implanted TiO₂ thin film photocatalyst available under visible light irradiation: metal ion-implantation and ionized cluster beam method. *J Synchrotron Radiat.* 8:569-571.

- Yang, J., Mei, S., Ferreira, J.M.F. (2001) Hydrothermal Synthesis of Nanosized Titania Powders: Influence of Tetra alkyl Ammonium Hydroxides on Particle Characteristics. *J. Am. Ceram. Soc.* 84:1696-1702
- Yao, Y., Ohko, Y. et al. (2008) Self sterilization using silicone catheters coated with Ag and TiO₂ nanocompositethin film. *Journal of Biomedical Materials Research Part B - Applied Biomaterials* ,
- Ye, Z., Zhang, H. H., Pan, H. B., Pan, H. Q. (2002) Spectral studies on nanosized titania photocatalysts prepared by different drying methods. *Guang Pu Xue Yu Guang Pu Fen Xi* 22:928-931.
- Yongbing Lou, Xiaobo Chen, Anna C. Samia, Clemens Burda.(2003) Femtosecond Spectroscopic Investigation of the Carrier Lifetimes in Digenite Quantum Dots and Discrimination of the Electron and Hole Dynamics via Ultrafast Interfacial Electron Transfer. *J. Phys. Chem. B*, 107(45), 12431
- Yoo, K., Choi, H., Dionysiou, D. D. (2005) Synthesis of anatase nanostructured TiO₂ particles at low temperature using ionic liquid for photocatalysis. *Catal.Comm.* 6:259-262.
- Yu JG, Zhao XJ, Zhao QN (2000) Effect of surface structure on photocatalytic activity of TiO₂ thin films prepared by sol-gel method. *Thin Solid Films* 379 (1-2): 7-14
- Yu, J. C., Yu, J., Zhao, J. (2002) Enhanced photocatalytic activity of mesoporous and ordinary TiO₂ thin films by sulfuric acid treatment. *App. Cat. B:Environmental* 36:31-43
- Zhang F, Zhao J, Shen T, Hidaka H, Pelizzetti E, Serpone N (1998) TiO₂-assisted photodegradation of dye pollutants. II. Adsorption and degradation kinetics of eosin in TiO₂ dispersions under visible light irradiation *Appl Catal B: Environ* 15:147-156
- Zhang J Z (1997) Ultra fast studies of electro dynamics in semiconductor and metal colloidal nanoparticles: Effects of size and surface. *Chem Res* 30:423-429

- Zhang, H.J. and Chen, G.H. (2009) Potent antibacterial activities of Ag/TiO₂ nanocomposite powders synthesized by a one - pot sol - gel method. *Environmental Science and Technology*, 43 (8), 2905 – 10.
- Zhang, Z., Wang, C.C., Zakaria, R., Ying, J.Y. (1998). Role of Particle Size in Nanocrystalline TiO₂-Based Photocatalysts. *J. Phys. Chem. B* 102:10871-10878
- Zhao J, X Yang (2003) Photocatalytic oxidation for indoor air purification: a literature review *Build. Environ.* 38:645–654.
- Zhu et al. (2005) Zhu, H. Y., Lan, Y., Gao, X. P., Ringer, S. P., Zheng, Z. F., Song, D. Y., Zhao, J. C. 2005. Phase Transition between Nanostructures of Titanate and Titanium Dioxides via Simple Wet-Chemical Reactions. *J. Am. Chem. Soc.*
- Zumdahl, S.S., & Zumdahl, S. A. (2003). *Chemistry*. Boston, MA: Houghton Mifflin Company.